

On the volume of number, ζ zero's and particle repulsion

JH - GeometricRH@gmail.com

28 January 2020

Contents

1	The Basel problem	1
1.1	Why the Basel problem	1
1.1.1	The sum formula	2
1.1.2	The product formula	2
1.1.3	The sum/product equality	3
1.2	Rational and Real numbers	3
2	The spatial aspect of zeta	5
2.1	Volume over zeta	5
2.2	The structure of Volume over zeta	6
2.3	Geometric progression	8
2.3.1	Progression and common ratio's	8
2.4	Making sense of zeta	10
2.4.1	Contrasting discrete and continuous aspects	11
2.4.2	From 'abstract spatial' to 'observed continuity'	12
2.5	Spherical scale-invariant proportion	14
2.5.1	Mapping to a circumference	14
2.5.2	Mapping to a surface area	15
3	The primorial function	17
3.1	Prime grouping	18
3.2	The quadrature constant	19
3.3	Mapping the continuum	20
3.4	Quadrature reference frame	21
3.5	Primorial 24 parts in 25 and hexagons	22
4	The Triangular numbers	25
4.1	Mapping the sum formula	25
4.2	Mathematical universe	26
4.3	The Planes	26
4.3.1	Projection Plane	26

4.3.2	Triangular Plane	27
4.4	Affected area for n is 3	28
4.4.1	Proportion above hypotenuse	28
4.4.2	Affected area in the limit	28
4.5	Triangular projection to Surface Area	28
4.5.1	Hybrid right and equilateral triangle	29
4.6	Area accounting in the plane	29
4.7	Zeta for s other than 2	32
4.8	Changes in Surface Area	33
4.8.1	Bounds of the phase shift	35
4.8.2	Longest root of a square area	35
4.9	Volume independent of number	36
4.10	Outside the limit	37
4.10.1	Zeta at the limit, the surface asymptote	38
4.10.2	Equilibrium at SA=V, Planck	39
4.11	The fractal argument for zeta	40
5	Chords	45
5.1	Hexagonal chords and Planck	45
5.2	Unity chords	46
5.2.1	Like a ladder up the wall	48
5.3	Root 2 equilibrium	50
5.4	Curvature and the plane	51
5.5	The root of curvature	54
5.5.1	Unity orthogonal to the sphere	55
6	A cartesian M-brane mono surface	57
6.0.1	Primorial 10 and PI	60
6.0.2	Necessarily convex	60
6.1	The M-brane exposed area	60
6.2	Slotting mechanism	63
7	Quadrature Geometric Framework	67
7.1	Primorial hexagon plus	68
7.2	One ring to enclose them all	68
7.2.1	Chords, almost created equal	68
7.2.2	Where does the unity chord live	70
7.2.3	The primorial connection	72
7.2.4	The forties	73
7.2.5	Powers of ten to infinity	73
7.3	The natural state as repository of potential	74

7.3.1	A box of chords	74
7.4	Prime interference	78
7.4.1	Observations	79
7.5	Geometric, density dependent primes	80
7.5.1	Pair correlation	80
7.6	Looking back from infinity	82
7.6.1	Pair correlation as function of volume	82
7.7	Zeta zero to proportional QGF chord	84
7.7.1	Stable QGF configuration	86
7.7.2	Interlaced zeta and repulsion	87
7.7.3	Naturally in pieces	87
7.7.4	Prime like distribution for all n	91
7.7.5	Zetas walk about on the diagonal	92
7.8	Prime stretching in the projection plane	95
7.8.1	The size of the plane	98
8	Spectrum of volume	103
8.1	Interval, chaos and strange attractor	103
8.2	Spectrum chain links	105
8.3	Spectrum midfield composite	107
8.4	At the edge of chaos, the primordial spectrum	109
8.4.1	25, primordial equilibrium	109
8.4.2	The spectrum for the primordials	111
8.4.3	Factors on the orthogonal diagonal	112
8.4.4	Equilibrium at the bow shock	112
8.5	The size of the mathematical universe	114

Chapter 1

The Basel problem

The focus in this document is not on the classic Riemann zeta function involving Complex Analysis, however, the results provide a solution for the distribution of the zeta zero's and consequently an answer to the Riemann hypothesis. This thesis covers the problem that superseded the Riemann zeta function, 'the Basel Problem', called after the Swiss city. At the university of Basel the Bernoulli brothers successively served as professor of mathematics (Jakob, 1687-1705, Johann, 1705-1748). Jakob Bernoulli stated the problem: Find a closed form for the infinite series

$$1 + \frac{1}{2^2} + \frac{1}{3^2} + \frac{1}{4^2} + \frac{1}{5^2} + \dots \quad (1.1)$$

This is the sum of the reciprocal squares of the natural numbers. This series is closely related to the harmonic series for which the Bernoulli brothers found proof for the divergence of the series

$$1 + \frac{1}{2} + \frac{1}{3} + \frac{1}{4} + \frac{1}{5} + \dots = \infty \quad (1.2)$$

The Basel problem, as sum of the reciprocal squares of the natural numbers, is the foundation for what later became inquiry in the distribution of the prime numbers among the natural numbers. After 330 years there are still open questions to be answered .

1.1 Why the Basel problem

In essence this paper starts in 1735, the year that Leonhard Euler in st. Petersburg found the answer to the Basel problem, he found the closed (exact) form surprisingly to add up to an irrational number

$$1 + \frac{1}{2^2} + \frac{1}{3^2} + \frac{1}{4^2} + \frac{1}{5^2} + \dots = \frac{\pi^2}{6} \quad (1.3)$$

It proved beneficial to take a step back and just look at the problem without any accumulated baggage of prior investigations.

1.1.1 The sum formula

The zeta function for $s=2$ is the infinite sum of reciprocal squares of the natural numbers :

$$\zeta(2) = \sum_n^{\infty} n^{-s} = 1 + \frac{1}{2^2} + \frac{1}{3^2} + \dots = \frac{\pi^2}{6} \quad (1.4)$$

The infinite sum of the shaded squares fig. 1.1, The sum formula adds up

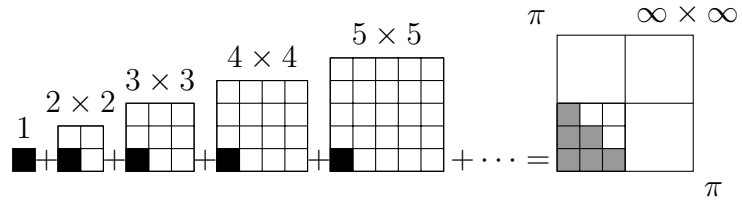


Figure 1.1: The sum formula

to $\frac{1}{6}$ of π^2 . Note that the closed form $\frac{\pi^2}{6}$ indicates that the rational squares add up to a fraction of an irrational surface with sides π .

1.1.2 The product formula

The zeta function for $s=2$ can also be stated as product over the primes:

$$\begin{aligned} \zeta(2) &= \prod_p^{\infty} (1 - p^{-2})^{-1} = \prod_p^{\infty} \frac{1}{1 - \frac{1}{p^2}} \\ &= 1 \times \frac{4}{3} \times \frac{9}{8} \times \frac{25}{24} \times \dots = \frac{\pi^2}{6} \end{aligned} \quad (1.5)$$

This can be represented as a product of square area ratios. The infinite product of the factors equals $\frac{1}{6}$ of π^2 . E.g. Note that the ratio $\frac{16}{15}$ between $\frac{9}{8}$ and $\frac{25}{24}$ does not appear because 4 is not a prime number. The rational quotients multiply out to an irrational square with sides π .

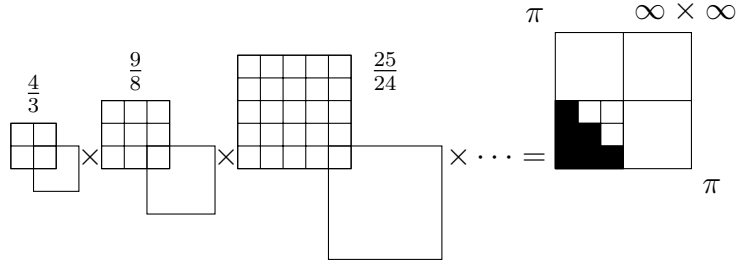


Figure 1.2: The product formula

1.1.3 The sum/product equality

The sum/product equality:

$$\sum_n n^{-s} = \prod_p (1 - p^{-s})^{-1} \quad (1.6)$$

The sum of the reciprocal squares of the natural numbers equals a infinite product of which the terms iterate over all prime numbers. The geometric projection of the sum and product formula shows the evolution of the formula to the result $\frac{\pi^2}{6}$ as a function of area. It is in precisely this mapping that a alternative pathway for investigation presented itself.

1.2 Rational and Real numbers

Wikipedia: Real numbers and topological properties

The rationals are a dense subset of the real numbers: every real number has rational numbers arbitrarily close to it.

A sum or product of Rational quantities should not add up, or multiply out, to a sum/product representing a Real number value.

Is the result $\zeta(2) = \frac{\pi^2}{6}$ a Real number or an infinitely close rational approximation?

The set of Real numbers \mathbb{R} and the set of Rational numbers \mathbb{Q} are diffusely interlaced on the Real axis, but never touch or share a coordinate. Or do they?

Chapter 2

The spatial aspect of zeta

Table 2.1 shows some known closed forms for the even values of 's', the closed forms for the odd values of 's' are unknown. Those for the even values have the form

$$\frac{\pi^s}{x} \quad (2.1)$$

With respect to symmetry naively one expects that the closed form for all 's' will be of the form:

$$\zeta(s) = \frac{n\pi^s}{x <= n\pi^s} \quad (2.2)$$

2.1 Volume over zeta

Wikipedia The inverse square law¹, in physics, is any physical law stating that a specified physical quantity or intensity is inversely proportional to the square of the

¹Wikipedia: inverse square law

Table 2.1: Zeta function values

s	Closed exact	Calculated value
1	no value	no value
2	$\frac{\pi^2}{6}$	1.644934067...
3	unknown	1.202056903...
4	$\frac{\pi^4}{90}$	1.082323234...
5	unknown	1.036927755...
6	$\frac{\pi^6}{945}$	1.017343062...

distance from the source of that physical quantity. The fundamental cause for this can be understood as geometric dilution corresponding to point-source radiation into three-dimensional space

A similar proportional symmetry exists between the result $\zeta(2) = \frac{\pi^2}{6}$ and the spherical volume enclosed by a surface area $SA = \pi^2$, expressed as twice the radius of such a volume.

Let $SA = \pi^2$

$$\begin{aligned} r_{sa} &= \sqrt{\frac{SA}{4\pi}} = \sqrt{\frac{\pi^2}{4\pi}} = \frac{\sqrt{\pi}}{2} \cong 0.8862269255 \\ V_{sa} &= \frac{4}{3}\pi r_{sa}^3 = \frac{4}{3}\pi \left(\frac{\sqrt{\pi}}{2}\right)^3 \cong 2.915569721 \\ \frac{V_{sa}}{\zeta(2)} &= 2r_{sa} \end{aligned} \tag{2.3}$$

2.2 The structure of Volume over zeta

The value volume over zeta is exactly twice the radius calculated for a sphere with $SA = \pi^2$. The function value $\zeta(2) = \frac{\pi^2}{6}$ represents a ratio which seems to sit in the middle of some dynamic process involving the expansion of a sphere. This becomes clear if we dissect the structure. The ratio $\frac{V_{sa}}{\zeta(2)} = 2r_{sa}$ has the form

$$\frac{V_{sa}}{\frac{1}{6}SA} = 2 \times r_{sa} \tag{2.4}$$

Assume that $2 \times r_{sa}$ is proportional to the radius of some next volume, the infinite sum of $\zeta(2)$ can be interpreted as the process that completes the inflation (by doubling of radius) from V_{sa} up to V_{next} . The assumed inflation has to start from some initial volume.

$$V_{sa} = \frac{4}{3}\pi (r_{sa})^3 = \frac{4}{3}\pi \left(\frac{\sqrt{\pi}}{2}\right)^3 \approx 2.915569721 \tag{2.5}$$

This V_{sa} is the volume after completion of $\zeta(2)$, therefore a division by 8 gives the initial volume: $V_{init} = \frac{V_{sa}}{8} \approx 0.3644462151$ is the supposed start volume. This numerical result is not very informative, a better way is to use scale invariant ratios.

The scale invariant ratios

V_{sa} itself is the end stage of a previous cycle
 $V_{init} \stackrel{def}{=} 1$ is the initial volume

Which makes $V_{sa} = 8 \times V_{init} = 8$, the end-stage of $\zeta(2)$, thus relabel for clarity, $V_{sa} \rightarrow V_{end}$

V_{end} is the stage before the next volume, therefore $V_{next} = 8 \times V_{end} = 64$

The interpretation of volume over zeta in light of the scale invariant ratios indicates a (snapshot of a) dynamic structure of 3 consecutive stages of inflation. Stages V_{end} and r_{end} represent the value for the middle volume that is reached at completion of the zeta function.

$$\begin{aligned} V_{init} &= 1 \rightarrow V_{end} = 8 \rightarrow V_{next} = 64 \\ r_{init} &= 1 \rightarrow r_{end} = 2 \rightarrow r_{next} = 4 \end{aligned} \quad (2.6)$$

To emphasize: $r_{end} = 2$, refers to twice the radius associated with V_{end} , and such a radius cannot belong to V_{end} in the regular sense. This means that V_{init} by method of completing the pattern must have a relative radius of $r_{init} = \frac{1}{2}$, because under this scheme volume over zeta returns twice the relative radius of the sphere. Now by logic of ratio,

$$sa_{end} = \frac{V_{end}(=8)}{r_{end}(=2)} = 4 \quad (2.7)$$

The surface area of a sphere grows with a factor 4 by doubling the radius. Thus the volume of the current iteration, V_{end} divided by the radius of the consecutive volume r_{end} , which is in fact the double radius found with V_{end} , gives the proportional multiplication factor of surface area by doubling of radius. Observe that it simultaneously represents a *growth factor of 4*, as well the scale invariant size of the current surface area.

$$sa_{init} = 1 \rightarrow sa_{end} = 4 \rightarrow sa_{next} = 16 \quad (2.8)$$

In equation 2.8, $sa_{end} = 4$ does refer to the surface area of the second iteration., e.g. $\{1, 4, 16, 64\}$, but in equation 2.7, $sa_{end} = 4$, in context of the ratio where $2r_{sa}$ refers to the consecutive volume, refers to the constant rate of growth of surface area between iterations. This aspect of a common ratio is also present for volume and radius, however, equation 2.7 as a ratio, will prove to be crucial. The ratio $\frac{V_{end}}{r_{end}} = 4$ is a constant value by necessity in this scheme, as we will see shortly.

$$\frac{V_{init}}{\left(\frac{V_{end}}{r_{end}}\right)} = \frac{1}{4} \quad (2.9)$$

The intimate relation (eq. 2.9) between the numerator and denominator begs for an explanation. Taken in unison they both encode for spherical aspects, but do so following different sequences involving the presumed spatial properties.

A seemingly three dimensional structure hovers just below the surface of the zeta function. However, it concerns an abstract object, abstract objects do not take up space in a physical sense. And although clear spatial aspects are identified, there are no spatial aspects discernible in the infinite sum/product of the zeta function itself, nor is there any connection with 3-dimensional attributes in the zeta algorithm.

This lack of spatial properties might point to the outline of an abstract mathematical object that can be identified as a first principle under-laying the emergence of physical three dimensional structure.

2.3 Geometric progression

Nothing in the abstraction of the zeta function indicates a connection to spherical geometry. The zeta function arrives at the same answer by two distinct procedures, the additive sum formula eq.1.1 and the multiplicative product formula eq. 1.5. At the core we find arithmetic and geometric sequences that outline spherical attributes interwoven in the set of rational numbers \mathbb{Q} . *Such abstract sequences by themselves, however, are not sufficient to cause/project spherical attributes in physical sense.*

Wikipedia In mathematics, a geometric progression, also known as a geometric sequence, is a sequence of numbers where each term after the first is found by multiplying the previous one by a fixed, non-zero number called the common ratio. For example, the sequence 2, 6, 18, 54, ... is a geometric progression with common ratio 3. Similarly 10, 5, 2.5, 1.25, ... is a geometric sequence with common ratio 1/2. Examples of a geometric sequence are powers r^k of a fixed number r, such as 2^k and 3^k . The general form of a geometric sequence is $\{a, ar, ar^2, ar^3, ar^4, \dots\}$ where $r \neq 0$ is the common ratio and a is a scale factor, equal to the sequence's start value.

2.3.1 Progression and common ratio's

The numerator of the general pattern (see equation 2.10), is simply expressed starting at *init vol #0 = $\frac{1}{2}$* and then progresses with a common ratio of 2.

$$\frac{\text{init vol } \#0 = \frac{1}{2}}{\left(\frac{v=1}{0.25}\right)}, \frac{\text{volume } \#1 = 1}{\left(\frac{v=8}{2}\right)}, \frac{\text{volume } \#2 = 2}{\left(\frac{v=64}{16}\right)}, \frac{\text{volume } \#3 = 4}{\left(\frac{v=512}{128}\right)} \quad (2.10)$$

Thus encoding an increasing volume as function of a doubling radius in a geometric progression with a common ratio 2,

$$\left\{ (V_0 = \frac{1}{2}), (V_1 = 1), (V_2 = 2), (V_3 = 4), \dots \right\} \quad (2.11)$$

This given the context, is indeed a sequence to encode for an expanding sphere, but void of proper context it is an arbitrary, unwarranted, choice and should just be interpreted as some linear sequence. The second part expressed in the denominator, is more specific and gives clues how to interpret the ratio as a whole. The value of the denominator is itself a ratio

$$\frac{\frac{1}{2}}{\left(\frac{v=1}{0.25} = 4\right)}, \frac{1}{\left(\frac{v=8}{2} = 4\right)}, \frac{2}{\left(\frac{v=64}{16} = 4\right)}, \frac{4}{\left(\frac{v=512}{128} = 4\right)} \quad (2.12)$$

Here the numerator starts at $v = 1$ and progresses with a common ratio of 8, $\{1, 8, 64, 512, \dots\}$. Note that this sequence is encoded as an 8-fold increase of volume proportional to a doubling of the radius. Yet another linear expression to encode for an expanding sphere given the context in which it is found. In the denominator the value represents $\frac{1}{4}$ of the volume in the numerator. This simple property makes that whole ratio of the denominator for each instance equal to 4, and thus encodes a static measure of surface area. And this is however simple, just as it should be, because found is a spatial ratio that encodes a ratio of volume over surface area at the completion of the infinite sum/product $\zeta(2)$,

$$S_{ratio} = \frac{V_{init} = 1}{\left(\frac{V_{end}=8}{r_{end}^3=2}\right)} = \frac{1}{4} \quad (2.13)$$

This is the pattern recognized in the inverse square law and the geometric progression of surface area by a common factor of 4, for each consecutive doubling of radius. And yes, this $\frac{V_{end}=1}{SA_{end}=4}$ only holds for the infinite sum/product $\zeta(2) = \frac{\pi^2}{6}$. The challenge is therefore to provide a natural mechanism which independent of the abstraction, can be shown to necessarily emerge from some identifiable first condition and necessarily self organizes such that it reflects the abstraction. Equation 2.12 becomes,

$$\frac{\left(\frac{1}{2}\right)}{4}, \frac{1}{4}, \frac{2}{4}, \frac{4}{4}, \dots \rightarrow \frac{1}{8}, \frac{1}{4}, \frac{1}{2}, 1, 2, 4, 8, \dots \quad (2.14)$$

The ratio as a whole reflects the same geometric sequence as the numerator V_{init} , it encodes an increasing volume as function of the radius being doubled in a geometric progression

$$\left\{ (V_0 = \frac{1}{2}), (V_1 = 1), (V_2 = 2), (V_3 = 4) \right\} \quad (2.15)$$

the only difference is that the sequence lags two iterations behind. And in fact, both expressions (numerator and ratio overall) will proof to be sequences of increasing surface area:

$$\begin{aligned} \{common\ ratio = 4\} \times & \left\{ \frac{1}{(8)}, \frac{1}{(4)}, \frac{1}{(2)}, 1, 2, 4, 8, \dots \right\} \\ = & sequence\ V_{init} \left\{ \frac{1}{2}, 1, 2, 4, 8, \dots \right\} \end{aligned} \quad (2.16)$$

2.4 Making sense of zeta

It makes sense to designate surface area as the primary expression of the zeta function because it is present as common ratio of the combined expression in numerator and denominator.

Apparently the zeta function expresses a continuous increment in surface area that does not ‘enclose’ a volume, but IS the volume.

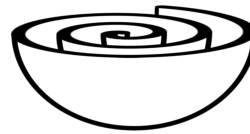


Figure 2.1: SA as a Volume

Fact is that in the geometric sequences any sense of continuous curvature is absent. It is the structure of the numerator and denominator of

$$SA_{ratio} = \frac{V_{init} = 1}{\left(\frac{V_{end}=8}{r_{end}^3=2} \right)} = \frac{1}{4}$$

that allows us to envision the trace of a spherical object shaped like a 3d spiral of surface area (fig. 2.1). It seems that the abstract sum exposes

aspects that are spatial in nature, *as if the algorithm $\zeta(2)$ actually traces some 3d object* while traversing the infinite series. The proposed hypothesis is the exact opposite such that the 3d structural aspects observed in nature, the tangible spatial aspects of 'space', might be merely an illusion. This presumed illusory aspect of 3-dimensional spatial aspect is also recognized in the holographic principle².

Once again the topological argument:

Wikipedia: Real numbers and topological properties

The rationals are a dense subset of the real numbers: every real number has rational numbers arbitrarily close to it.

... The rationals are a dense subset of the real numbers: every real number has rational numbers arbitrarily close to it. A related property is that rational numbers are the only numbers with finite expansions as regular continued fractions

In light of the topological argument, sec based on the sum of reciprocal squares of the natural numbers, one would not suspect such a sum to produce anything else but a rational value. Continuity as property of the Real numbers will be exposed as an illusion caused by topological projection, whereby the sets \mathbb{Q} and \mathbb{R} are merely distinguished by choice of perspective.

2.4.1 Contrasting discrete and continuous aspects

$$\text{spatial ratio} \rightarrow \frac{\text{(initial volume)}}{\frac{\text{(end volume}}{\text{end radius}}} \rightarrow \frac{V_{init} = 1}{\frac{(V_{end}=8)}{r_{end}=2}} \rightarrow \frac{1}{4} \quad (2.17)$$

The spatial ratio, (equation 2.17) is discrete, consists of rational values which describe scale invariant ratios. This structure of scale invariant ratios can be interpreted in terms of spherical geometry.

The structure $\frac{V_{sa}}{\zeta(2)} \equiv 2r_{sa}$ as limit of the product $\zeta(2) = \frac{\pi^2}{6}$, indicates that V_{sa} refers to an end volume, and that $\frac{\pi^2}{6}$ refers to $\frac{1}{6}$ the surface area of this volume $sa = \pi^2$. This leaves the impression that the infinite product of the zeta function represents a complete cycle during which some volume expands by doubling of its radius, from the first term of the infinite series to the last.

Abstract concepts do not have spatial properties nor do they exhibit dynamic behavior in any physical sense, so what does '*some volume expands by doubling of its radius*' in essence mean? Postulated is an abstract spatial object under-laying the nature of numbers. This abstraction exposes spherical

²wikipedia:Holographic principle

properties like radius, circumference and volume *detached from any apparent physical context*. The detachment from spatial dimensions is clear because the zeta algorithm does not operate on a data set obtained from a spatial context, be it sampled from nature or derived from some abstract model of nature. All that is derived from the function value $\zeta(2) = \frac{\pi^2}{6}$ are patterns that match geometric sequences and a apparently Real number function value that might be a infinitely close rational approximation.

The conjecture is that discrete accumulation, be it abstract numerically or wave/particle like as observed in physics, follows a first principle that might be described as 'pre-mathematical'. This first principle forces both numerical abstract models and/or physical reality to emerge such that the structure of both systems are clearly of common descent but not necessarily contingent on each other.

In other words, this first principle must be self evidently present in abstract numerical models and physical systems such that it has explanatory power for the effectiveness of mathematics in modeling natural systems, or reversely, the ability to gain new mathematical insight from observing nature.

The hypothesized 'pre-mathematical' first principle, as will be presented, follows from the theory of convex sets and is surprisingly simple to recognize in context of physical reality. It is in the physical implementation that we find the bridge to the Riemann zeta function and the proof for the conjecture 'all zeros have real part one half'. This means that a model for the distribution of the zeta zeros and the source for particle repulsion will be known from first principle and likewise rooted in basic mathematical principles.

As stated in chapter 1, we will not use complex analysis, we will arrive at the zeta zeros from another angle. For this build a new analytic tool and start by contrasting the mathematical abstraction of the sum of reciprocal squares and its supposed spatial attributes against spatial attributes of spherical geometry as observed in natural systems.

2.4.2 From 'abstract spatial' to 'observed continuity'

$$\begin{aligned}\zeta(s) &= \prod_p^{\infty} (1 - p^{-s})^{-1} = \frac{1}{1 - \frac{1}{2^2}} \times \frac{1}{1 - \frac{1}{3^2}} \times \frac{1}{1 - \frac{1}{5^2}} \times \dots \\ &= \frac{4}{3} \times \frac{9}{8} \times \frac{25}{24} \times \dots = \frac{\pi^2}{6} \rightarrow \frac{\text{surface area}}{\text{some value}}\end{aligned}\tag{2.18}$$

The zeta function value seems to indicate the inflation of a volume with respect to an initial volume. It does so because it has in it the radius for the successive cycle of inflation. Clearly any numerical quantity derived from appropriate context can be interpreted to represent length, area, volume,

time, any applicable dimensional quality. *Such a context is for the zeta function, an infinite product over the primes (all primes) or infinite sum over the natural numbers (all numbers) not obvious at all.*

Why do we find a relation to the inverse square law and spherical geometry? Numerically a ‘volume’ has inflated, and the process expresses this in a value that encodes a spatial ratio (see equation 2.17). The ratio $\frac{\pi^2}{6}$ appears to be based on a surface area π^2 and must thus be proportional to the volume it encloses. The first aspect to take note of is that the zeta function expresses no elements of spherical geometry, i.e. Only rational numerical values, line segments if you will, are the sole constituents of the function value.

Because spatial aspects, if at all present, do not follow from the zeta algorithm, care has to be taken not to inadvertently introduce spatial aspects. How to prevent erroneous introduction of those aspects?

Consider the following formulas

$$V = \frac{4}{3}\pi r^3 \text{ yields the volume of a sphere}$$

$$r = \sqrt[3]{\frac{V}{(\frac{4}{3}\pi)}} \text{ yields the radius from a given volume.}$$

$$SA = 4\pi r^2 \text{ yields the surface area of a sphere}$$

$$r = \sqrt{\frac{SA}{4\pi}} \text{ yields the radius from a given surface area}$$

In each case the spatial aspect is represented by either raising the radius to a power, or reversely, taking the n_{th} root of the value $r^3 = \frac{V}{(\frac{4}{3}\pi)}$ for volume or $r^2 = \frac{SA}{4\pi}$ for surface area. The factors $(\frac{4}{3}\pi)$ and (4π) represent the curvature detached from spatial aspects.

As the subject of investigation is why the Real number value of $\zeta(2) = \frac{\pi^2}{6}$ follows from, in essence, a rational context. We do assume however that spatial attributes like volume, surface and length are illusory aspects of reality. So when contrasting the apparent spatial aspects of the sum of reciprocal squares we have to take care not to unwittingly introduce spatial aspects like $V = l \times h \times w$ when the assumption is there are no analogues to tangible spatial aspects represented in the sum of reciprocal squares.

For instance if we cube a radius we define a volume, and reversely, if we apply the formula $r = \sqrt[3]{\frac{V}{(\frac{4}{3}\pi)}}$ the assumption is that $|\frac{4}{3}\pi r^3|$ represents a volume, be it derived from some model with spatial properties, or from measurements obtained from some spatial context. The function $\zeta(2) = \frac{\pi^2}{6}$ represents neither the former nor the latter, therefor, to take a cube root in this context, for instance $r = \sqrt[3]{x}$, is in essence an operation that presupposes volume, and thus introduces a spatial context in the results. A context not present in the zeta function algorithm to begin with. Therefore the correct action is to obtain the initial- and end-radius conform the formula $r = \sqrt[3]{\frac{V}{(\frac{4}{3}\pi)}}$,

but omit reducing spatial aspects as if they represent volume. This simply means to stop short of reducing the cubic root in order to obtain the regular 1-dimensional radius, but instead work with the cubed value as is: $r^3 = \frac{V}{(\frac{4}{3}\pi)}$. Simply put, if the question “who or what cubed that value?”, can not be answered, then assume it is not cubed at all, after all, the function $\zeta(2)$ is nothing more than a sum/product of rational values which as such has no relation to any spatial context.

The cubed radius $r^3 = \frac{V}{(\frac{4}{3}\pi)}$ can be approached alternatively and has a deep connection to $\frac{V_{sa}}{\zeta(2)} = 2r_{sa}$. This connection leads to a two dimensional model that, like holographic models, causes an illusion/projection of three dimensional space. To confirm this conjecture of the illusory aspect of spatial properties a model is needed to explain how it is that we experience a 3 dimensional reality.

2.5 Spherical scale-invariant proportion

Assuming the zeta function encodes a scale-invariant proportion of surface area (SA), a rather naive approach provides more insight. Mapping any value for $\zeta(s) = \frac{\pi^s}{x}$ to a circumference, surface area or for instance cubic value, can be achieved by using the appropriate numerator and retain proportionality in the denominator, $\frac{\pi^s}{\pi^s \zeta(s-1)} >= 1$. A mapping of zeta for π^2 gives

$$\zeta(2) = \frac{\pi^2}{6}, \zeta(3) = \frac{\pi^2}{8.210596...}, \zeta(4) = \frac{\pi^2}{9.118906528...} \quad (2.19)$$

2.5.1 Mapping to a circumference

Scaling to $\zeta(2) = \frac{2\pi}{x}$ a circumference over a radius. Calculate the (s-1) derivative of the numerator and preserve proportionality with respect to that derivative in the denominator. e.g. for $\zeta(2)$ where $s=2$, it takes the first derivative to map π^2 to $2\pi^1$: $f(\pi) = \pi^2 \rightarrow f'(\pi) = 2\pi$:

$$\begin{aligned} \zeta'(2) &= \frac{2\pi}{(2\pi)(\frac{\pi^2}{6})^{-1}} = \frac{2\pi}{3.819718634} = \frac{2\pi}{(\frac{24}{2\pi})} \\ &\rightarrow \frac{\text{circumference}}{\text{radius}} \end{aligned} \quad (2.20)$$

Obviously the function value for $\zeta(2)$ must be known in order to feed back in this formula, however, it is the mapping that will provide insight into the

inner structure of the zeta function.

$$\begin{aligned}\zeta'(s) &= \frac{n\pi}{(n\pi)\left(\frac{\pi^s}{\pi^{s-\varepsilon}}\right)^{-1}} = \frac{n\pi}{(n\pi) - \varepsilon} >= 1 \\ &\rightarrow \frac{\text{circumference} \propto 2\pi}{|\text{radius}| <= 2\pi}\end{aligned}\quad (2.21)$$

This pattern will hold for all ‘s’. Because ‘s’ is the exponent of the numerator, the algorithm can be generalized for all ‘s’ by application of the factorial function. For s=5,

$$\begin{aligned}f''''(x^5) &= sx^{s-1} \rightarrow x^5 \rightarrow 5x^4 \rightarrow 20x^3 \rightarrow 60x^2 \rightarrow 120x^1 \\ f''''(\pi^5) &= 5!\pi = 5 \times 4 \times 3 \times 2 \times 1\pi = 120\pi\end{aligned}\quad (2.22)$$

The (s-1) derivative of π^s translates to $s!\pi$ and allows for the following closed formula for all s:

$$\frac{\pi^s}{(\pi^s)(\zeta(s))^{-1}} \rightarrow \frac{1}{(1)(\zeta(s))^{-1}} \rightarrow \frac{s!\pi}{(s!\pi)(\zeta(s))^{-1}}\quad (2.23)$$

And because this is a ratio, proceed by simplifying to the first derivative of $\zeta(s)$ by multiplying the ratio with 2 over ‘s’ factorial, and map all $\zeta(s)$ to the radius $r = 2\pi$:

$$\frac{2}{(s!)} \times \frac{s!\pi}{x} = \frac{2\pi}{(s!)x}\quad (2.24)$$

The general pattern: the denominator for all ‘s’ is smaller than the numerator, the quotient will approach 1 in the limit, i.e. the denominator will approach 2π :

$$\frac{s!\pi}{(s!\pi)(\zeta(s))^{-1}} \rightarrow \frac{x}{x - \varepsilon} > 1\quad (2.25)$$

2.5.2 Mapping to a surface area

Table 2.2 lists the first 6 values for s showing the mapping to 2π . The last column in this table shows the shorthand version for mapping the zeta function to $SA = \pi^2$, or to any πn . For the purpose of this thesis we continue with the values proportional to π^2 as shown in the rightmost column, *ratio* $\propto \pi^2$.

Table 2.2: Zeta as a scale invariant proportion

s	value	<i>preserving</i> \propto	<i>ratio</i> $\propto 2\pi$	<i>ratio</i> $\propto \pi^2$
	$\zeta(s)$	$\frac{s!\pi}{(s!\pi)(\zeta(s))^{-1}}$	$\frac{s!\pi}{x}$	$\frac{2}{s!} \times \frac{s!\pi}{x}$
1	no value yet			
2	$\frac{\pi^2}{6}$	$\frac{2\pi}{(2\pi)(1.644934066848)^{-1}}$	$\frac{2\pi}{3.819718634}$	$\frac{2\pi}{3.819718634}$
3	1.202056903159	$\frac{6\pi}{(6\pi)(1.202056903159)^{-1}}$	$\frac{6\pi}{15.68108454}$	$\frac{2\pi}{5.22702818}$
4	$\frac{\pi^4}{90}$	$\frac{24\pi}{(24\pi)(1.082323233711)^{-1}}$	$\frac{24\pi}{69.66331438}$	$\frac{2\pi}{5.80276198}$
5	1.036927755143	$\frac{120\pi}{(120\pi)(1.036927755143)^{-1}}$	$\frac{120\pi}{363.5654621}$	$\frac{2\pi}{6.059424368}$
6	$\frac{\pi^6}{945}$	$\frac{720\pi}{(720\pi)(1.017343061984)^{-1}}$	$\frac{720\pi}{2223.386383}$	$\frac{2\pi}{6.176073286}$
∞	$\frac{\pi^\infty}{\infty}$			$\frac{2\pi}{2\pi}$

Chapter 3

The primorial function

The primorial function is similar to the factorial function for the natural numbers but involves the product over the primes.

$$P_n\# = \prod_{k=1}^n P_k = 2 \times 3 \times 5 \times 7 \times \cdots \in \mathbb{N} \quad (3.1)$$

Table 3.1, page 18 lists:

1. P_n , the consecutive primes
2. $P_n\#$, the primorials
3. $(P_n\#)^{-1}$, the inverse primorials
4. P_s , the partial sum of $(P_n\#)^{-1}$ up til P_n
5. ΔP_s , the difference $\frac{(\sqrt{2})^{-1}}{P_s}$
6. $\uparrow\downarrow$, upper and lower bound alternating odd/even n

The partial sum of the inverse primorials P_s approaches the inverse square root of 2, $(\sqrt{2})^{-1} \simeq 0.7071067812$, but falls short by some factor. The primorial delta ΔP_s is the discrepancy between $(\sqrt{2})^{-1}$ and the limit of P_s which has a closed form $\sqrt{\frac{2\pi}{2.5^2}}$:

$$\lim_{n \rightarrow \infty} \Delta P_s = \frac{(\sqrt{2})^{-1}}{P_s} = \sqrt{\frac{2\pi}{2.5^2}} \simeq 1.00265131 \cdots \in \mathbb{R} \quad (3.2)$$

Table 3.1: Primorial root 2 approach

n	P_n	$P_n\#$	$(P_n\#)^{-1}$	$P_s = \sum_{k=1}^n (\prod_{k=1}^n P_k)^{-1}$	ΔP_s	$\uparrow\downarrow$
1	2	2	$\frac{1}{2}$	$\frac{1}{2}$	$\sqrt{2}$	ub
2	3	6	$\frac{1}{6}$	$\frac{2}{3}$	$\frac{\sqrt{2}-1}{2}$	lb
3	5	30	$\frac{1}{30}$	$\frac{7}{10}$	$\frac{\sqrt{2}-1}{7}$	ub
4	7	210	$\frac{1}{210}$	0.7047619048	1.00332719	lb
5	11	2310	$\frac{1}{2310}$	0.7051948052	1.002711274	ub
6	13	30030	$\frac{1}{30030}$	0.7052281052	1.002663927	lb
7	17	510510	$\frac{1}{510510}$	0.7052300641	1.002661142	ub
8	19	9699690	$\frac{1}{9699690}$	0.7052301671	1.002660995	lb
9	23	223092870	$\frac{1}{223092870}$	0.7052301716	1.002660989	ub
10	29	6469693230	$\frac{1}{6469693230}$	0.7052301718	1.002660989	lb
∞	∞			$\sim (\sqrt{2})^{-1}$	$\sqrt{\frac{2\pi}{2.5^2}}$	

3.1 Prime grouping

The grouping of the primes in an upper and lower bound, column $\uparrow\downarrow$, becomes apparent by analyzing the partial sum increment for each step with respect to the total increment so far. To apply the progressive sum, an additive function, over the primorial function, a multiplicative function, is inspired by the sum/product equality where a sum over the integers is equal to a product over the primes:

$$\sum_n n^{-s} = \prod_p^\infty (1 - p^{-s})^{-1} \quad (3.3)$$

Table 3.2, page 19 lists the partial sum increment for each row in table 3.1 in the column P_s increment.

1. P_n , the consecutive primes
2. $\uparrow\downarrow$, upper and lower bound alternating odd / even n
3. P_s increment, the step wise increment in P_s from previous to current row
4. $\frac{lb}{ub}$, the ratio between the P_s increment for grouped rows $\frac{(2n)}{(2n)-1}$

5. $\Delta \frac{lb}{ub}$, the ratio between the first row and current row $\frac{(2n)}{(n=1)}$

Table 3.2: Primorial lb/ub oscillation

n	P_n	$\uparrow\downarrow$	P_s increment	$\frac{lb}{ub}$	$\Delta \frac{lb_{n \rightarrow \infty}}{lb_{n=1}} = 3 \frac{lb}{ub}$
1	2	ub		$\frac{1}{2}$	
2	3	lb		$\frac{1}{6}$	$\frac{1}{3}$
3	5	ub	$\frac{16}{10} = 0.5333\dots$		
4	7	lb	0.1714285714	0.3214285714	0.964285714
5	11	ub	0.5337662338		
6	13	lb	0.1714618715	0.3212302701	0.96369081
7	17	ub	0.5337681926		
8	19	lb	0.1714619746	0.3212292844	0.963687853
9	23	ub	0.5337681971		
10	29	lb	0.1714619747	0.321229282	0.963687846
∞	∞		$\sim (\sqrt{2})^{-1}$	$0.32 = \frac{1}{3.125}$	$\frac{24}{25} = 0.96$

The clear oscillation between a upper and lower bound follows from taking the current partial sum (P_s for row n) minus the increment so far (P_s increment for row $n - 1$). The column $\frac{lb}{ub}$ contains the ratio between lower and upper bound for each group. Column $\Delta \frac{lb_{n \rightarrow \infty}}{lb_{n=1}} = 3 \frac{lb}{ub}$ contains the progressive ratio between the current $\frac{lb}{ub}$ row pair with respect to the ratio of the first $\frac{lb}{ub}$ row pair, $(\frac{lb}{ub})_{n=1} = \frac{1}{3}$.

3.2 The quadrature constant

The square of ΔP_s is defined as the quadrature constant.

$$\mapsto = (\Delta P_s)^2 = \frac{2\pi}{2.5^2} \simeq 1.005309649 \dots \in \mathbb{R} \quad (3.4)$$

The partial sum increment, P_s increment, table 3.2, shows a peculiar alternating progression. The current partial sum $P_s \rightarrow n$ minus the increment so far, oscillates between a lower and a upper bound of approximately $ub = \frac{1}{2}$ and $lb = \frac{1}{6}$. The upper and lower bounds alternate row by row and group the primes like $\{2, 3\}, \{5, 7\}, \{11, 13\}, \{17, 19\}$, etc. in some periodic fashion.

For the first two terms $\{2, 3\}$ the ratio is exact, $\frac{lb}{ub} = \frac{1}{3}$, the last two terms in the table $\{23, 29\}$ approach $\frac{lb}{ub} \simeq 0.3212292821 \sim \frac{1}{\pi}$. The primorials, and

thus the inverse and sum thereof, are rational values. The ratio lb/ub will, by the topological property of the real numbers, approach $\sim \frac{1}{\pi}$, but must be a rational approximation. By application of the derived quadrature constant $\varphi = \frac{2\pi}{2.5^2}$ the limit can be determined to be exact, $\frac{1}{\pi} \times \varphi = 0.32 \in \mathbb{Q}$.

The quadrature constant φ indicates that a one to one correspondence exist between the Rational numbers \mathbb{Q} , and Real numbers \mathbb{R} such that:

$$\mathbb{Q} \varphi = \mathbb{R} \leftrightarrow \frac{\mathbb{R}}{\varphi} = \mathbb{Q} \quad (3.5)$$

which implies

$$(\forall x \in \mathbb{R}) (\exists! q \in \mathbb{Q}) (x(\varphi)^{-1} = q) \quad (3.6)$$

The set of rational numbers \mathbb{Q} is countable infinite and can be paired with the natural numbers \mathbb{N} , which implies that if the hypothesis is correct, the real numbers \mathbb{R} are also countable infinite. Pairing, not by in the limit

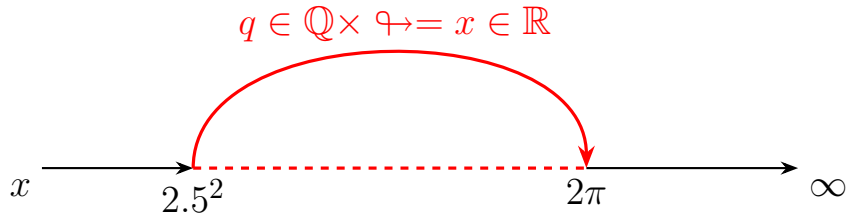


Figure 3.1: Quadrature constant - leap

approaching arbitrarily close to a partner, but rather leap frogging over an infinity of real and rational numbers (see fig.3.1) to a distinct value.

3.3 Mapping the continuum

Picture 3.2 shows, not to scale, the outer circle \mathbb{R} at radius $x = 1$, and the inner circle \mathbb{Q} at radius $x = (\varphi)^{-1}$. Both circumferences represent the continuum \mathbb{R} but both differ in length due to the difference in radius. For every arbitrary small change in angle the radius cuts each circle in exactly 1 distinct dimensionless coordinate $\frac{1}{\mathbb{R}}$. This is counter-intuitive, how can the coordinate be dimensionless if circumferences that differ in length are divided up in essentially the same number of coordinates? We see that at $\angle 180^\circ$ radius 1 gives $c = \frac{2\pi \times 1}{2} = \pi$ and for radius $(\varphi)^{-1}$ it is $c = \frac{2\pi \times (\varphi)^{-1}}{2} = 3.125$. Apparently the 'width of a coordinate', on a circumference encodes some property other than 'gradient in spread of arc'. Because radii intersect concentric circles at $\frac{1}{\mathbb{R}} \in \mathbb{R}$, a dimensionless point, this leads to a intimate and

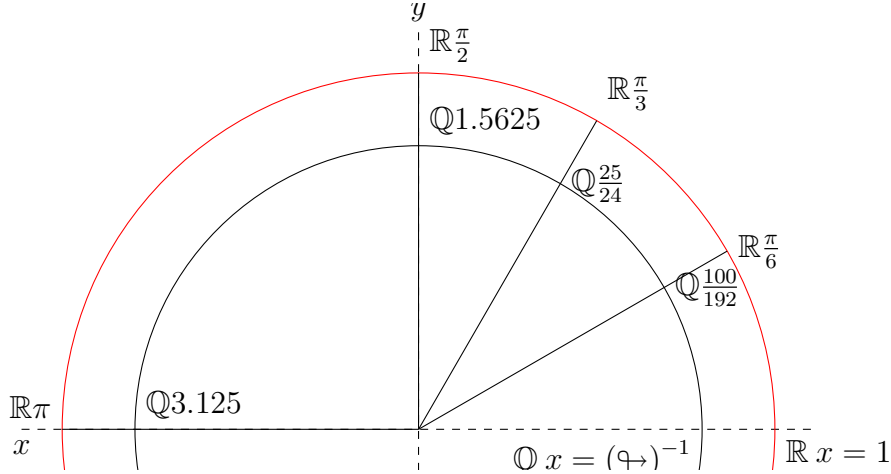


Figure 3.2: Quadrature continuum

unique connection between the sets \mathbb{Q} and \mathbb{R} . The circle is the continuum \mathbb{R} , and measures $\frac{2\pi}{\mathbb{R}} = 1$. The quadrature constant $\varphi = \frac{2\pi}{2.5^2}$ provides a smooth mapping from \mathbb{Q} to \mathbb{R} if we define \mathbb{Q} as a circle with radius $r = (\varphi)^{-1}$, and \mathbb{R} as a circle with radius $r = 1$. A rotation over 180° results for radius 1 in $c = \pi \in \mathbb{R}$ and for radius $(\varphi)^{-1}$ to $c = 3.125 \in \mathbb{Q}$. Apparently the radius has a curvature distorting the observers view such that discrete rational number intervals seem to spread out and project as indeterminable (irrational) real number values. As if a number-theoretical uncertainty principle exists with a horizon \mathbb{R} projected at a factor $\Delta r_{rq} = \frac{2\pi}{2.5^2} = \varphi$ from any arbitrary point chosen in \mathbb{Q} .

There exist a observational limit at radius 2π which transforms any discrete interval in what seems to be a continuum of real numbers. If we choose position at $r = \frac{2\pi}{\varphi} = 2.5^2$, or $\frac{2\pi}{\varphi}$ from the horizon at \mathbb{R} , we snap back on the grid of rational coordinates at \mathbb{Q} . Both coordinates π and 3.125 map to the exact same coordinate but only differ by perspective. Apparently distinct rational inputs map to distinct irrational outputs because intrinsically $\mathbb{Q} \equiv \mathbb{R}$.

3.4 Quadrature reference frame

Figure 3.3 is a Cartesian construction with compass and (unmarked) straight-edge. The construction simply begins with straight line 'A', a random point 'B', and a circle centered on 'B' of as yet undetermined radius. Now define the radius to $r = 5$ and construct 'E = 2.5' and 'F = 2.5²'. Proceed by constructing the square. This results in a square and circle of approximately

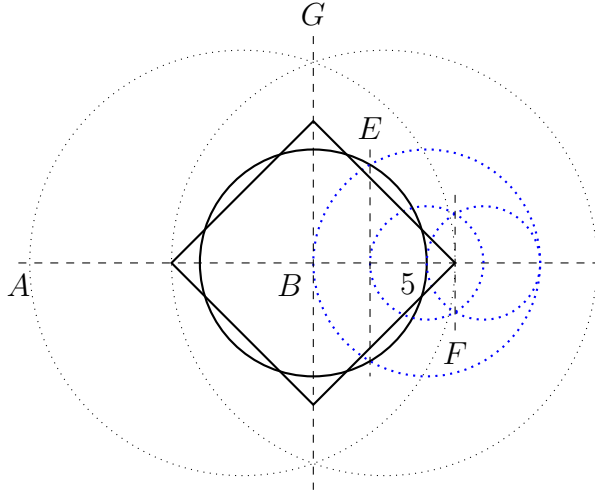


Figure 3.3: Quadrature reference frame

the same area¹. Transcendental numbers are not constructible with a set of compasses and (unmarked) straight edge², but in this reference frame we are able to construct an exact solution for $A_{\square} = A_{\circ}$.

$$\begin{aligned} A_{\square} &= \left(2.5^2\sqrt{2}\right)^2 = 78.125 \in \mathbb{Q} \\ A_{\circ} &= \pi 5^2 = 78.125 \nrightarrow \in \mathbb{R} \end{aligned} \quad (3.7)$$

In a strict Cartesian sense, clearly $A_{\square} \neq A_{\circ}$, however, we did not simply declare $A_{\square} = A_{\circ}$, but rather defined a geometric context in which the equality exist. Assuming the hypothesis correct this is expressed by

$$\mathbb{Q} \nrightarrow = \mathbb{R} \leftrightarrow \frac{\mathbb{R}}{\nrightarrow} = \mathbb{Q} \quad (3.8)$$

3.5 Primorial 24 parts in 25 and hexagons

Each distinct dimensionless point (coordinate) addressed on area A_{\square} maps to exact one, yet indeterminable fuzzy surface like, 'distributed coordinate' on the area A_{\circ} . This aspect of 'fuzzy spread' is closely related to the distribution of the (non trivial) zeros of the Riemann zeta function for which a model will be presented in chapter 7.

The outline of that model starts with defining the geometry in which to place the quadrature constant \nrightarrow . The placement is almost derived in

¹Wikipedia: Squaring the circle

²Wikipedia: Constructible number

figure 3.3, point $F = 2.5^2$. In fact $F \leftrightarrow = 2\pi$, which is in fact the horizon, or observational limit at radius 2π . Point 'F' functions as a pole at radius $x = 2.5^2$ and is the reference point from which all $x \in \mathbb{Q}$ are calculated. The primorial delta $P\Delta = 0.96$ (see table 3.2 page 19) defines the x-coordinate $P\Delta \times 2.5^2 = 6$ in figure 3.4.

$$P\Delta = \frac{24}{25} = 0.96 \quad (3.9)$$

We find in fact that the x-axis can be subdivided in exactly 25 parts of $\frac{1}{4}$, and that $\frac{24}{25} \times 2.5^2 = 6$, which makes the pole a 25 : 1 scale unit circle.

$$pole = \frac{2.5^2}{2\pi (\leftrightarrow)^{-1}} \propto \frac{25}{25} \propto 1 \quad (3.10)$$

The pole at $\frac{25}{25}$ can therefore be unambiguously constructed starting from any inscribed hexagon which, enforced by $P\Delta$, projects at $x = \frac{24}{25}$ within this geometric framework. Lastly, observe that the inverse of the primorial delta, multiplied by the quadrature constant, gives an angle of $60^\circ = \frac{\pi}{3}$. The hexagonal chord and the associated equilateral triangle will be a further crucial key element in this hypothesis.

$$P_* = (P\Delta)^{-1} \leftrightarrow \rightarrow \frac{\pi}{3} = 60^\circ \quad (3.11)$$

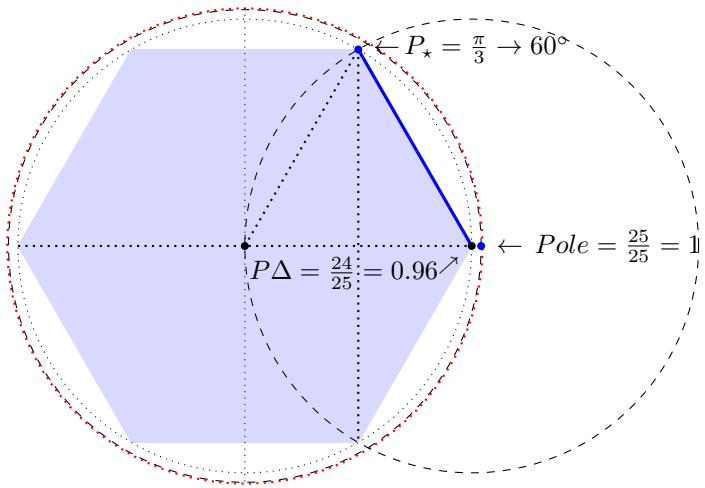


Figure 3.4: Primorial hexagon

Chapter 4

The Triangular numbers

Wikipedia: A triangular number or triangle number counts objects arranged in an equilateral triangle, [...].

The nth triangular number is the number of dots in the triangular arrangement with n dots on a side and is equal the sum of the n natural numbers from 1 to n.

$$T_n = \frac{n(n+1)}{2} = 0, 1, 3, 6, 10, 15, 21, 28, 36, \dots$$
$$n = \frac{\sqrt{8x+1}-1}{2} \rightarrow n \in \mathbb{N} \rightarrow T_n = x \quad (4.1)$$

4.1 Mapping the sum formula

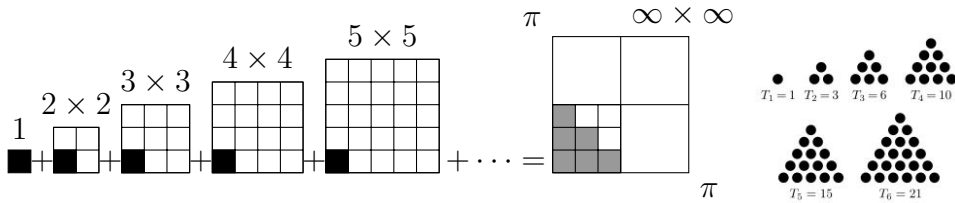


Figure 4.1: The sum formula and first six triangular numbers

The sum formula mapped as in figure 4.1, is a rather naive graphical representation of the zeta function value for $\zeta(2)$. Is the infinite sum of reciprocal squares connected to the triangular numbers? The final result after adding the whole infinity of reciprocal squares can be represented as such, but does it offer any explanatory powers to do so?

4.2 Mathematical universe

The triangular numbers and the zeta function are mathematical abstractions that can not in them selves exhibit dynamical behavior, nonetheless, we find that the under laying numerical sequence does reflect some tangible dynamical process. The conclusion therefor must be that numerical abstraction necessarily depends on, derives from, what is considered to be the physical nature of the world we observe. Overall we find that it seems as if observing a dynamic structure in a continues state of collapse. In fact this notion of *mathematics emerging from physical reality* and state of collapse is exactly what needs to be modeled for the hypothesis to be correct.

Figure 4.1 showing the area $A = \pi^2$ divided in 4 quadrants represents the mathematical universe, a complete convex set¹. Figure 4.1 does not have explanatory power for the dynamic behavior, that will be handled in chapter 7. In this chapter the apparent fractal property of self-similarity and dynamic fingerprint will be identified, the lower left (3_{th}) quadrant will be shown to represent the end state of the area as a whole.

4.3 The Planes

4.3.1 Projection Plane

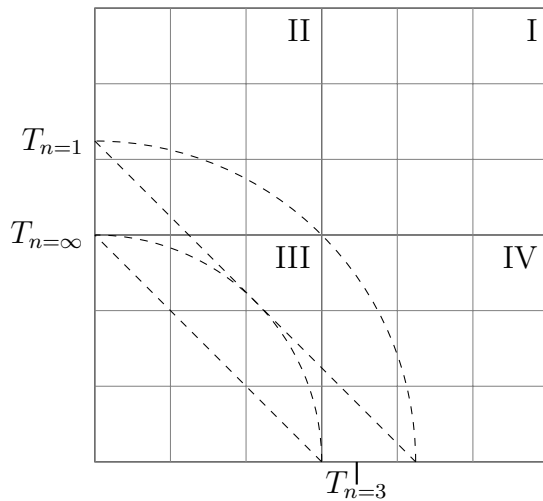


Figure 4.2: The projection plane

¹Wikipedia:A complete convex set

The projection plane A_{\square} (fig. 4.2) measures 1×1 unit, subdivided into 4 quadrants, numbered from the top right, anticlockwise I, II, III and IV. This plane is assigned a scale with sides of length $1 : \pi$ and thus defines the projection plane to $A_{\square} = \pi^2$, i.e. the continuum \mathbb{R}^2 . The marker $T_{n=3}$ on the x-axis, (also projects on the y-axis), marks the extend of a isosceles right angle triangle measuring $\frac{1}{6}A_{\square} = \frac{\pi^2}{6}$. Similarly the two arcs at $x = 0.5$ and $x = \sqrt{2}^{-1}$ define the two hypotenuses, $T_{n=0}$ as upper bound and $T_{n=\infty}$ as lower bound, below which the triangular numbers project as area of the continuum \mathbb{R}^2 , also as isosceles right angle triangles.

4.3.2 Triangular Plane

The rational projection of the triangular numbers is contained within the limits of quadrant III, the triangular plane A_{Δ} (see fig. 4.3). The n_{th} triangular number $T_n = \frac{1}{2}n(n + 1)$ projects on a $n \times n$ grit from the lower left corner up to and over the diagonal running from upper left to lower right. The 3×3 projection of $T_{n=3}$ results in a grit of 9 squares of which 6 are occupied.

$$T_{n=3} = \frac{1}{2}n(n + 1) = 1.5 \times 4 = 6 \quad (4.2)$$

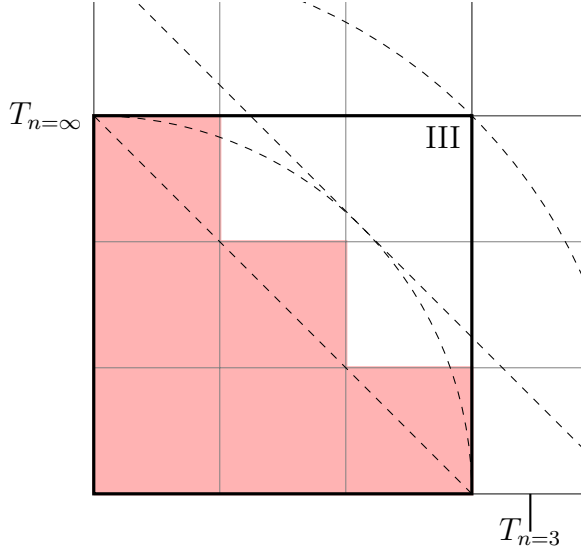


Figure 4.3: The triangular plane

4.4 Affected area for n is 3

See table 4.1, page 31. Each triangular number can be expressed as a set of discrete areas, e.g. the 6 filled squares in the 3×3 grid contained in quadrant III for $n=3$. The total affected area can be expressed in relation to:

- The projection plane: $T_{n=3} \rightarrow A_{\square} = \frac{6}{4 \times 9} = \frac{6}{36} = \frac{1}{6}$
- The triangular plane: $T_{n=3} \rightarrow A_{\Delta} = \frac{6}{9}$

4.4.1 Proportion above hypotenuse

Except for the limiting case $\lim_{n \rightarrow \infty}$, there is a portion of the affected area that projects above the hypotenuse. The sum of the triangles projected above the hypotenuse also add up to an area, for $n = 3$ this adds up to:

- Proportional to the projection plane: $T_{n=3} \rightarrow A_{\square} = \frac{n}{2} (2n)^{-2} = \frac{1}{24}$
- Proportional to the triangular plane: $T_{n=3} \rightarrow A_{\Delta} = \frac{n}{2} (n)^{-2} = \frac{1}{6}$

4.4.2 Affected area in the limit

At $\lim_{n \rightarrow \infty} T_n \rightarrow T_n = \infty$ the affected area is infinite dens, solely consisting of dimensionless points. This leaves no affected area remaining above the hypotenuse of quadrant III, for a total of $A_{\Delta} = \frac{1}{2} \rightarrow A_{\square} = \frac{A_{\Delta}}{A_{\square}} = \frac{1}{8}$. In this configuration the hypotenuse of the affected area will be $c = \frac{1}{2}\sqrt{2} \propto \frac{\pi}{2}\sqrt{2}$.

4.5 Triangular projection to Surface Area

The area projected by square area units in the triangular plane A_{Δ} , can also be represented by a continuous triangular section of the projection plane A_{\square} as a whole *with right angle sides* (note the emphasis) $a = b = \sqrt{2A_{\Delta}}$.

Such a projection for the triangular numbers will exceed the bounds of quadrant III for all triangular numbers with exception for the limiting case which projects on the diagonal of quadrant III, see fig.4.4. The hypotenuse of $Area \rightarrow T_{n=3} = 6$ has length: $c_{n=3} = \sqrt{2 \times Area} \times \sqrt{2} = \sqrt{24}$. The hypotenuse at $T_{n=3}$ sections off exactly the affected area as shown in the triangular projection $\frac{1}{6} = \frac{1}{8} + \frac{1}{24}$. In essence providing a continuous representation of the discrete triangular projection. By this procedure both $T_{n=3}$ and $\zeta(2) = \frac{\pi^2}{6}$ are mapped to the projection plane. The emphasis on “*with right angled sides*” has a purpose, a triangle number counts objects arranged in an equilateral triangle and not in a right sided triangle.

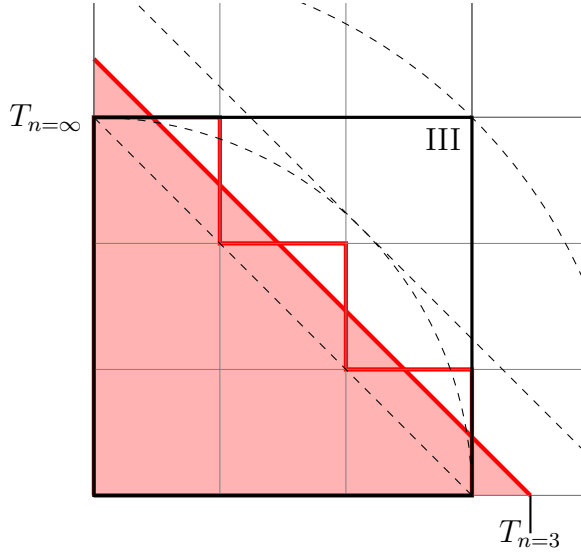


Figure 4.4: Triangular to projection plane

4.5.1 Hybrid right and equilateral triangle

There is one aspect that makes the right angled projection a model for a equilateral triangle and that is the arrangement of the triangular numbers. Note that $T_{n=3}$ projects 3 unit squares along the x and y axis, but also 3 units along the diagonal. *The projection is equilateral when expressed in numbers of units.* Figure 4.5 shows the area which any triangular grid can possibly occupy when projected as continuous area. In fig.4.5 the total area below the hypotenuse for $T_{n=3}$ is $\frac{1}{8} + \frac{1}{24} = \frac{1}{6}$. The remainder of the shaded area between $T_{n=3}$ and the limit at $T_{n=0} = (\sqrt{2})^{-1}$ measures $\frac{1}{2}(\sqrt{2}^{-1})^2 - \frac{1}{6} = \frac{1}{12}$. The process starts with $Area = \frac{1}{2}(\sqrt{2}^{-1})^2 - \frac{1}{6} = \frac{1}{12}$ and this area reduces as the cycle approaches $\lim_{n \rightarrow \infty} \rightarrow A_\Delta = \frac{1}{2} \rightarrow \frac{A_\Delta}{A_\square} = \frac{1}{8}$, a difference of $\frac{1}{8} - \frac{1}{12} = \frac{1}{24}$ which in the triangular projection is the part of the affected area exceeding the hypotenuse of the triangular plane.

4.6 Area accounting in the plane

The Bernoulli brothers found proof for the divergence of the harmonic series (eq. 1.2, page 1) $1 + \frac{1}{2} + \frac{1}{3} + \frac{1}{4} + \dots = \infty$.

Consider that the triangular number $T_{n=1}$ projects in a 1×1 grid in the

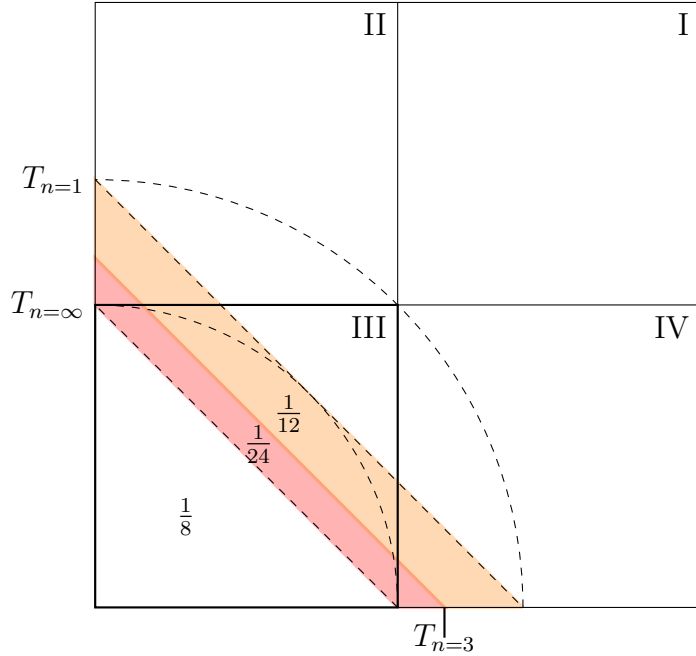


Figure 4.5: Exceeding the bounds of the Triangular plane

triangular plane and has $a = \sqrt{2 \times \frac{1}{4}} = \sqrt{2}^{-1}$, and furthermore that the harmonic series is equivalent to $\zeta(1) = 1 + \frac{1}{2^1} + \frac{1}{3^1} + \frac{1}{4^1} + \dots$.

In table 4.1, page 31 we find that the maximum affected area is $A_{\square} = \frac{1}{4}$. Table 2.1, page 5, "Zeta function values", lists "no value" for $\zeta(1)$, the harmonic series. However, in this particular reference frame a definite closed value can be assigned to the harmonic series by completing the pattern:

$$\zeta(1) = 1 + \frac{1}{2^1} + \frac{1}{3^1} + \dots = 1 + \frac{1}{2} + \frac{1}{3} + \dots = \frac{\pi^2}{4} \quad (4.3)$$

This needs to be justified for $\zeta(1)$. Considering that the mathematical universe is A_{\square} , where do the function values $\zeta(s) \forall s \neq 2$ project on the projection/triangular plane? The answer is intriguing, first the context for $\zeta(2)$ should be clear.

Table 4.1, page 31, shows three sections, connecting Cartesian triangular projection and associated spherical geometry.

1. section A_{Δ} *Triangular plane*: "Discrete" lists the area affected, "Continue" lists the associated right angle sides $a = b$ for the projection (fig. 4.4, onto the projection plane).

Table 4.1: Discrete triangular - Continues projection plane

A_{Δ} Triangular plane					A_{\square} Projection plane	Proportional SA
Discrete		Continue			$\lim_{n \rightarrow \infty} a = \frac{1}{2} \rightarrow r_q = \frac{0.5}{a}$	$r_q \rightarrow r_x$
$\propto A_{\Delta}$	$\propto A_{\square}$	Sides ab		Closed	Calculated	radius $r_x \propto SA$
n	T_n	$\frac{T_n}{n^2}$	$\frac{T_n}{4n^2}$	A	$a = \sqrt{2} \times A$	$r_q = \sqrt{\frac{n}{n+1}}$
						$r_q = \frac{0.5}{a}$
						$r_x = \frac{r_q}{\sqrt{P\Delta(\Downarrow^{-1})}}$
1	1	1	$\frac{1}{4}$	$\frac{1}{4}$	$\sqrt{2}^{-1}$	$\sqrt{\frac{1}{2}}$
2	3	$\frac{3}{4}$	$\frac{3}{16}$	$\frac{3}{16}$	$\sqrt{(2\frac{2}{3})^{-1}}$	$\sqrt{\frac{2}{3}}$
3	6	$\frac{6}{9}$	$\frac{6}{36}$	$\frac{1}{6}$	$\sqrt{\frac{1}{3}}$	$\sqrt{\frac{3}{4}}$
4	10	$\frac{10}{16}$	$\frac{10}{64}$	$\frac{5}{32}$	$\sqrt{\frac{10}{32}}$	$\sqrt{\frac{4}{5}}$
5	15	$\frac{15}{25}$	$\frac{15}{100}$	$\frac{3}{20}$	$\sqrt{\frac{3}{10}}$	$\sqrt{\frac{5}{6}}$
6	21	$\frac{21}{36}$	$\frac{21}{144}$	$\frac{7}{48}$	0.5400617249	$\sqrt{\frac{6}{7}}$
7	28	$\frac{28}{49}$	$\frac{28}{196}$	$\frac{1}{7}$	0.5345224838	$\sqrt{\frac{7}{8}}$
8	36	$\frac{36}{64}$	$\frac{36}{256}$	$\frac{9}{64}$	0.5303300859	$\sqrt{\frac{8}{9}}$
∞	∞		$\frac{1}{8}$	0.5		1
						1
						$\propto SA = \frac{4}{3}\pi^2$

2. section A_{\square} Projection plane: “Closed” lists the from “n” derived “intermediate radius” as the closed formula $r_q = \sqrt{\frac{n}{n+1}}$, the “Calculated” value for $r_q = \sqrt{\frac{n}{n+1}}$ is derived from the ratio to which the limit is approached, $r_q = \frac{0.5}{\sqrt{2 \times A}}$ (eq. 4.4, page 31)
3. section Proportional SA: the conversion of the “intermediate radius” using the primorial structure. Listed is the proportional surface area associated with the radius $r_x = \frac{r_q}{\sqrt{P\Delta(\Downarrow^{-1})}}$. By ratio $SA \propto \frac{4\pi(r_x)^2}{\pi^2}$ we find that the mapping for $T_{n=3}$ relates to $SA = \pi^2$ by application of the primorial ratios $P\Delta$ and \Downarrow .

$$\lim_{n \rightarrow \infty} \rightarrow a = \sqrt{2 \left(\frac{T_n}{4n^2} \right)} = \sqrt{2 \left(\frac{1}{8} \right)} = \frac{1}{2} \rightarrow r_q = \frac{0.5}{a} = 1 \quad (4.4)$$

The progression from $a = \sqrt{2}^{-1}$ to the limit $a=0.5$ can be, evidently, expressed as a ratio $r_q = \frac{0.5}{a}$, which has as closed form $r_q = \sqrt{\frac{n}{n+1}}$. Table 4.1, shows that the primorial ratios reflect some intimate connection between two

distinct worlds, the flat Cartesian triangular projection and the curved surface area of spherical geometry.

At $n = 3$, table 4.1, we find that the affected triangular area amounts to $A = \frac{A_{\square}}{6}$, and that the proportional surface area is π^2 . Assumed spatial aspect of $\zeta(2) = \frac{\pi^2}{6}$ is closely related to $T_{n=3}$ by $P\Delta$ and \leftrightarrow , which follow from the primorial function, and therefor from the prime numbers.

Is this merely a mathematical coincidence for $\zeta(2)$?

4.7 Zeta for s other then 2

Table 4.2: Projection plane range for all s

s	$\zeta(s)$	$\frac{\pi^2}{(\pi^2)(\zeta(s)^{-1})}$	$a = \sqrt{2A}$	$r_q = \frac{0.5}{a}$	$r_x = \frac{r_q}{\sqrt{P\Delta(\leftrightarrow^{-1})}}$	$SA \propto \pi^2$
1	$\frac{\pi^2}{4}$	$\frac{\pi^2}{4}$	$\sqrt{2 \times \frac{1}{4}} = 0.7071067812$	$\sqrt{2}^{-1}$	$\frac{\sqrt{0.5}}{\sqrt{P\Delta(\leftrightarrow^{-1})}} = 0.7236012546$	$SA \propto \frac{6}{9}\pi^2$
2	$\frac{\pi^2}{6}$	$\frac{\pi^2}{6}$	$\sqrt{2 \times \frac{1}{6}} = 0.5773502692$	$\sqrt{\frac{3}{4}}$	$\frac{\sqrt{\frac{3}{4}}}{\sqrt{P\Delta(\leftrightarrow^{-1})}} = 0.8862269255$	$SA \propto \pi^2$
3	$\frac{\pi^2}{8.210596}$	$\frac{\pi^2}{8.210596}$	$\sqrt{2 \times \frac{1}{8.210596}} = 0.4935460224$	1.013076749		
4	$\frac{\pi^4}{90}$	$\frac{\pi^2}{9.118906528}$	$\sqrt{2 \times \frac{1}{9.118906528}} = 0.4683209821$	1.067643851		
5	$\frac{\pi^2}{9.518121541}$	$\frac{\pi^2}{9.518121541}$	$\sqrt{2 \times \frac{1}{9.518121541}} = 0.4583944753$	1.090763582		
6	$\frac{\pi^6}{945}$	$\frac{\pi^2}{9.701359231}$	$\sqrt{2 \times \frac{1}{9.701359231}} = 0.4540447984$	1.101212924		
∞	$\frac{\pi^\infty}{\infty}$	$\frac{\pi^2}{\pi^2}$	$\sqrt{2 \times \frac{1}{\pi^2}} = \frac{1}{\pi}\sqrt{2} = 0.4501581581$	$\sqrt{\frac{\pi^2}{8}}$	$\frac{\sqrt{\frac{\pi^2}{8}}}{\sqrt{P\Delta(\leftrightarrow^{-1})}} = 1.136630193$	$SA \propto \frac{\pi^2}{6}(\pi^2)$

Table 4.2 tabulates the values for $s = \{1, \dots, 6, \infty\}$, where for $s = 1$ the proposed value $\frac{\pi^2}{4}$ is used.

The values for $\zeta(s > 2)$ in column $a = \sqrt{2A}$ all calculate to a value $\sqrt{2A} < 0.5$. This means that none of the $\zeta(s > 2)$ will be expressed in the

infinite range of triangular numbers $T_n(a) = [\sqrt{2}^{-1}, 0.5]$, as if they do not exist at all. They do, however, have a limit at $\frac{1}{\pi}\sqrt{2}$. The value for $\zeta(s=1)$ in column $SA \propto \pi^2$ lists $SA \propto \frac{6}{9}\pi^2$, this result hints at the fractal property if interpreted as a result of dynamic behavior, but does not confirm conclusively that $\zeta(1) = \frac{\pi^2}{4}$ is valid. The interpretation of $A_{\square} = \frac{6}{9}\pi^2$ is that it indicates *a previous cycle of $\zeta(2) = \frac{\pi^2}{6}$ when the ratio affected cells for the triangular plane reached $A_{\Delta} = \frac{6}{9}$* . The fraction $\frac{6}{9}$ is associated with the affected area of the triangular plane A_{Δ} in the third quadrant of the projection plane A_{\square} resulting from $\zeta(2) = \frac{\pi^2}{6}$, and here we find this configuration superimposed on the projection plane $A_{\square} = \frac{6}{9}\pi^2$ as if it is the triangular plane. At $\zeta(1)$ the affected area of the projection plane A_{\square} is $\frac{6}{9}$, mirroring the triangular plane A_{Δ} at $\zeta(2)$. The value $\zeta(2) = \frac{\pi^2}{6}$, indicates that both projection plane and triangular plane are projections of the same area π^2 at two distinct moments of some recursive process.

The configuration/function value $\zeta(2) = \frac{\pi^2}{6}$ seems to represent some equilibrium, see equation 4.5.

$$\begin{aligned} T_{n=1} &\propto SA = \frac{2}{3}\pi^2 = 2\pi \times P_{\star} \\ \zeta(2) &= \frac{\pi^2}{6} \rightarrow 4\left(\frac{\pi^2}{6}\right) \propto SA = \frac{4}{6}\pi^2 = 2\pi \times P_{\star} \\ \zeta(1) &\propto SA = \frac{6}{9}\pi^2 = 2\pi \times P_{\star} \end{aligned} \quad (4.5)$$

4.8 Changes in Surface Area

The triangular cycle $T_{n\{1,\dots,\infty\}}$ only holds $\zeta(s)$ for $s \in \{1, 2\}$, values for $\zeta(s > 2)$ are not represented within the triangular cycle. Those values cannot be mapped as triangular number grid in quadrant III, however, the values can be mapped as affected area in the mathematical universe of A_{\square} .

In table 4.1, page 31 we find that the value for $\zeta(2)$ coincides with $n = 3 \rightarrow a = \sqrt{2 \times \frac{1}{6}}$ and a proportional $SA = \pi^2$. At the start of the triangular cycle we find $T_{n=1} \rightarrow r_x \propto SA = \frac{6}{9}\pi^2$, the total increment in the range $\zeta(1) \rightarrow \zeta(2)$ is therefore $\left(\frac{A_{\square}}{A_{\Delta}}\right) \times \left(\frac{\pi^2}{\frac{6}{9}\pi^2}\right) = 4 \times \frac{3}{2} = 6$. The projection for $\zeta(\infty)$ (see table 4.2, page 32) yields the radius for a sphere with $SA \propto \left(\frac{\pi^2}{6} \times \pi^2\right)$ which is an increment in surface area by a factor $\zeta(2) = \frac{\pi^2}{6}$ in the range $\zeta(2) \rightarrow \zeta(\infty)$. However, because the values for $\zeta(s > 2)$ fall outside the

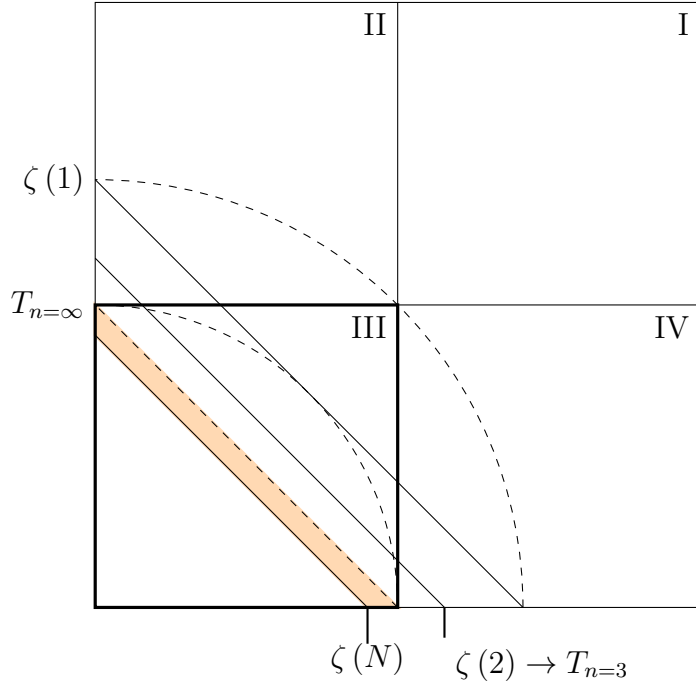


Figure 4.6: Projection plane extended zeta

bounds of the triangular projection, we established that the mapping to A_Δ does not apply. Instead, those values indicate the projection to some future state in a continuous collapse of surface area.

The values for $s > 2$ for the Projection plane/Triangular plane assembly can be interpreted as *reflecting a relative position/distance removed from the current equilibrium at value $\zeta(2)$* . In this sense the triangular numbers projected onto the projection plane A_\square can be interpreted as *a scale invariant snapshot of any stage in hypothesized state of continuous collapse*. Which, of course, implies that for this to be true, also the natural numbers $n \in \mathbb{N}$ must be interpreted as a set of labels attached to relative positions on a gliding scale.

For now we assume this dynamical aspect as a given, and proceed under the assumption that this geometric model represents a phase shift in the mathematical universe that, during hypothesized collapse, geometrically fixates the relative positions of those labels.

4.8.1 Bounds of the phase shift

The phase shift projects within static bounds on the projection plane A_{\square} . We find values for $SA \propto \frac{6}{9} \times \pi^2$, $SA = 1 \times \pi^2$, and $SA \propto \frac{\pi^2}{6} \times \pi^2$ (see table 4.2, page 32). As found previously, the scale factor $\left(\frac{A_{\square}}{A_{\Delta}}\right) = 4$ is key because the triangular plane, or rather quadrant III it projects in, is clearly the scale invariant continuation of the projection plane A_{\square} . We see that with respect to scale, $\left(\frac{A_{\square}}{A_{\Delta}}\right) \times \frac{\pi^2}{6} \propto \frac{6}{9}\pi^2$. The apparent increment in surface area from π^2 to $\frac{\pi^2}{6} \times \pi^2$ between $s = 2$ and $s = \infty$ is, however, a dynamical interpretation imposed on what essentially is a mathematical abstraction, so there must be some real world context in which proposed phase shift can be identified as part of some dynamical process in space/time reality. In chapter 8 a proposal to explain the nature of this phase shift will be formulated, and a relation will be identified between the conservation laws, the nature of vacuum energy and the cosmological constant Λ .

First identify the static numerical pattern that seems to occurs at the point of equilibrium for the ratio affected area:

- For the projection plane A_{\square} , numerator and denominator are $A_{\square} \rightarrow \frac{6^n}{6}$
- For the triangular plane A_{Δ} , numerator and denominator are $A_{\Delta} \rightarrow \frac{6^{n+1}}{9}$

Thus the increase of the affected area progresses in a $1 : 4$ ratio (see eq. 2.17, page 11),

$$\begin{aligned} \frac{6^0 = 1}{6} A_{\square} &\rightarrow \frac{6^1 = 6}{9} A_{\Delta} \\ \frac{6^1 = 6}{6} A_{\square} &\rightarrow \frac{6^2 = 36}{9} A_{\Delta} \end{aligned} \tag{4.6}$$

which indicates the total affected area of A_{Δ} must be $\frac{6}{6}A_{\square} = 1A_{\square}$ or corrected for scale in-variance $\frac{A_{\Delta}}{A_{\square}}A_{\square} = \frac{1}{4}A_{\square} = A_{\Delta}$ for each iteration. The total affected area of A_{Δ} is therefore $A_{\Delta} = \frac{A_{\square}}{4} = 100\%$ and therefor justifies $\zeta(1) = \frac{\pi^2}{4}$.

4.8.2 Longest root of a square area

The affected area $A_{\Delta} = 100\%$ gives the maximum value for the right angled side of the projection plane A_{\square} ; $a = \sqrt{2 \left(\frac{1}{4}\right)} = \sqrt{\frac{1}{2}} = \sqrt{2}^{-1}$. The hypotenuse from $a = \sqrt{2}^{-1}$ to $b = \sqrt{2}^{-1}$ is off course $c = a\sqrt{2} = 1$, the hypotenuse of

the mathematical universe $A_{\square} = \pi^2$. Longer lines that represent the root of a square area, do not exist in our mathematical universe. Further in this chapter a connection is made between this longest line and Planck's constant, $\hbar \approx \sqrt{\frac{\sqrt{\pi^2}\sqrt{2}}{4}}2\pi \approx 6.621895274$. Longer lines representing the root of a square area would imply that the count of elements $\lim_{n \rightarrow \infty} T_n \rightarrow \#n \in \mathbb{N} > \infty$, which is nonsensical. The maximum right angled side value for the affected area projection is $\lim_{n \rightarrow \infty} T_n \rightarrow A_{\Delta} = \frac{1}{2} \rightarrow a = \sqrt{2A_{\Delta}}\sqrt{2} = \sqrt{2}^{-1} \approx 0.707$.

Continuing the cycle brings us at ratio $\frac{6^2=36}{6}A_{\square} \rightarrow \frac{6^3=216}{9}A_{\Delta}$ or $6A_{\square} \rightarrow 24A_{\Delta}$ for a total affected area of $\frac{A_{\Delta}}{A_{\square}} = \frac{6}{24} = \frac{1}{4}A_{\square}$, the ratio stays the same $\frac{1}{4}$ ad infinitum.

$$T_{n=1} \rightarrow a = \sqrt{2 \left(\frac{T_n}{4n^2} \right)} = \sqrt{2}^{-1} \quad (4.7)$$

This seems to confine us to an infinite cycle during which only $\zeta(2)$, and by completing the pattern $\zeta(1)$, play a roll within the bounds of the infinite series of $\lim_{n \rightarrow \infty} \rightarrow T_n \rightarrow \#n \in \mathbb{N}$.

4.9 Volume independent of number

The maximum size of the right angled side is $a = \sqrt{2}^{-1}$. In the limit $\lim_{n \rightarrow \infty} \rightarrow T_n \rightarrow \#n \in \mathbb{N}$ the right angled sides contain each $\#n \in \mathbb{N}$, but also the hypotenuse $c = \#n \in \mathbb{N}$ (see subsection 4.5, Triangular projection to surface area). All 3 sides count $\#n \in \mathbb{N}$ elements of equal area. Application of the multiplication factor $\sqrt{2}$ to account for “absolute size” measured over the 45° hypotenuse makes no sense, this because in the limit both the straight angled sides and the hypotenuse consist of an equal number of dimensionless points and therefor represent lines of equal length, i.e. forming a distorted equilateral triangle.

There is a limit beyond $\lim_{n \rightarrow \infty} \rightarrow T_n$, out of reach for the window provided by T_n , see table 4.2 - 'Projection plane range for all s'. There for $s=2$ we find that $\sqrt{2 \times \frac{1}{6}} = \sqrt{\frac{2}{3}} = 0.5773502692$ and we know that the limit for the triangular projection is: $a = \sqrt{2 \times \frac{1}{8}} = 0.5$ i.e. the length of triangular plane A_{Δ} sides a and b , effectively the lower limit reached by the triangular projection. For all $\zeta(s > 2)$ the values for $a = \sqrt{2A}$ overshoot the lower limit $\lim_{n \rightarrow \infty} T_n \rightarrow a = 0.5 \rightarrow A_{\square} = \frac{1}{8}$ e.g. $\zeta(3) \rightarrow \sqrt{2 \times \frac{1}{8.210596}} = 0.4935460224 \rightarrow \frac{A_{\Delta}}{A_{\square}} = \frac{1}{8.210596}$. This can be understood as a function of volume, $\frac{1}{8}$ affected area as limit

implies the reduction of a volume by cutting its radius in half, $V_1 \times \frac{1}{8} = V_0$. To find values in the range $\frac{\pi^2}{8.210596} \rightarrow \frac{1}{8.210596} < \frac{1}{8}$ must, by completing the pattern, imply this fraction is addressing a volume that is part of a secondary cycle, one that further reduces to $V_0 \times \frac{1}{8} = V_{-1} = \left(\frac{1}{8}\right)^2 = \frac{1}{64}$. However, in the limit the current cycle resets numerically back to the start of infinity, see eq.4.7. This occurs because, as hypothesized, the frame of reference presented by the zeta function consists of a static numerical pattern of affected surface area at the point of equilibrium $\zeta(2) = \frac{\pi^2}{6}$.

4.10 Outside the limit

Not all hypotenuses are created equal. All values $\zeta(s) \forall s (1 < s \leq 2)$ result in $a = \sqrt{2A} \geq 0.5$, i.e. the resulting hypotenuse is $(\sqrt{2}^{-1} \leq a\sqrt{2} \leq 1)$. These values represent the complete range of the triangular projection cycle (fig. 4.6). The limit for the triangular projection in A_Δ , $c \geq \sqrt{2}^{-1}$, is geometrically hard coded by the premise that the triangular projection has to be a grid of n^2 overlay-ed on A_Δ , such that it completely fills quadrant III of the projection plane A_\square . Figure 4.6 depicts a shaded area between the

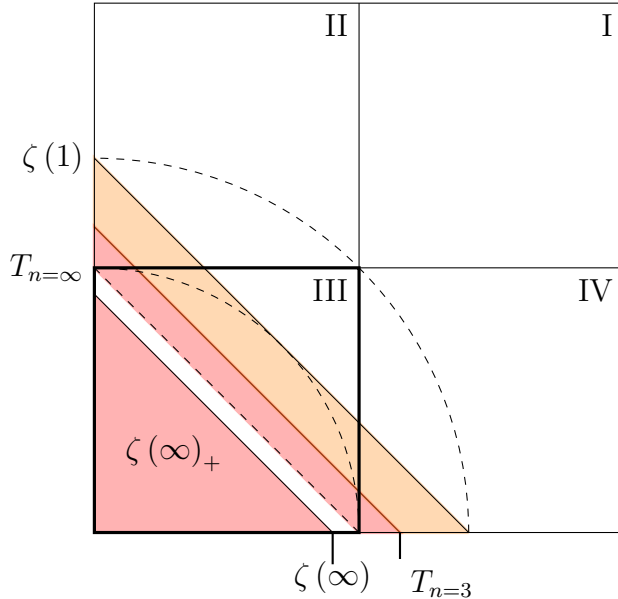


Figure 4.7: Projection plane bulk

hypotenuse at $\zeta(N)$ and the hypotenuse at $T_{n=3} \rightarrow a = 0.5$, this is the projection domain for $\zeta(s > 2)$. The first value that projects outside the cycle

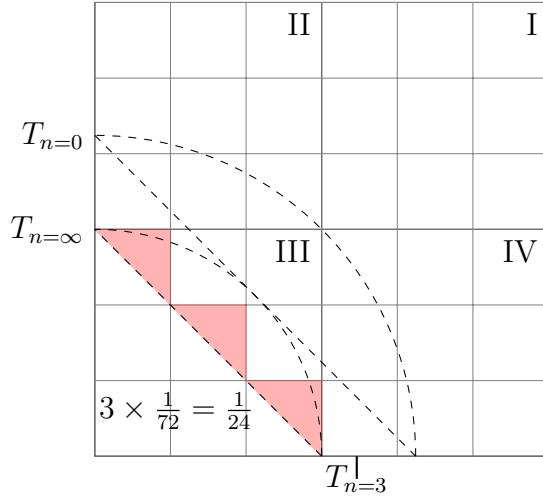


Figure 4.8: The triangular plane bulk

is $\zeta(3) \rightarrow \sqrt{2 \times \frac{1}{8.210596}} = 0.4935460224$ and the last $\zeta(\infty) \rightarrow \sqrt{2 \times \frac{1}{\pi^2}} = \frac{1}{\pi}\sqrt{2} = 0.45015815814$. For values of $a = \sqrt{2A} < 0.5 \rightarrow a^2 < \frac{A_{\square}}{4}$ the resulting affected surface area consists of insufficient dimensionless points to generate a triangular grid of $\frac{N}{2}(N+1)$.

For all function values $\zeta(s)$ an associated surface area exists, each of those have right angled sides $a = \sqrt{2A}$ in the projection plane. However, lacking a reference frame like the projection/triangular plane assembly would make it impossible to say if this surface area is defined by a mapping to T_n , or falls outside the static bounds of the phase shift. In such case all hypotenuses do seem to be created equal.

This is not a trivial observation, because it brings us to the Riemann hypothesis, can it simply be that a proof for the Riemann hypothesis, ‘All non trivial zeros have real part one half’, is unobtainable because the tool of complex analysis simply lacks the proper reference frame to distinguish between classes of non trivial zeros? In chapter 7 a proposition to answer this question will be formulated.

4.10.1 Zeta at the limit, the surface asymptote

The range for the triangular numbers is $a = [\sqrt{2^{-1}}, 0.5]$, in this range only the values for $\zeta(1)$ and $\zeta(2)$ occur as discrete projection of $\lim_{n \rightarrow \infty} T_n$:

$$\zeta(2) \rightarrow a = \sqrt{2 \times \frac{1}{6}} = 0.57735026922 \rightarrow (\sqrt{2^{-1}} \geq a \geq 0.5) \quad (4.8)$$

The values for $\zeta(s > 2)$ project to quadrant III of the projection plane A_{\square} , but not in its triangular plane A_{Δ} identity because the value is out of bounds for $a = [\sqrt{2}^{-1}, 0.5]$. However, the argument for scale invariance still applies, quadrant III scales to $A_{\square} = \pi^2$. Figure 4.7 depicts the shaded triangle $\zeta(\infty)_+$. By $\lim_{s \rightarrow \infty} a = \sqrt{2A} \geq \frac{\sqrt{2}}{\pi}$ the shaded area $\zeta(\infty)_+$ lays beyond $\lim_{s \rightarrow \infty} \zeta(s)$. Completing the pattern analogues to $\zeta(2) \rightarrow a =$

$$\sqrt{2A} = \sqrt{2 \times \left(\frac{\pi^2}{6}\right)} \rightarrow \sqrt{2 \times \left(\frac{1}{6}\right)} \text{ gives } \zeta(\infty) \rightarrow a = \sqrt{2 \times \left(\frac{[\pi^2]}{\pi^2}\right)} \rightarrow a = \sqrt{2 \times \left(\frac{1}{\pi^2}\right)} = \frac{1}{\pi}\sqrt{2} = 0.4501581581.$$

Then follows $r_q = \frac{0.5}{a} = (0.900316316)^{-1}$. The associated radius for the sphere is $r_x = \frac{r_q}{\sqrt{p\Delta(\infty)^{-1}}} = 1.136630193$ and yields a surface area of $SA = 4\pi(r_x)^2 = \pi^2 \left(\frac{\pi^2}{6}\right)$ (see table 4.2). A factor $\frac{\pi^2}{6}$ bigger than our universe, the projection plane. Because some collapsing surface area is assumed, the scale factor $\frac{A_{\Delta}}{A_{\square}} = \frac{1}{4}$ needs to be observed.

The algorithm produces for $s=1$, $\zeta(1) = \frac{\pi^2}{4} \rightarrow SA = \frac{6}{9}\pi^2 = 4 \times \frac{\pi^2}{6}$. For $s=2$, $\zeta(2) = \frac{\pi^2}{6} \rightarrow SA = \pi^2 = 4 \times \frac{\pi^2}{4}$.

This means that the initial configuration of $\zeta(1)$ is also the final configuration of $\zeta(2)$, this is sufficient to describe the recursion in terms of the phase shift with exclusion of the values for $s > 2$.

Likewise the result for $\zeta(\infty) \rightarrow SA = \frac{\pi^2}{6}(\pi^2)$ is a factor 4 too big. Therefore $SA = \frac{1}{4} \left(\pi^2 \left(\frac{\pi^2}{6}\right)\right)$ scales to the universe. Plugging in this value produces

a surface area $SA = \frac{1}{4} \times \frac{\left(\pi^2 \left(\frac{\pi^2}{6}\right)\right)}{\pi^2} = \frac{\pi^2}{24}$. This is a significant result because $3 \times \frac{1}{72} = \frac{1}{24}$ is exact the area that exceeds the hypotenuse of the triangular plane for $\zeta(2)$, see figure 4.8, page 38. The hypotenuse of the triangular plane is off course the limit $\lim_{n \rightarrow \infty} T_n$. The value $SA = \frac{\pi^2}{24}$ remaining after $\lim_{s \rightarrow \infty} \zeta(s)$ is exact the value $\zeta(2) = \frac{\pi^2}{6}$ that correlates with a 4-fold reduction in surface area by recursive application of $\zeta(2)$.

Herein is the proof that $\lim_{s \rightarrow \infty} \zeta(s)$ is fully contained within the limits of $\lim_{n \rightarrow \infty} T_n$, al be it that $\zeta(s) \forall s \in (2, \infty) \ni T_n$. The Spatial ratio $S_{ratio} = \frac{1}{4}$, see equation 2.17 on page 11, only holds for the infinite sum/product $\zeta(2) = \frac{\pi^2}{6}$.

4.10.2 Equilibrium at SA=V, Planck

The value $\zeta(1) = \sum_n n^{-1} = \frac{\pi^2}{4}$ completes the pattern for $\zeta(s) \forall s \in \mathbb{N}$ and seems sufficiently justified. Crucial is that only $\zeta(2)$ maps to a discrete solution in T_n . Also does $\zeta(1)$ but this is by completing the pattern. What

is special about $\zeta(2) = \frac{\pi^2}{6}$ operating on a unit surface area π^2 is the ratio $(\frac{1}{8} + \frac{1}{24} = \frac{1}{6})$. Herein we find a profound key to the solution, one that is of significance in connecting the dots between $\zeta(2)$ and physics.

The transition $\pi^2 \rightarrow \frac{\pi^2}{8}$ can be interpreted as a function of volume but $\zeta(2)$ is expressed as a function of (surface) area. At the function value of $\zeta(2)$ a unique point of equilibrium occurs that sits at the source of the emergence of Planck's constant $h = 6.62607015 \times 10^{-34} \text{ J.s.}$. The projection plane exposes a point of equilibrium between volume and surface area, $\zeta(2)$, at which Surface Area and Volume can be recognized as expressions of one underlying principle. Table 4.3 'The base of Planck's constant', gives a break down for the formulae of surface area and volume.

Table 4.3: The base of Planck's constant

SA	V	
$4\pi r^2$	$\frac{4}{3}\pi r^3$	$/\pi$
$4r^2$	$\frac{4}{3}r^3$	$/4$
r^2	$\frac{1}{3}r^3$	$/r^2$
1	$\frac{1}{3}r^1$	x^2
$SA = 1$	$V = \frac{1}{9}$	$SA \propto (\frac{1}{8} + \frac{1}{24}) \propto V$

For every unit surface area $SA = 1$, there is $V = \frac{1}{9}$ unit of volume. The ratio is defined as $T_h \stackrel{def}{=} 1 + \frac{1}{9} = 0.9^{-1} = 1.11111\dots$ from which Planck's constant $h = 6.62607015 \times 10^{-34} \text{ J.s.}$ is approached by $h_* = \sqrt{T_h} \times 2\pi \sim h \rightarrow \Delta h \approx \frac{2201}{2200}$. The equilibrium follows from the fractal argument for zeta.

4.11 The fractal argument for zeta

Figure 4.9 on page 41 depicts a recursive regression of the triangular plane, quadrant III, as found in the configuration for $\zeta(1) \rightarrow SA \propto \frac{6}{9}\pi^2$. The fractal iteration in the lower left cell of quadrant III occupies $\frac{1}{6}$ of the affected area of quadrant III. If we assume the recursive product $\prod_n \zeta(2)^n = \{1, \frac{1}{6}, \frac{1}{36}, \frac{1}{216}, \frac{1}{1296}, \dots\}$ then for each iteration we find that the ratio affected area $\zeta(2) = \frac{\pi^2}{6}$ must have the scale invariant ratio $SA = \pi^2$, i.e. represent the universe of the projection plane A_{\square} as a whole. At the same time we find that a relation exist between $\zeta(s) \forall s \in \{1, 2, \infty\}$. There is an equivalence between the calculated SA value of $\zeta(s)$ and the function value of $\zeta(s+1)$,

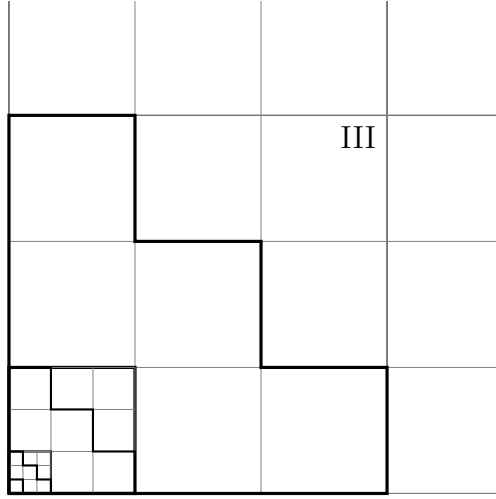


Figure 4.9: Projection plane regression

see eq. 4.9.

Tabel 4.2, page 32

$$\left\{ \frac{\pi^2}{4} \times \frac{8}{3} = \frac{6}{9} \pi^2 \right\} \xrightarrow{SA=A} \left\{ \frac{\pi^2}{6} \times 6 = \pi^2 \right\} \xrightarrow{SA=A} \left\{ \frac{\pi^2}{\pi^2} \times \frac{\pi^2}{6} (\pi^2) = \frac{\pi^2}{6} (\pi^2) \right\}$$

Unit $\pi^2 = 1$

$$\left\{ \frac{1}{4} \times \frac{8}{3} = \frac{6}{9} (1) \right\} \xrightarrow{SA=A} \left\{ \frac{1}{6} \times 6 = 1 \right\} \xrightarrow{SA=A} \left\{ \frac{1}{1} \times \frac{1}{6} (1) = \frac{1}{6} (1) \right\}$$

Scale invariant : $4 \times A_\Delta = A_\square$

$$\left\{ A_\square \times \frac{1}{6} = SA \right\} \xrightarrow{SA=A} \left\{ \frac{A_\square}{6} \times 6 = SA \right\} \xrightarrow{SA=A} \left\{ A_\square \times \frac{1}{6} = SA \right\}$$

(4.9)

This results in a regression pattern where the values appear to project in a region $\frac{A_\Delta}{9}$ of the universe measuring $\frac{9}{9} = 1\frac{1}{8}$. This proportion can be interpreted as a volume wrapped by a (continuously reducing) surface area.

Table 4.4: Zeta, the SA/Volume equilibrium

s	$\frac{1}{4} \propto A_{\square}$		$\frac{6}{9} \propto A_{\triangle}$		$ratio \propto \zeta(2)$
	# \square cells A_{\square}	# \blacksquare cells A_{\blacksquare}	# \triangle cells A_{\triangle}	# \blacktriangle cells A_{\blacktriangle}	
0	$6^0 = 1$	$\frac{3^0}{6^0} = 1$	$3^0 = 1$	$\frac{6}{9} \times 3^0 = \frac{6}{9}$	$\frac{6^0}{6} = \frac{9}{6}$
1	$6^1 = 6$	$\frac{3^1}{6^1} = \frac{1}{2}$	$3^1 = 3$	$\frac{6}{9} \times 3^1 = 2$	$\frac{6^1}{6^2} = 3$
2★	$6^2 = 36$	$\frac{3^2}{6^2} = \frac{1}{4}$	$3^2 = 9$	$\frac{6}{9} \times 3^2 = 6$ ★	$\frac{6^2}{6^3} = 6$ ★
3	$6^3 = 216$	$\frac{3^3}{6^3} = \frac{1}{8}$	$3^3 = 27$	$\frac{6}{9} \times 3^3 = 18$	$\frac{6^3}{6^4} = 12$
4	$6^4 = 1296$	$\frac{3^4}{6^4} = \frac{1}{16}$	$3^4 = 81$	$\frac{6}{9} \times 3^4 = 54$	$\frac{6^4}{6^5} = 24$
5	$6^5 = 7776$	$\frac{3^5}{6^5} = \frac{1}{32}$	$3^5 = 243$	$\frac{6}{9} \times 3^5 = 162$	$\frac{6^5}{6^6} = 48$

The function $\zeta(2) = \frac{\pi^2}{6}$ represents the scale invariant ratio of affected surface area and/or volume, where volume is defined by $V = \frac{1}{6}\zeta(2)$. Realizing that each second iteration results in $SA = \frac{1}{9}$ of the initial $SA = \pi^2$ it is of course not discernible whether there exist such thing as an even or odd cycle, for all intents and purposes $SA = V$. What must be true is that each iterative step results in a scale invariant projection of the universe that is expressed by $\zeta(2) = \frac{\pi^2}{6}$ as fraction of surface area. If $\pi^2 = 1$ then we find that volume and surface area are interchangeable, see table 4.3) $T_h = 0.9^{-1} = 1 + \frac{1}{9}$ and table 4.4 for $s = 2$:

$$V = \left(\sqrt{\frac{\pi^2}{4\pi}} \right)^3 \times \frac{4}{3}\pi \approx 2.915569721 \rightarrow V = \left(\sqrt{\frac{1}{4}} \right)^3 \times \frac{4}{3} = \frac{1}{6} \quad (4.10)$$

$$\zeta(2)^2 \approx 2.705808084 \rightarrow V^2 = \left(\frac{1}{6} \right)^2 = \frac{9^{-1}}{4} = \frac{T_h}{40}$$

This is a fractal, A_{\square} is to $\zeta(2)$ as $\zeta(2)$ is to $\frac{1}{9}A_{\triangle}$ (fig.4.9), at which point a equilibrium exists between surface area and volume. Surface area is expressed as

$$\begin{aligned} \zeta(2)^n \rightarrow SA &= \frac{A_{\square}}{6^n} = \left(\frac{1}{6} \right)^n \\ &= \left\{ 1, \frac{1}{6}, \frac{1}{36}, \frac{1}{216}, \frac{1}{1296}, \dots \right\} \end{aligned} \quad (4.11)$$

and volume as

$$\begin{aligned}\zeta(2)^n \rightarrow V &= \frac{1}{4} \left(\frac{A_{\square}}{T_h} \right) = \frac{A_{\square}}{6^{n+1}} \\ &= \left\{ \frac{1}{6}, \frac{1}{36}, \frac{1}{216}, \frac{1}{1296}, \dots \right\}\end{aligned}\tag{4.12}$$

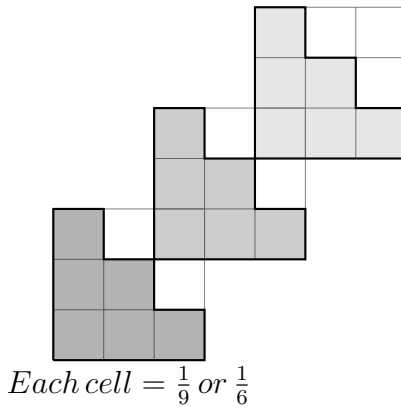


Figure 4.10: Fractal stack

The pattern is self-similar in regression (fig. 4.9) where each iteration is the application of $\zeta(2)^{n+1}$ on the area representing the scale invariant universe A_{square} . In figure 4.10, page 43 the same regression is depicted, only this time the scale invariance is preserved where each regressive step is proportionally equal to the former and the overlap is $\frac{1}{9}$ for the completed square. This stacking will lead to exposing the connection between the zeta zero's and prime numbers. The base of Planck's constant $h = 6.62607015 \times 10^{-34} J.s.$, (table 4.3) $T_h = 0.9^{-1} = 1 + \frac{1}{9}$ is the ratio between the start of the cycle $\frac{9}{9} = 1$, and the end of the cycle $\frac{1}{9}$ expressing the depletion of volume as function of reduced surface area. In fig. 4.9 we observe that with each successive iteration the projection plane A_{\square} repeats with $\frac{\pi^2}{9} \rightarrow 4$ cells of which the bottom left cell projects A_{Δ} , the proportional size regresses as

$$\begin{aligned}A_{\square n} = 1 \rightarrow A_{\square n+1} &= \frac{4}{9} = \frac{1}{10} (4T_h) = 0.444\dots \\ \Delta \lim_{n \rightarrow \infty} \rightarrow \frac{(3^n)^2}{(3^n)^2 - 1} &= \left\{ \frac{9}{8}, \frac{81}{80}, \frac{729}{728}, \frac{6561}{6560}, \frac{59049}{59048}, \dots \right\} = 1 \rightarrow \Delta - \frac{1}{8}\end{aligned}\tag{4.13}$$

Chapter 5

Chords

5.1 Hexagonal chords and Planck

A hexagonal chord has the same dimensions as the radius for the circle it inscribes, $a = \cos\left(\frac{\pi}{3}\right) = \frac{1}{2}$, $b = \sin\left(\frac{\pi}{3}\right) \rightarrow c = \sqrt{a^2 + b^2} = 1$ (figure 3.4, page 23). In table 4.1, page 31, we find $x \rightarrow a$ and $y \rightarrow r_q$, where $y \rightarrow r_q$ by the closed formula:

$$r_q = \forall n \sqrt{\frac{n}{n+1}} \rightarrow \left\{ \sqrt{\frac{1}{2}}, \sqrt{\frac{2}{3}}, \sqrt{\frac{3}{4}}, \dots \right\} \quad (5.1)$$

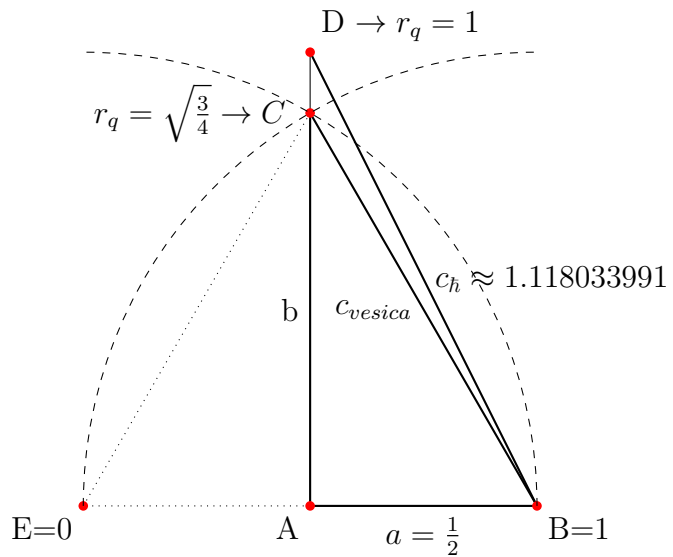


Figure 5.1: Hexagonal chord versus \hbar

Figure 5.1, page 45, shows two chords:

1. Chord c_{vesica} is a hexagonal chord and related to the triangular projection by the proportion of side b . In table 4.1 we find $n = 3 \rightarrow r_q = \left| \sqrt{\frac{3}{4}} \right|$. However, because here we find $a \neq \frac{1}{2} \rightarrow a = 0.5773502692$, the tuple for $n = 3$ does not represent $\triangle ABC$. Calculating \overline{BC} with this value produces $\sqrt{(a)^2 + (r_q)^2} = 1.040833 \neq 1$. Side b is interesting because the absolute value $r_q = \left| \sqrt{\frac{3}{4}} \right|$ conforms to the scale invariant value $b = \sin(\frac{\pi}{3})$ present in $90^\circ 60^\circ 30^\circ$ hexagonal triangles.
2. $\triangle ABD$, with chord c_h , has side b extended to $b = 1$. This triangle matches the last tuple in the table, but $\triangle ABD$ does not conform to a $90^\circ 60^\circ 30^\circ$ triangle. See table 4.1 on page 31, where we find $n = \infty \rightarrow r_q = 1$ and $a = 0.5 \rightarrow \cos(\frac{\pi}{3}) = 0.5$.

5.2 Unity chords

In the following we will abuse the Pythagorean theorem to suite our needs. The experimentally deduced value of Planck's constant is $h = 6.62607015 \times 10^{-34} J.s.$. Observe that if we counter intuitively apply the Pythagoras theo-

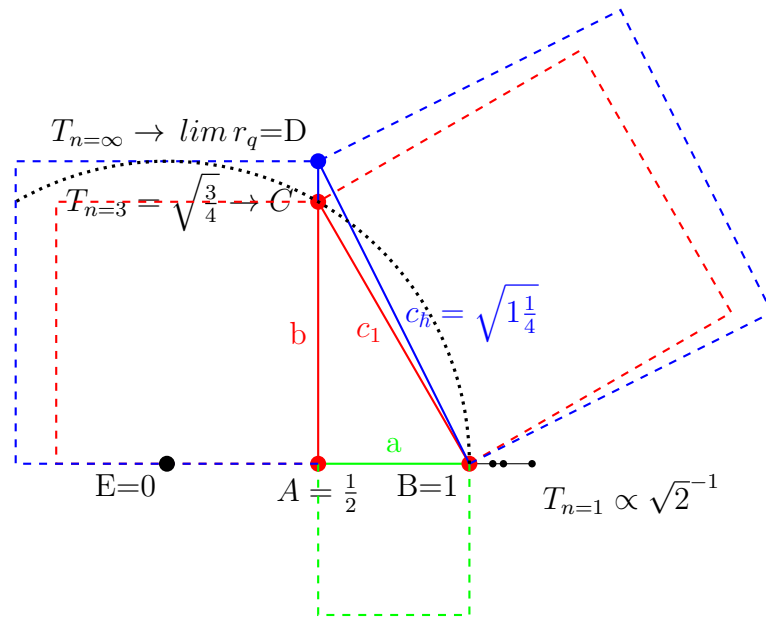


Figure 5.2: Planck base - Unity chord

rem by assuming \overline{BC} as if \overline{AC} , then any $\angle ABC = \frac{\pi}{3} = 60^\circ$ right angled triangle has a ratio $\sqrt{1\frac{1}{4}} = \frac{\sqrt{5}}{2}$ derived by $c_h = \sqrt{(BC)^2 + (AB)^2} = \sqrt{1^2 + 0.5^2} = \sqrt{1\frac{1}{4}} = \frac{\sqrt{5}}{2}$. We find Planck's constant by: $h = \frac{\sqrt{c_h} \times 2\pi}{\sqrt{q\pi}} \approx 6.626091764\dots \rightarrow \Delta h \sim 2.1728 \times 10^{-5}$. This is not just a mathematical coincidence and can be placed in a rigid meaningful context labeled 'Unity chords' which justifies the abuse of the Pythagorean theorem. Equation 5.2 on page 47 gives the associated values as found in table 4.1, page 31.

$$\begin{aligned}\overline{BC}^2 + \overline{AB}^2 &= 1\frac{1}{4} \rightarrow c_h = \sqrt{(BC)^2 + (AB)^2} \\ n = 4 \rightarrow a &= \left[\sqrt{2}^{-1}, \frac{1}{2} \times \left(\sqrt{\frac{4}{5}} \right)^{-1} \right] \rightarrow \left[\sqrt{2}^{-1}, \sqrt{\frac{10}{32}} \right] \\ n = 3 \rightarrow r_q &= \left[\sqrt{\frac{3}{4}}, 1 \right]\end{aligned}\quad (5.2)$$

In figure 5.2 on page 46, this principle "Unity chord" is shown as a function of area for T_n where $n \in \{3, \infty\}$. The extended part of side b, $\overline{CD} = \Delta\zeta(2)$ starts at $n = 3 \rightarrow r_q = \sqrt{\frac{3}{4}}$. Before the extension the area $A_{\overline{AC}} = \overline{AC}^2 = \sqrt{\frac{3}{4}}^2 = \sin\left(\frac{\pi}{3}\right)^2 = \frac{3}{4}$. Then after extension $A_{\overline{AD}} = \overline{AD}^2 = 1^2 = \frac{4}{4}$. The square area in figure 5.2 defined by $A_{\overline{AD}} = \frac{4}{5}$ of the square area defined by $A_{\overline{BD}}$. Extending side b from $\overline{AC} = \sqrt{\frac{3}{4}} \rightarrow \overline{AD} = 1$ has the net effect *Area* $\frac{3}{4} : 1$, a growth factor of $1\frac{1}{3}$. That same extension for side c from $\overline{BC} = 1 \rightarrow \overline{BD} = \sqrt{1^2 + (\frac{1}{2})^2}$ has the net effect *Area* $\frac{3}{4} : 1$, a growth factor of $1\frac{1}{4}$.

The unity chords are defined by the hypotenuses in a specific range and the associated right angled triangles are *all assumed to represent a distorted representation of a hexagonal triangle, $\angle 60^\circ 30^\circ 90^\circ$* . In figure 5.2 the projection of $T_n \rightarrow a$ for $n \in \{1, 2, 3\}$ (the three dots to the right of coordinate 'B') seem not to fit the schema. This figure 5.2 is not the whole picture. The chords on the x-axis project in the range $a \rightarrow [\sqrt{2}^{-1}, \frac{1}{2}]$ while in figure 5.2 they all radiate from $\angle ABC$. This is however not the case in the triangular projection, see table 4.1, the values for the y-axis slide down to up, and the values for the x-axis slide right to left. This results, plugging in the values a and r_q for each tuple $\angle\theta = \tan\left(\frac{r_q}{a}\right)$, in chords angled between 45° and 63.43° varying in length between $\sqrt{0.5 + 0.5} = 1$ to $\sqrt{1 + 0.25} \approx \hbar^2$.

5.2.1 Like a ladder up the wall

The triangular projection (tbl. 4.1) for $n = \infty$ lists the values $a = \sqrt{2A} = 0.5$ and $r_q = \frac{0.5}{a} = 1$. In fig. 5.4 two ranges are projected.

$$1. \text{ Range x-axis } a \rightarrow [\sqrt{2}^{-1}, 0.5]$$

$$2. \text{ Range y-axis } r_q \rightarrow [\sqrt{2}^{-1}, 1]$$

This sliding ratio defines a range for modeling the triangular projection as a succession of chord's ranging between length $\sqrt{(\sqrt{2}^{-1})^2 + (\sqrt{2}^{-1})^2} = 1$ and $\sqrt{(\frac{1}{2})^2 + 1^2} = \frac{\sqrt{5}}{2}$. Figure 5.3 shows both extremes and their intersection at $\sim 54.74^\circ$. The gradient shows the chord density for $n \rightarrow [1, \dots, 80]$ and the migration of the intersection point along the arc, which in the limit, approaches 90° .

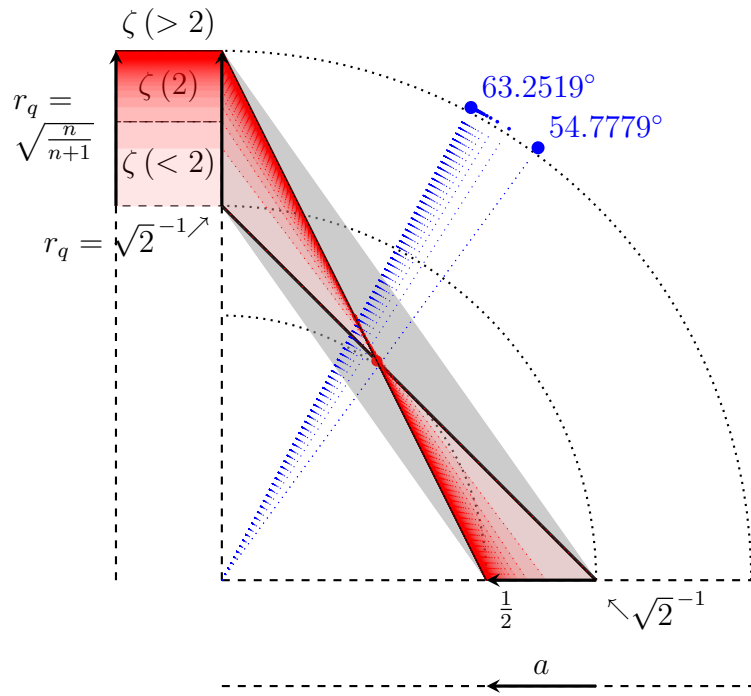
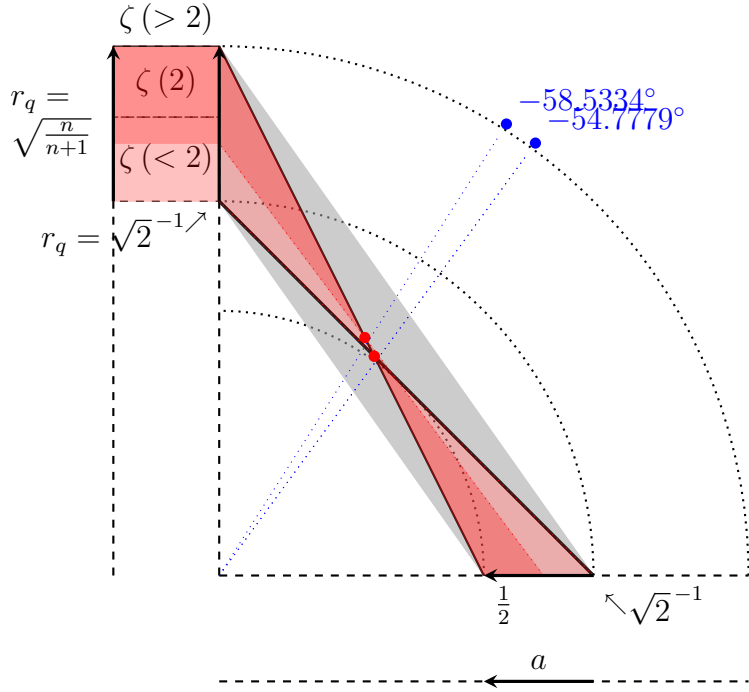


Figure 5.3: Triangular numbers - (a, R_q) chord density

Because we assume a distorted representation of a hexagonal triangle in each case, geometrically the unity chords must have $\angle ABC = \frac{\pi}{3} = 60^\circ$ and be part of right angled triangles with a hypotenuse $\sqrt{1\frac{1}{4}} = \frac{\sqrt{5}}{2}$, by counter

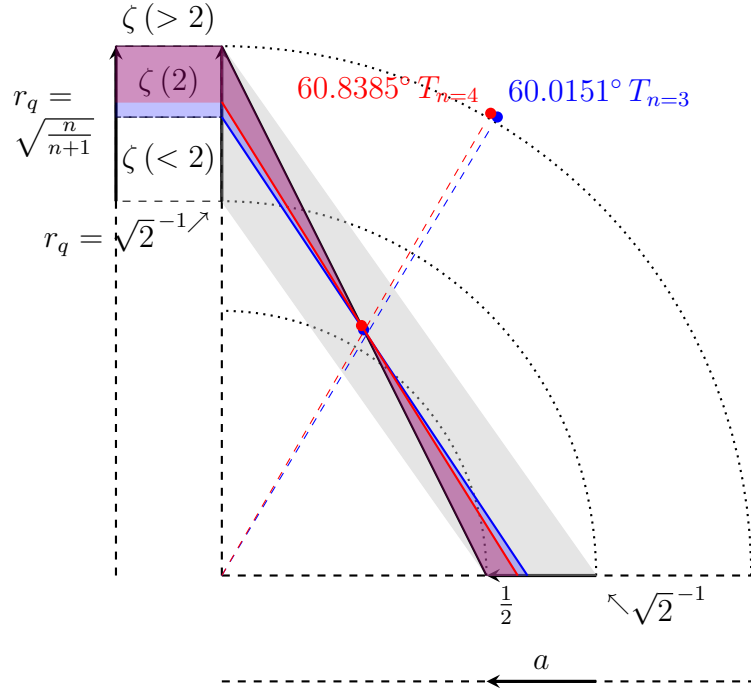
Figure 5.4: Plot Triangular $T_{n=1}$ and $T_{n=2}$

intuitively application of the Pythagoras theorem by treating \overline{BC} as if \overline{AC} of course. The range in which the unity chords project is wedged between $(a = \sqrt{2}^{-1}, r_q = \sqrt{2}^{-1}) \rightarrow T_n = 1$ and $(a = \frac{1}{2}, r_q = 1) \rightarrow T_{n=\infty}$. Observe that the only natural occurring hexagonal chord wedged between $a = 0.5$ and $r_q = \sqrt{\frac{3}{4}}$ does not occur in the triangular projection as discrete interval, see table 4.1. Note that the area enclosed for all tuples in table 4.1 comes to $\forall n \rightarrow \frac{a \times r_q}{2} = \frac{1}{4}$. An infinite set of coordinates in between can accommodate such a chord, and therefore unity chords must exist such that;

$$\forall x \in \mathbb{R} \exists U_{chord} \rightarrow y = \sqrt{\frac{3}{4}} \leq r_q \leq 1 \text{ and } x = \frac{0.5}{y}$$

For any pair of coordinates (a, r_q) a hypotenuse exists, but only those that occur in the triangular projection, see table 4.1 on page 31 conform to the spatial ratio $S_{ratio} = \frac{V_{init}}{\left(\frac{V_{end}}{r_{end}}\right)} = \frac{1}{4}$, see equation 2.17, page 11.

The triangular projection defines a discrete point of equilibrium between Cartesian area and spherical surface where $A = \frac{T_n}{4n^2} \rightarrow \frac{a}{b}\pi^2$ and $A = \frac{a \times r_q}{2} = \frac{1}{4}$. One observation is the area of the 1 by 2 rectangle and its diagonal $\sqrt{5}$. Let

Figure 5.5: Planck base - Transition $T_{n=3}$ to $T_{n=4}$

$c = \frac{\sqrt{5}}{2} \approx \hbar^2$ be the circumference of a sphere. Then the surface area of that sphere is $r = \frac{c}{2\pi} \rightarrow SA = 4\pi r^2 = \frac{4}{10^{99}} = (2.5 \leftrightarrow)^{-1}$. In this reference frame we have an infinite series of chords $c \propto \sqrt{1\frac{1}{4}} = \frac{\sqrt{5}}{2}$, each marking an iterative step in a cycle projecting the triangular numbers, of which the third iteration marks of the conclusion of $\zeta(2) = \frac{\pi^2}{6}$, see figure 4.1, page 25.

5.3 Root 2 equilibrium

The ratio $\sqrt{1\frac{1}{4}} = \frac{\sqrt{5}}{2}$ means that for every hexagonal chord the proportionality to Planck's constant holds. Which makes this occurrence of Planck's constant kind of a banality. This will be proven a feature, not a bug. In context of a $\sqrt{2}^{-1}$ power series we find quite a unique occurrence for the unity chord. In figure 5.6 the tuple for n=2 in table 5.1, page 52, is depicted. From the triangles $\triangle ABC$ and $\triangle DBE$, $\triangle ABC$ does not occur in table 4.1 as a triangular projection, but we used it in figures 5.1, page 45 and 5.2, page 46. Now in figure 5.6 the "Unity" aspect that integrates triangle $\triangle ABC$ in the set of periodic chords as depicted in figure 5.2 comes to light by the association with triangle $\triangle DBE$. Here the first thing to take note

of, is that both triangles in this configuration are indeed hexagonal. The angles $\angle CAB$ and $\angle EDB$ are both 90° and $\angle ABC$ and $\angle EBD$ are both 60° . Further, the point of origin for both triangles is B. It is easy to see that by decreasing segment \overline{CE} , labeled $\Delta\zeta(2)$, will map both triangles in one to one correspondence. We recognize the chord \overline{BC} in a somewhat peculiar place for a hexagonal chord in figure 5.2, page 46, namely it is the chord h_{init} between $r_q = \sqrt{2}^{-1}$ and $a = \sqrt{2}^{-1}$ that corresponds with the hypotenuse in figure 4.6, page 34, at the extend of $\zeta(1)$. This indicates that triangle $\angle ABC$ is the end phase of a cycle, in this model the hypotenuse at $\zeta(1)$ indicates a 4-fold decrement in surface area. The chord \overline{BE} on the other hand does also associate with the end of a cycle, it is the limit of the triangular cycle. See $n = \infty$ in table 4.1, page 31. The conclusion must be that both \overline{BC} and \overline{BE} are in fact one and the same, they stand back to back, occupy the same space, are merely separated by choice of perspective. One way of looking at it is to assume that both triangles $\triangle ABC$ and $\triangle DBC$ are conjoined along their chords and model a spherical triangle as depicted in figure 5.7, page 54. Together they can be envisioned to form $\triangle A'B'C'$, but will encompass in fact the entire surface area because of the scale invariant property of volume. This in turn will clarify again the surface area vs volume equilibrium as shown in figure 4.9, page 41. The associated surface area ratio is $SA_{\infty h} = (\sqrt{2}^{-1} \times \frac{\sqrt{5}}{2})^2 = (1.6)^{-1} \rightarrow \Delta \frac{1+\sqrt{5}}{2} \sim \varphi^2$ And the surface area of the final state confronts us with a beautiful factor 10,

$$\begin{aligned} SA_{c=1} &= (\sqrt{2}^{-1} \times 1)^2 \times 4\pi = 2\pi \\ &\rightarrow (SA_{\infty h})^{-1} \times SA_{c=1} = 10 \varphi \end{aligned} \tag{5.3}$$

5.4 Curvature and the plane

The ordering of triangular numbers in the triangular plane raises the question what a number precisely entails. In the limit $\lim_{n \rightarrow \infty} T_n \rightarrow a = \sqrt{2A}$ consists of all natural numbers counting of all triangular numbers. This is also the case for the hypotenuse c which has exactly as many members as the sides a and b by nature of their arrangement. This makes all sides of the triangle in count of represented numbers equally sized. We identified chords \overline{BC} and \overline{BE} as two expressions of one and the same chord (fig. 5.6) and the process in which segment \overline{CE} decreases until in the limit both triangles are in a one to one correspondence. The moment that the chords \overline{BC} and \overline{BE} merge into 1, numerically a equilateral triangle $\triangle ADE$ is realized where

Table 5.1: Hexagonal equilibrium

		a	$ b $	c	c_h	360°	$\pi \text{ rad}$
n	$(\sqrt{2})^{-n}$ $\rightarrow \sqrt{\frac{1}{2^n}}$	$(\sqrt{2})^{-n}$ $\rightarrow \sqrt{\frac{1}{2^n}}$	$\sqrt{\frac{3}{2^n}}$	$\sqrt{a^2 + b^2}$ $\rightarrow \sqrt{\frac{1}{2^n} + \frac{3}{2^n}}$	$\sqrt{a^2 + c^2}$ $a \times \sqrt{5}$	$\left(\frac{b_n}{b_2}\right) \cdot 60^\circ$	$\left(\frac{b_n}{b_2}\right) \cdot \left \sqrt{\frac{3}{4}}\right $
0	1	1	$\sqrt{\frac{3}{1}}$	$\sqrt{\frac{4}{1}}$	$1 \cdot \sqrt{5}$	120°	$\frac{2\pi}{3}$
1	0.70710...	$\sqrt{\frac{1}{2}}$	$\sqrt{\frac{3}{2}}$	$\sqrt{\frac{4}{2}}$	$\sqrt{\frac{1}{2}} \cdot \sqrt{5}$	84.8528°	$\frac{2\pi}{3 \times \sqrt{2}}$
2★	0.5	$\sqrt{\frac{1}{4}}$	$\sqrt{\frac{3}{4}}$	1	$\sqrt{\frac{1}{4}} \cdot \sqrt{5}$	60°	$\frac{2\pi}{6} \star$
3	0.35355...	$\sqrt{\frac{1}{8}}$	$\sqrt{\frac{3}{8}}$	$\sqrt{\frac{1}{2}}$	$\sqrt{\frac{1}{8}} \cdot \sqrt{5}$	42.4264°	$\frac{2\pi}{6 \times \sqrt{2}}$
4	0.25	$\sqrt{\frac{1}{16}}$	$\sqrt{\frac{3}{16}}$	$\sqrt{\frac{1}{4}}$	$\sqrt{\frac{1}{16}} \cdot \sqrt{5}$	30°	$\frac{2\pi}{12}$
5	0.17678...	$\sqrt{\frac{1}{32}}$	$\sqrt{\frac{3}{32}}$	$\sqrt{\frac{1}{8}}$	$\sqrt{\frac{1}{32}} \cdot \sqrt{5}$	21.2132°	$\frac{2\pi}{12 \times \sqrt{2}}$
6	0.125	$\sqrt{\frac{1}{64}}$	$\sqrt{\frac{3}{64}}$	$\sqrt{\frac{1}{16}}$	$\sqrt{\frac{1}{64}} \cdot \sqrt{5}$	15°	$\frac{2\pi}{24}$
7	0.08839...	$\sqrt{\frac{1}{128}}$	$\sqrt{\frac{3}{128}}$	$\sqrt{\frac{1}{32}}$	$\sqrt{\frac{1}{128}} \cdot \sqrt{5}$	10.6066°	$\frac{2\pi}{24 \times \sqrt{2}}$
8	0.0625	$\sqrt{\frac{1}{256}}$	$\sqrt{\frac{3}{256}}$	$\sqrt{\frac{1}{64}}$	$\sqrt{\frac{1}{256}} \cdot \sqrt{5}$	7.5°	$\frac{2\pi}{48}$
9	0.04419...	$\sqrt{\frac{1}{512}}$	$\sqrt{\frac{3}{512}}$	$\sqrt{\frac{1}{128}}$	$\sqrt{\frac{1}{512}} \cdot \sqrt{5}$	5.3033°	$\frac{2\pi}{48 \times \sqrt{2}}$
10	0.03125	$\sqrt{\frac{1}{1024}}$	$\sqrt{\frac{3}{1024}}$	$\sqrt{\frac{1}{256}}$	$\sqrt{\frac{1}{1024}} \cdot \sqrt{5}$	3.75°	$\frac{2\pi}{96}$
11	0.0221...	$\sqrt{\frac{1}{2048}}$	$\sqrt{\frac{3}{2048}}$	$\sqrt{\frac{1}{512}}$	$\sqrt{\frac{1}{2048}} \cdot \sqrt{5}$	2.6517°	$\frac{2\pi}{96 \times \sqrt{2}}$
12	0.015625	$\sqrt{\frac{1}{4096}}$	$\sqrt{\frac{3}{4096}}$	$\sqrt{\frac{1}{1024}}$	$\sqrt{\frac{1}{4096}} \cdot \sqrt{5}$	1.875°	$\frac{2\pi}{192}$
	$\star \rightarrow b = \sqrt{\frac{3}{4}} = \sin\left(\frac{\pi}{3}\right) \approx 0.8660254038$				$\star \rightarrow (P\Delta)^{-1} \looparrowright$		

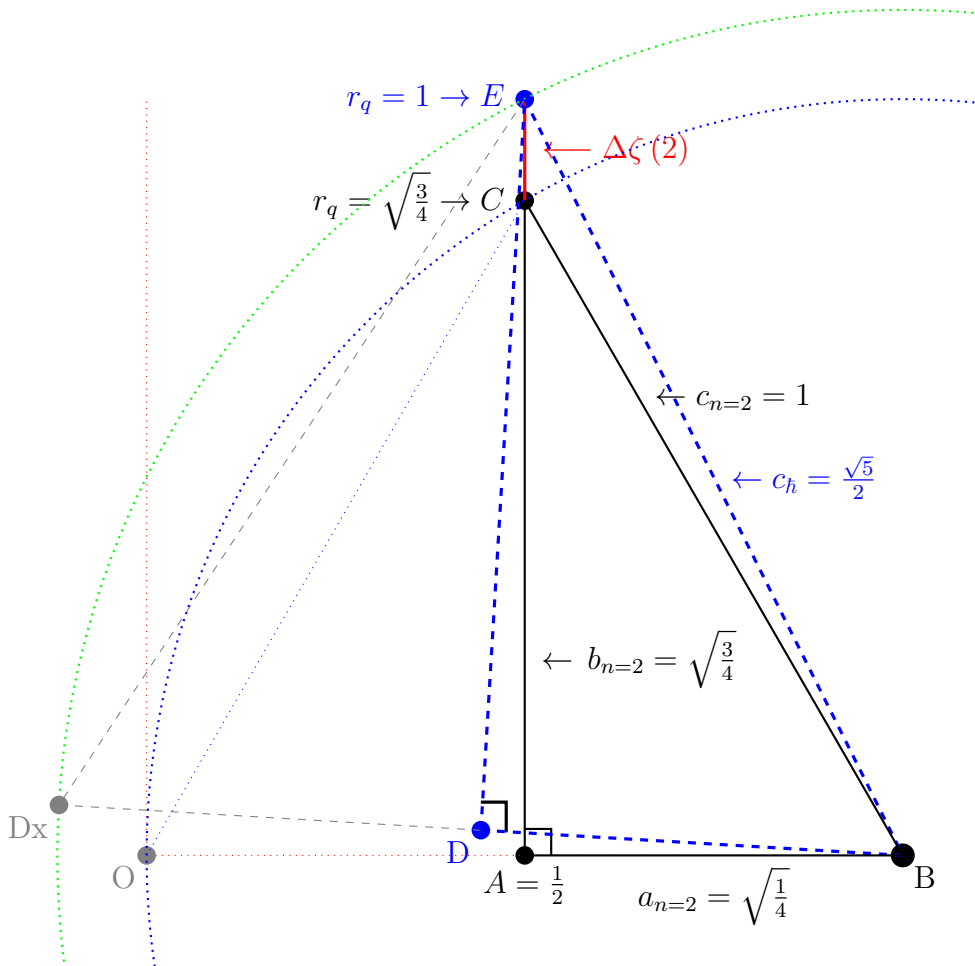


Figure 5.6: Root 2 equilibrium

$\overline{AE} = \overline{DE} = \overline{AD} \rightarrow \overline{AD} = (\overline{AB} + \overline{BD} = 1)$. In numerical sense this configuration resembles a 90° right angled polar triangle on a spherical surface (fig.5.7), three angles that is, total $3 \times 90^\circ = 270^\circ$ where the area itself represents the complete count of Natural numbers.

Such a triangle fits 8 times on the surface of a sphere and this must mean that the Surface area is a scale invariant model of volume. This clearly is the point of equilibrium, the surface area is at the point of $V_0 \rightarrow \frac{1}{8}V_1$ and in the configuration as depicted in figure 4.9. This configuration can only be depicted as a square surface area $A = \pi^2$ because the moment this configuration is reached, the only measure in this new state of our mathematical universe is the size of the chords spanning the surface as great circles. And

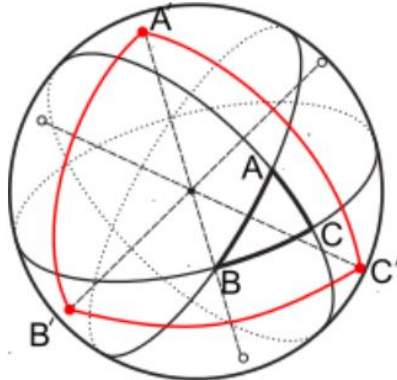


Figure 5.7: Spherical triangle

already established was that “The hypotenuse from $x = \sqrt{2}^{-1}$ to $y = \sqrt{2}^{-1}$ is off course $c = a\sqrt{2} = 1$ and longer lines, that represent the root of a square area, do not exist in our universe.” (see subsection 4.8.2).

5.5 The root of curvature

The root of curvature, or at least the sense there is such a thing as curvature, is illustrated in figure 5.6. At any given moment the universe is in a state where the chords c_1 and c_h are simultaneously observable, measurable, but can only be recognized in there distinct identity as either Cartesian or part of spherical geometry. In this figure the spherical identity must be from chord $c_h = \frac{\sqrt{5}}{2}$ because the length exceeds the maximum length feasible in our mathematical universe. Conjoining both chords leaves us with two possible configurations to represent those chords. United in the hypotenuse $c = \pi\sqrt{2}$ or as the great circle $c=2\pi$, notably the equator, joining two hemispheres. The scale invariant ratios “square root of two” and the “circumference of a circle” are one and the same entity. The projection plane measures $A_{\square} = \pi^2$ with a hypotenuse $c_h = \pi\sqrt{2}$. The unit surface area is $SA = \pi^2$ with an associated circumference of $c_{sa} = 2\pi\sqrt{\frac{\pi^2}{4\pi}} = \sqrt{\pi^3}$, and yields a ratio $\Delta_{\infty} \stackrel{def}{=} c_{ratio} = \frac{c_{sa}}{c_h} = \frac{\sqrt{2\pi}}{2} = 1\frac{1}{4} \times \sqrt{\frac{\pi}{2}}$. $\Delta_{\infty} \rightarrow \frac{2.5}{0.8} = \frac{\pi}{\frac{\pi}{2}} \rightarrow \pi = \frac{2.5}{0.8} \Leftrightarrow$ Because a surface area is defined by $SA = 4\pi r^2$ and this area is subdivided in 8 polar triangles the relative radius for a surface area $SA = 8\pi^2$ is $r_{T\infty} = \sqrt{\frac{8\pi^2}{4\pi}} = \sqrt{2\pi} = 2.5 \times \sqrt{\frac{\pi}{2}}$, or with $\pi = 1 \rightarrow r_{T\infty} \sqrt{\frac{8}{4}} = \sqrt{2}^{-1}$. In table 5.1 the schema is based on a root 2 power series $r_x \rightarrow \left\{ \dots \times \sqrt{2}^{-1} \times \sqrt{2}^{-1} \times \sqrt{2}^{-1} \times \sqrt{2}^{-1} \times \dots \right\}$ and

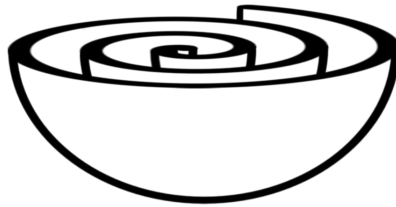


Figure 5.8: M-brane hemisphere mono surface

it is the triangular number cycle irrespective of coordinate system, reference frame, that iterates in continuous perpetuity through that cycle. In table 4.1 the cycle starts with $a = \sqrt{2}^{-1}$ and ends with $a = \frac{1}{2}$, in what seems a infinity of iterative steps reducing the radius. A perpetual reducing radius produces a surface area that has a unique radial length for each separate surface coordinate it intersects. For regular spherical surfaces this will mean a stack of identical x and y coordinates at each unique radial distance. It is in the continuous regression of surface area that lays a clue hinting at a 2 dimensional surface structure that wraps around a singularity, the surface asymptote found earlier. Figure 5.8 is a model of one hemisphere of such a surface. A Cartesian flat version will be presented. The 2D surface itself stands model for a 3D space spiraling in on itself, any radius intersecting this spiral stands orthogonal on 3D space. M-brane hemisphere mono surface

This is a M-brane mono surface with a bulk (void) separating the surface layers wrapping over and over. The shape of the surface area of this (two hemisphere) structure, given the bulk infinitely thin and ignoring the subsurface spiral, is approaching that of a sphere. With the singularity as center of this structure, any perfect sphere with fixed radius will cut as a ghost through this surface and only have two (2) coordinates in common with that surface, those are the conjoined surface coordinate(s) $\{C, E\}$ and the coordinate at the absolute center B, see figure 5.6.

5.5.1 Unity orthogonal to the sphere

Taking another look at figure 5.6 it becomes clear what is represented. As \overline{CE} shortens \overline{BE} approaches the point at which \overline{BC} stands orthogonal to the surface of the sphere. As that point is reached then \overline{BC} and \overline{BE} share the same radius. There is one aspect to take note of and that is the angle. \overline{BC} and \overline{BE} are at that point orthogonal to the surface of the sphere, however, no radius can be orthogonal to the surface of the M-brane. A better way to

look at it is that because the sphere only intersects the spiral at one point, a continuous decreasing radius will visit each coordinate at the spiral without exception. At certain radial distances it must be the case that the shared coordinate is at the point of equilibrium, see figure 4.9 and table 4.4. In principle the decreasing radius paints the surface of the spiral as a space filling curve, linear and missing no spot. This is what we see expressed in figure 5.6, only from that perspective it is the spheres surface being painted, after all, we are dealing with an infinite set of orthogonal unity chords, see figure 5.2 for $h_{init} = h_{lim} = \frac{\sqrt{5}}{2}$. The question to ask is however, “did you not notice your radius decreasing?”

Chapter 6

A cartesian M-brane mono surface

Figure 6.1 shows 4 ways in which $\frac{\pi^2}{6}$ can be represented as a function of affected area. Configurations A and B are those of the projection and triangular plane. Configuration C is more straightforward, but configuration D will be the one to take center stage. The hypotenuse $c_D = \sqrt{\left(\frac{1}{3}\right)^2 + 1^2} = \sqrt{T_h} \approx \hbar$,

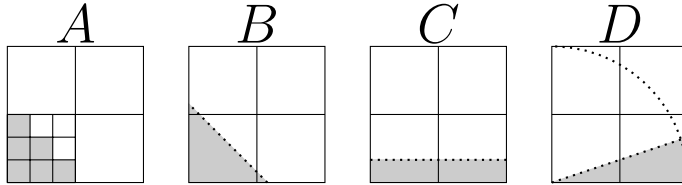
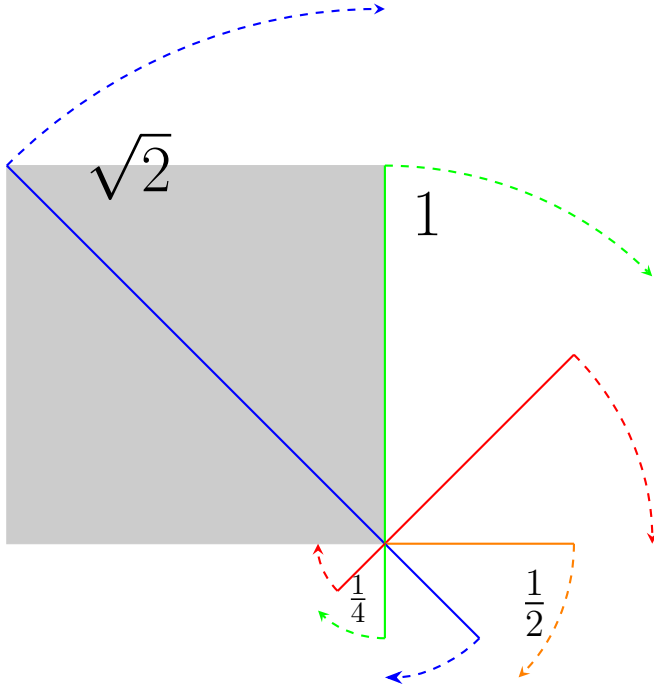


Figure 6.1: Some $\frac{1}{6}$ affected area configurations

see table 4.3, subsection 4.10.2, and figure 4.9. The x-coordinate for the intersection with the arc $x_D = \cos\left(\tan^{-1}\left(\frac{1}{3}\right)\right) = \sqrt{(T_H)^{-1}}$. The affected area in all those configurations is delimited by exact the value found in the fractal argument for zeta, only here the relation between angle and radius is significant. In figure 6.2, the radius contracts according to table 5.1, column $(\sqrt{2})^{-n}$. Starting with the hypotenuse $\sqrt{2}$, depicted in the shaded square, representing the initial state of the mathematical universe operated on. One iteration of $\sqrt{2}^{-1}$ further we find radius “1” representing the continuum \mathbb{R} and therefor the shaded area stands model for $1 = \mathbb{R}^2 \propto \pi^2$. This is the starting point for $n = 0 \rightarrow \sqrt{\frac{1}{2^n}} \rightarrow a = 1$. The radii stand in specific relation to each other, they are grouped in sequences of 3 radii, spanning a surface over $\pi rad \rightarrow 180^\circ$. This is depicted in figure 6.3. Line

Figure 6.2: M-brane mono surface $\sqrt{2}$ contraction

$\overline{AG} = \sqrt{2}$ is the longest line in our universe and the next iteration gives $\overline{AG} \times \sqrt{2}^{-1} = \overline{AD} = 1$. The triangular shapes are not just for illustrative purposes. Line $\overline{GF} > \overline{AG}$ and cannot exist in the universe therefor the first shape $\triangle AFG$ has to extend the universe bounds which would defy the meaning “universe”. The absolute size of the area $A = \angle AFG = \frac{1}{2}$, and as such does not violate the bounds, therefore the set of points exist in some continuous relation contained within the mathematical universe. In table 5.1 we find the family of chords that represent sets of points that would appear to express spherical attributes, see column c_h containing values proportional to $\sqrt{5}$. In figure 6.3 triangle $\triangle BCD$ consists of two triangles $\triangle ACD$ and $\triangle ABC$. Line $\overline{CD} = c_h = \frac{\sqrt{5}}{2}$ (see figure 5.6), one would erroneously expect to fit the universe because $\overline{CD} < \overline{AG}$. This would be mistaken because of the fractal argument (section ??) in relation to a continuously collapsing surface, each iteration expresses a evolutionary stage of the surface and is a scale invariant measure of the universe. Area $\triangle ABC = \frac{\triangle ACD}{4}$, represents the same evolution as depicted in the projection plane, triangular plane model. Therefor $\overline{CD} \propto \overline{BC}$, both lines represent $c_h = \frac{\sqrt{5}}{2}$ in relative proportion. The relative proportion in this diagram is recognizable in the triangular projection, see table 4.1, as $\overline{CD} = \sqrt{\frac{1}{4}} \times \sqrt{5} \rightarrow T_{n=4} \rightarrow \left(r_q = \sqrt{\frac{4}{5}}\right)^{-1}$ and

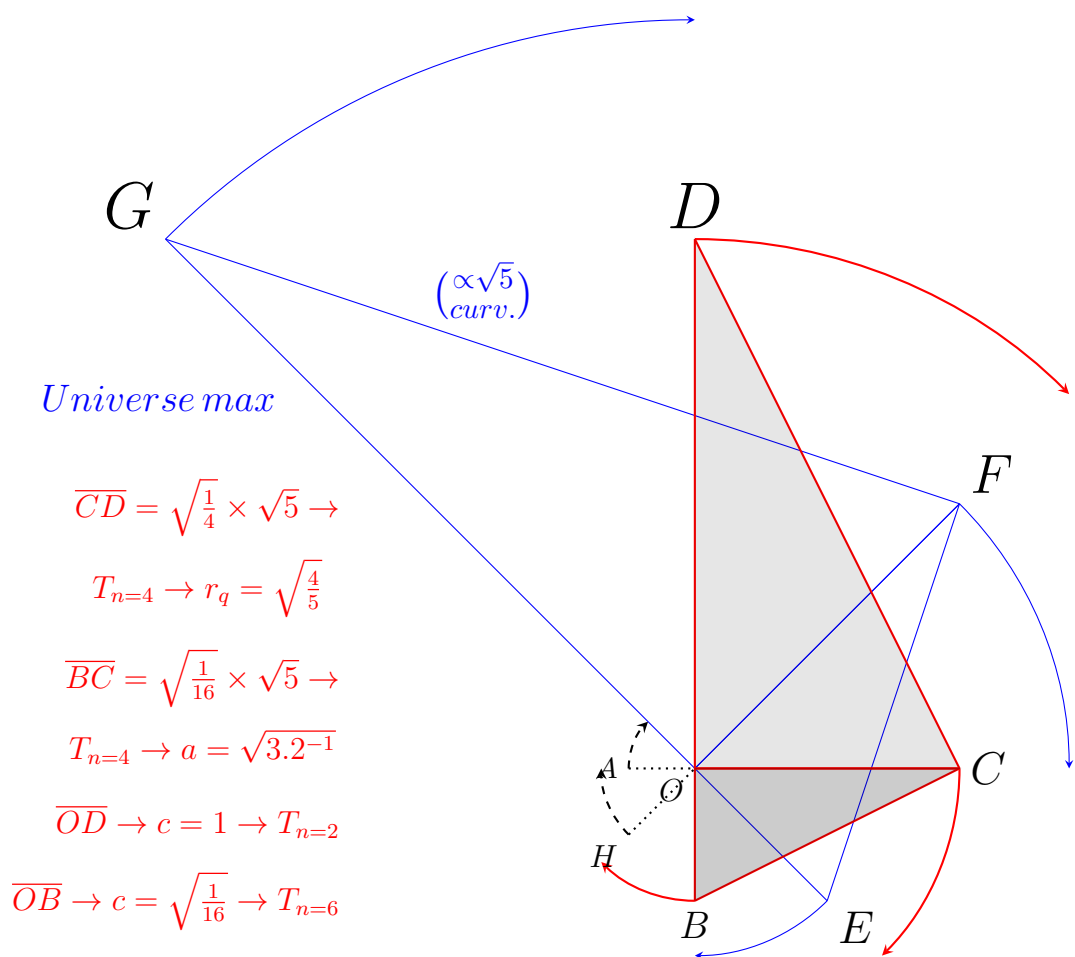


Figure 6.3: M-brane mono surface radii group III

$$\overline{BC} = \sqrt{\frac{1}{16}} \times \sqrt{5} \rightarrow T_{n=4} \rightarrow a = \sqrt{(3.2)^{-1}}.$$

6.0.1 Primorial 10 and PI

Taking a close look at $\overline{BC} = \sqrt{\frac{1}{16}} \times \sqrt{5} = \sqrt{(3.2)^{-1}}$ we have to notice that $(3.2)^{-1} = \frac{\pi^{(+)^{-1}}}{10}$, the limit of the primorial lower- upper-bound is $\frac{1}{3.125} = \frac{1}{\pi^{(+)^{-1}}} \text{ (table 3.2 on page 19, column } \frac{lb}{ub} \text{). The range of } P_s \text{ increment} = [0.5, \sqrt{2}^{-1}] \text{ processes one cycle from } (\overline{AC} \rightarrow \overline{AB}) \propto 2 \times 45^\circ = 90^\circ \text{ or } (2 \times \overline{AB} = \overline{AC}) \propto \left(2 \times [0.5, \sqrt{2}^{-1}]\right) = \left(2 \times \frac{\pi^{(+)^{-1}}}{10}\right) = \frac{\pi^{(+)^{-1}}}{5} = (1.6)^{-1}, \text{ the inverse of the hexagonal equilibrium surface area ratio (equation 5.3).}$

6.0.2 Necessarily convex

This brings us back to the root of curvature (figure 5.6) where chords are observable, but must be so in either a Cartesian or Spherical identity because they have to fit the bounds as a straight line between two vertices in some continues expression without exceeding the bounds of the universe . In short, the universe is a complete convex set where all edges between vertices are straight. In spite of that some appear curved because in a Cartesian reference frame the set of points would appear to project outside the universe, hence those sets are perceived as if having properties of spherical geometry.

6.1 The M-brane exposed area

In figure 6.4 the regression is depicted as successive squares of the radii. Each iterative step is depicted as a full triangular cycle of $45^\circ \rightarrow \sqrt{2}^{-1} \times \sqrt{2} = \frac{1}{2}$. A partition of the area has no overlap with previous and subsequent areas, those are indicated A through E, measure $\frac{1}{4}$ of the current iteration and $\frac{1}{2}$ of the subsequent iteration. By symmetry it takes two iterations $(\overline{AC} \rightarrow \overline{AB}) \propto 2 \times 45^\circ = 90^\circ$ reach a 4-fold reduction in area. Figure 6.5 by ratio of successive iteration $(A \rightarrow B) \propto 45^\circ$ shows that Surface Area and Volume are in fact out of phase expressions of surface area. $A_4^{\frac{1}{4}} : B_8^{\frac{1}{8}} \rightarrow B_4^{\frac{1}{4}} : C_8^{\frac{1}{8}}$ or $SA_4^{\frac{1}{4}} : V_8^{\frac{1}{8}} \rightarrow SA_4^{\frac{1}{4}} : V_8^{\frac{1}{8}}$. Volume is defined as wrapped surface area. The third iteration is associated with $T_{n=3}$. There if we project a intermediate iteration onto $\frac{5}{6}$ of the completed cycle, then we find ourselves at the point depicted in configuration D (fig. 6.1). The hypotenuse of the remaining triangular area is $c_{tan} = \sqrt{1^2 + \left(\frac{1}{3}\right)^2} = \sqrt{T_h} \approx \hbar$. M-brane mono surface zeta equilibrium

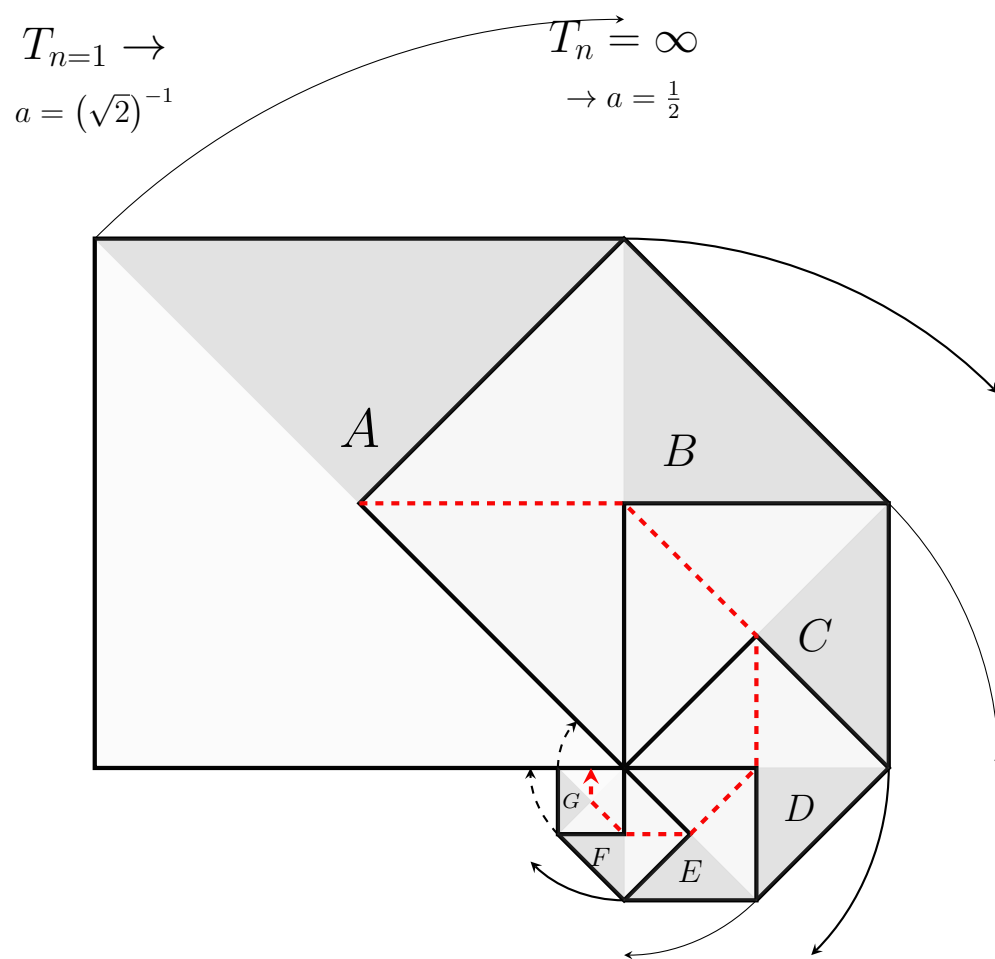


Figure 6.4: M-brane mono surface area contraction

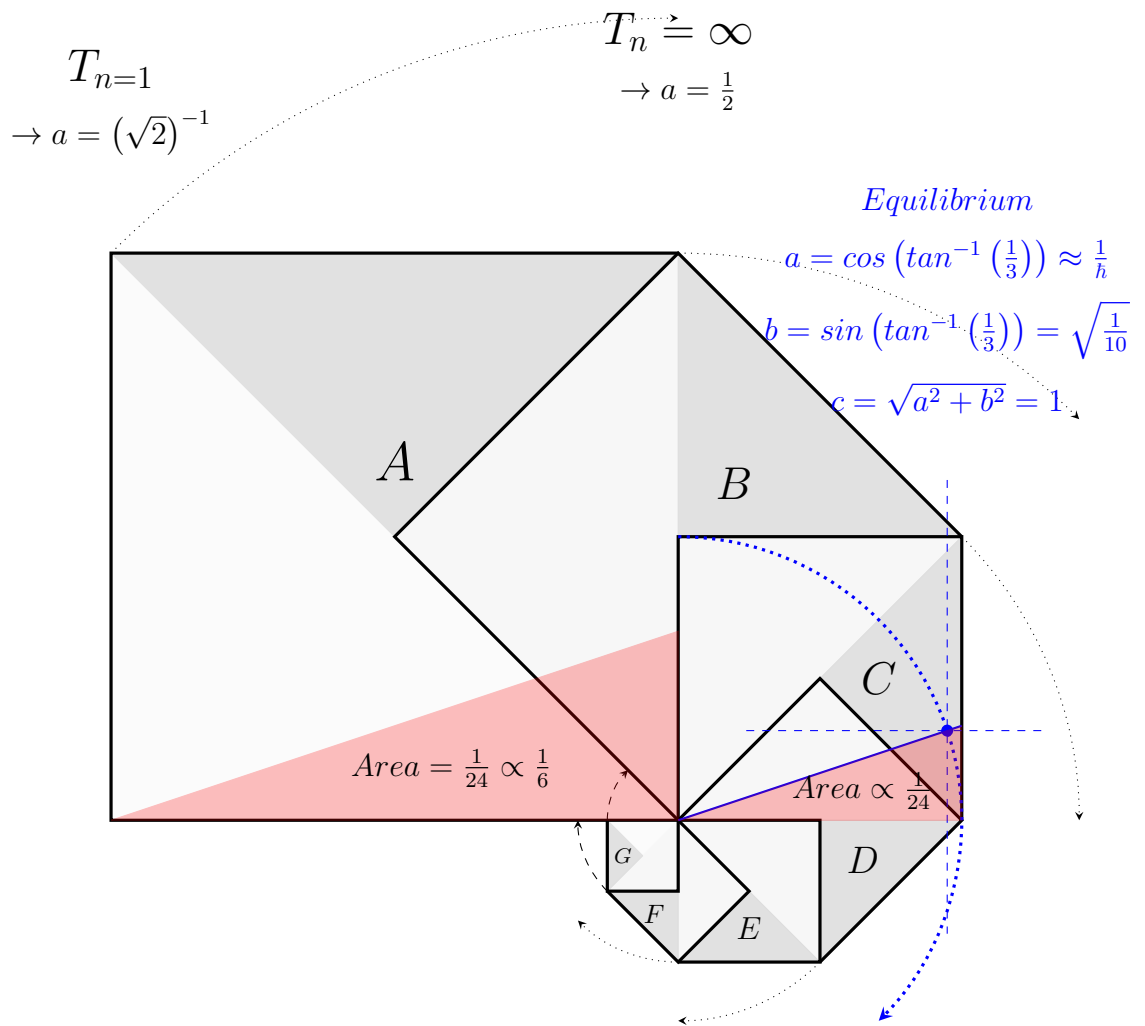


Figure 6.5: M-brane mono surface zeta equilibrium

In figure 6.6 (page 64) it is really more convenient to use the 360° system. The base of each iteration by scale invariance is always proportional to 1, $\overline{AB} \rightarrow a = 1$, $\overline{BC} \rightarrow b = \frac{1}{3}$ and $\overline{AC} \rightarrow c = \sqrt{a^2 + b^2} = \sqrt{T_h} \approx 1.054092553\dots \rightarrow \sqrt{c_{unity}} = \sqrt[4]{1\frac{1}{4}} \approx 1.057371263\dots$. By design we know that the total area below the hypotenuse is $Area \triangle ABC = \frac{1}{6}$. This we will express in fractions of 60, $Area \triangle ABC = \frac{10}{60}$. $Area \triangle AED = \frac{9}{60}$ and therefore remains $Area \square EBCD = \frac{1}{60}$. The coordinates for point D are $D_x = \cos(\tan^{-1}(\frac{1}{3})) = (\sqrt{T_h})^{-1}$ and $D_y = \sin(\tan^{-1}(\frac{1}{3})) = (\sqrt{10})^{-1}$ yielding an area $Area \triangle AED = \frac{9}{60} = 0.15 \rightarrow \frac{360}{24} = 15$. The sum of areas $\triangle AED + \square EBCD = \triangle ABC = \frac{1}{6}$ is equivalent to $\frac{9}{60} \times T_h = \frac{1}{6}$. The radii grouping in cycles of 90° (figure 6.3) has a point of equilibrium at the transfer from $\frac{9}{90}$ to $\frac{10}{90} \rightarrow \frac{1}{10}$ to T_h as function of decreasing area. This final value $\frac{10}{90} = T_h$ is as found in figure 4.9 where the value indicates the repetition of the projection plane. The proportionality is convenient. In here we find (60° is to 360° as $(\frac{1}{6})^\circ$ is to 1°) and therefor (0.15 is to 0.9 as 15° is to 90°). For $1\pi \frac{360^\circ}{2\pi} \approx 57.29577951\dots^\circ$ we can apply $1\pi rad = \frac{360^\circ}{2.52} \times (\leftrightarrow)^{-1} = 57.6 \times (\leftrightarrow)^{-1} \approx 57.29577951\dots^\circ$. The scale invariance obscures a beautiful aspect of $a = \overline{AB}$. In table 6.1 we find at $n = 2 \rightarrow Spherical calculated = 0.32 \rightarrow 0.32 = \frac{1}{\pi(\leftrightarrow)^{-1}}$, this $0.32 = \frac{1}{3.125}$ is the limit for $\frac{lb}{ub}$ from the primordial oscillation (table 3.1). The cycle starts of with $A=1$ and two iterations further we end up with $A = (\frac{1}{3.125})^2$. Therefor the initial area must have been $A = ((0.32)^2)^{-1} = (0.1024)^{-1} = 9.765625 = \pi^2 \times (\leftrightarrow)^{-2}$.

6.2 Slotted mechanism

The scale invariance of geometric proportions such as $\sqrt{2}$ and π means that without frame of reference the size of the object they are derived from is unknowable. To complicate matters further, knowing and following algorithms demand agency. There is no such thing as “agency” in an emergent system rooting in first principle. What mechanism would be capable of forcing a mathematical abstraction onto physical systems. How can any physical process take note of any mathematical abstract notion of oscillation and behave accordingly? Well, it can not, it only appears to stabilize each time while in reality, as we will show, the collapse is a ongoing process and quantized in discrete pulses. The mathematical structure is emerging from first principles from within the physical structure, it can be derived from observation. The fractal argument for zeta just tells us that there exist one specific point at which: A_\square is to $\zeta(2)$ as $\zeta(2)$ is to $\frac{1}{9}A_\Delta$, at which point a equilibrium exists

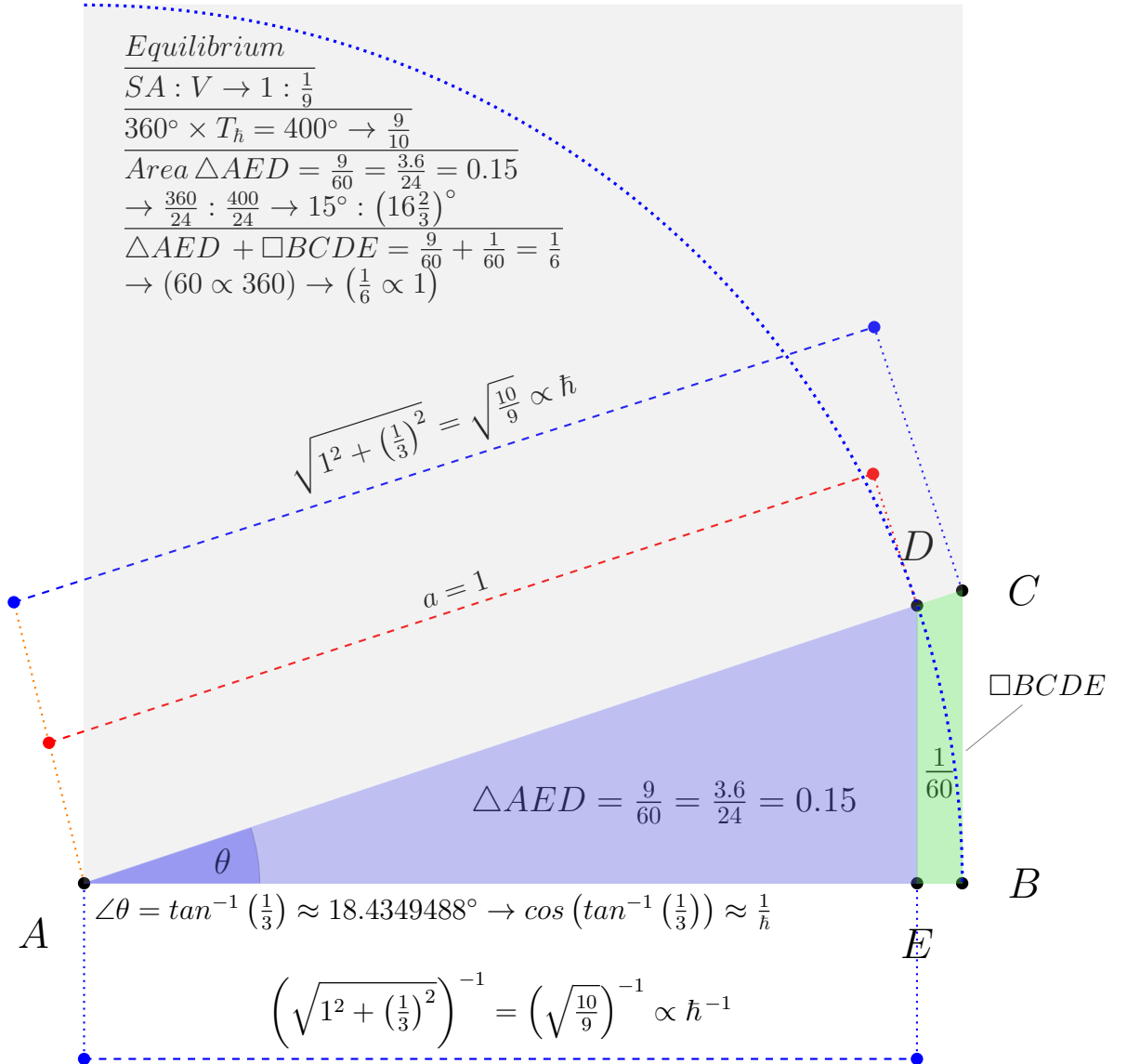


Figure 6.6: M-brane mono surface - detail 9 over 60

Table 6.1: 4/5 proportion Spherical vs Cartesian projection (exc. \nrightarrow)

n	<i>Cartesian</i>		<i>Spherical</i>			$\Delta \frac{\text{Cartesian}}{\text{Spherical}}$
	$\sqrt{2}^{-1}$	Calculated	$\left(\frac{4}{5}\sqrt{2}^{-1}\right)^n \leftrightarrow \sqrt{\pi(\nrightarrow)^{-1}}^{-n}$	Calculated	Closed	
0	1	$\sqrt{2}^0$	1	$\sqrt{\pi(\nrightarrow)^{-1}}^0$	$2^0 \times 10^0$	1
1	0.70710...	$\sqrt{2}^{-1}$	0.5656854249...	$\sqrt{\pi(\nrightarrow)^{-1}}^{-1}$	$2^{2.5} \times 10^{-1}$	$(1\frac{1}{4})^1$
2★	0.5	$\sqrt{2}^{-2}$	0.32	$\sqrt{\pi(\nrightarrow)^{-1}}^{-2}$	$2^5 \times 10^{-2}$	$(1\frac{1}{4})^2$
3	0.35355...	$\sqrt{2}^{-3}$	0.181019336...	$\sqrt{\pi(\nrightarrow)^{-1}}^{-3}$	$2^{7.5} \times 10^{-3}$	$(1\frac{1}{4})^3$
4	0.25	$\sqrt{2}^{-4}$	0.1024	$\sqrt{\pi(\nrightarrow)^{-1}}^{-4}$	$2^{10} \times 10^{-4}$	$(1\frac{1}{4})^4$
5	0.17678...	$\sqrt{2}^{-5}$	0.057926187...	$\sqrt{\pi(\nrightarrow)^{-1}}^{-5}$	$2^{12.5} \times 10^{-5}$	$(1\frac{1}{4})^5$
6	0.125	$\sqrt{2}^{-6}$	0.032768	$\sqrt{\pi(\nrightarrow)^{-1}}^{-6}$	$2^{15} \times 10^{-6}$	$(1\frac{1}{4})^6$
7	0.08839...	$\sqrt{2}^{-7}$	0.01853638...	$\sqrt{\pi(\nrightarrow)^{-1}}^{-7}$	$2^{17.5} \times 10^{-7}$	$(1\frac{1}{4})^7$
8	0.0625	$\sqrt{2}^{-8}$	0.01048576	$\sqrt{\pi(\nrightarrow)^{-1}}^{-8}$	$2^{20} \times 10^{-8}$	$(1\frac{1}{4})^8$
9	0.04419...	$\sqrt{2}^{-9}$	0.0059316416...	$\sqrt{\pi(\nrightarrow)^{-1}}^{-9}$	$2^{22.5} \times 10^{-9}$	$(1\frac{1}{4})^9$
10	0.03125	$\sqrt{2}^{-10}$	0.0033554432	$\sqrt{\pi(\nrightarrow)^{-1}}^{-10}$	$2^{25} \times 10^{-10}$	$(1\frac{1}{4})^{10}$

between the (intra dimensional) interface, surface area is volume and visa versa. At no point this fact tells us how this can be the cause for any natural process to ‘react to and or branching of’, no matter if Planck’s constant appears in such a geometric construction. The real question that comes up is, why does observation of nature led to answers indicative of constant recurrence of what mathematically seems to express one extremely rare instance in some continuous flow. $\zeta(2) = \frac{\pi^2}{6}$ has a very specific role to play in the envisioned structure. The fractal siblings projection plane $A_{\square} = \frac{\pi^2}{6}$ and the triangular plane $A_{\triangle} = \frac{\pi^2}{4}$ represent a continuously collapsing structure, it is $\zeta(2) = \frac{\pi^2}{6}$ that represents the configuration that is at the cusp of each discrete moment in time. Next a proposal for a structure that has exactly the properties sought for will be detailed, one with an integrate slotting mechanism, the Quadrature Geometric Framework

Chapter 7

Quadrature Geometric Framework

The QGF is based on the properties of a complete convex set, complete because no points exist outside the set, the set is the complete universe. Convex set From Wikipedia

Illustration of a convex set which looks somewhat like a deformed circle. The (black) line segment joining points x and y lies completely within the (green) set. Since this is true for any points x and y within the set that we might choose, the set is convex. Illustration of a non-convex set. Since the red part of the (black and red) line-segment joining the points x and y lies outside of the (green) set, the set is non-convex. In convex geometry, a convex set is a subset of an affine space that is closed under convex combinations More specifically, in a Euclidean space, a convex region is a region where, for every pair of points within the region, every point on the straight line segment that joins the pair of points is also within the region. For example, a solid cube is a convex set, but anything that is hollow or has an indent, for example, a crescent shape, is not convex. The ‘Quadrature Geometric Framework’ is a model for a ‘first principle’, an ‘ab initio’ condition that underpins behavior of units in both mathematics (numbers), as physics (wave/particles) and be

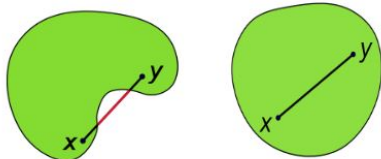


Figure 7.1: Convex set

shown to emerge independently with the physical realm.

7.1 Primorial hexagon plus

The basis for the QGF is derived from the primorial hexagon, figure 3.4. The QGF (figure 7.2 has a pole at $2.5^2 = \frac{2\pi}{\varphi}$ and at $2\pi = 2.5^2 \times \varphi$, see the zoomed in section on the lower right. This dual notation is by design, for all intents and purposes these coordinates 2π and 2.5^2 are to be considered one and the same and only separated by arbitrary choice of perspective. The illustration shows chords within the bounds of the pole (2π and 2.5^2) and chords stretching out beyond the pole, also indicated is a chord at infinity orthogonal to the x-axis. The chords belong to n-gon that have two identities.

- Scale invariant. The scale invariant coordinates for the n-gon are simply the x-coordinate $x=n$ for the circumscribed circle, this is the identity from which the chord length is calculated.
- Absolute. Because the pole at $\frac{25}{25} = 2.5^2 = 1$ all n have a absolute coordinate relative to the (chosen) pole. The absolute coordinate for a n-gon is $q = \frac{n}{2.5^2}$, e.g. $n=6 \rightarrow q = \frac{6}{2.5^2} = \frac{24}{25} = 0.96$

7.2 One ring to enclose them all

Each arbitrary x-coordinate can be designated as pole, that x coordinate becomes the unit and spawns its unique set of n-gons. This is done by selecting a $q \in \mathbb{Q}$ and if needed change perspective by $x \in \mathbb{R} = q \times \varphi$, using a φ with sufficient decimal expansion. Mathematically both the region drawn inside the pole as well the region extending beyond lay within the convex set. It is the pole at $2.5^2 \rightarrow 2\pi$ that represents the boundary of the infinite plane of the QGF, not the boundary that divides $x < pole < x$. e.g. $\frac{6}{2.5^2} = \frac{24}{25} = 0.96 < pole < \frac{7}{2.5^2} = \frac{28}{25} = 1.12$ spans the pole seamlessly. In physical systems however, this pole represents the ‘boundary’ of the universe, the point at infinity as you will. The region that geometrically projects beyond 2π and 2.5^2 to infinity, will in physical projection overlay the area $[6, 2\pi]$. The pole at $2.5^2 \varphi = \frac{2\pi}{\varphi}$ can be understood to behave in physical sense as end of a medium and a (maximum elastic) reflector.

7.2.1 Chords, almost created equal

The scale invariant coordinates for the n-gon are simply the x-coordinate $x=n$ for the circumscribed circle. From this the length of the chords can

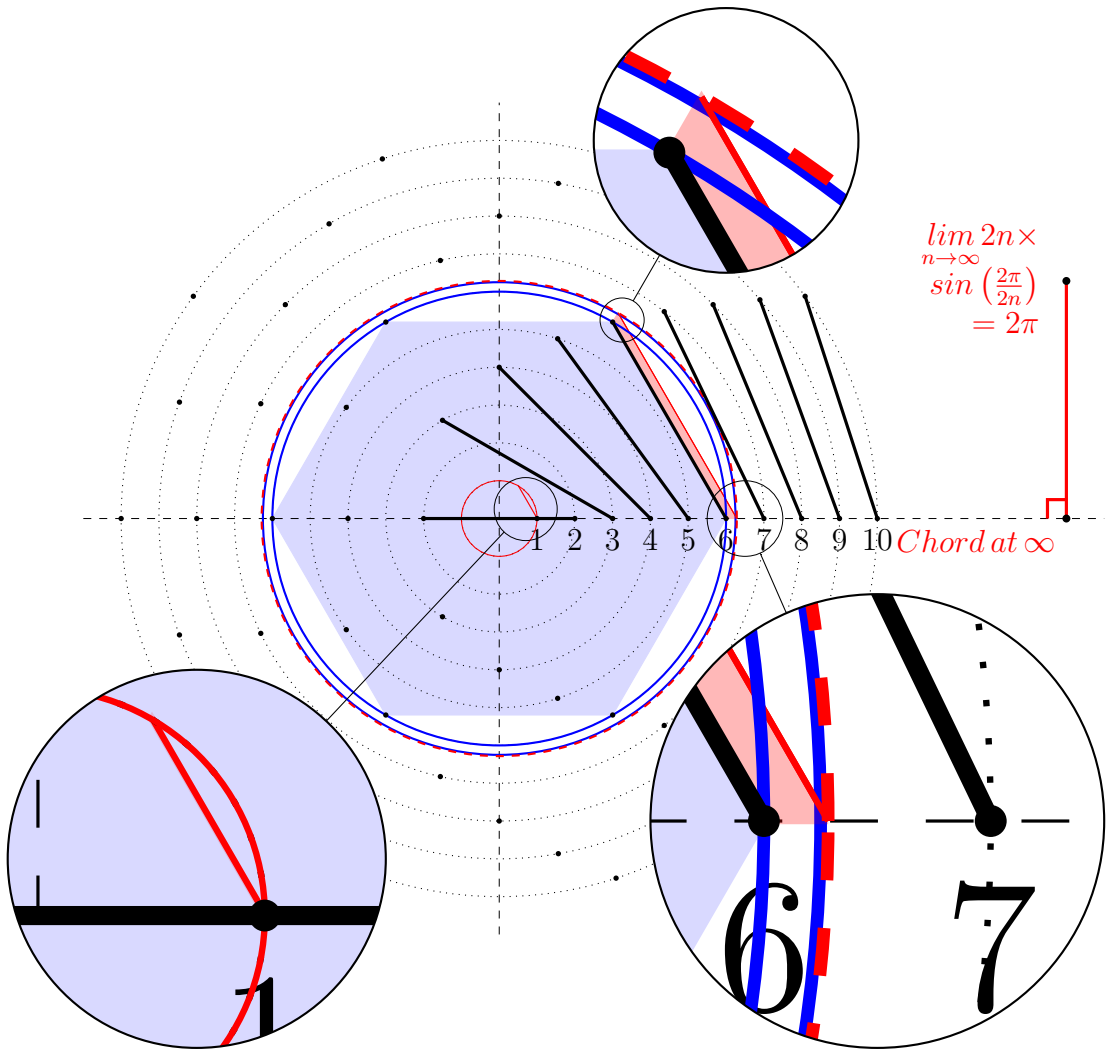


Figure 7.2: Quadrature Geometric Framework

Table 7.1: QGF standard chord and deviation

n	$c_n = \sin\left(\frac{2\pi}{2 \times n}\right)$	$closed$	$cl_n = 2n \times c_n$	$\Delta \frac{cl_n}{cl_6}$		
1	0	0	0	0	0	
2	1		4	0.666666...	$\frac{2}{3}$	
3	0.8660254038★	$\sqrt{\frac{3}{4}}$	5.196152423★	0.8660254038★	$\propto \zeta(2)$	
4	0.7071067812	$\sqrt{2}^{-1}$	5.656854249	0.9428090415	$\frac{2}{3}\sqrt{2}$	
5	0.5877852532		5.877852523	0.9796429872		
6	0.5		6★	1	$\sin\left(\frac{\pi}{2}\right)$	$\Delta \frac{2}{\pi}$
7	0.4338837391		6.074372348	1.012395391		
8	0.3826834324		6.122934918	1.040481718		
16	0.195090322		6.242890305	1.047197551		
∞			2π	$\frac{\pi}{3} \rightarrow (\Delta \frac{2}{\pi}) \times \zeta(2)$	P_*	

be easily calculated by $cl_n = 2n \times \sin\left(\frac{2\pi}{2 \times n}\right)$. The unit chord from which all others are measured (table 7.1) is the chord for $n = 6 \rightarrow cl_6 = 2 \times 6 \times \sin\left(\frac{2\pi}{2 \times 6}\right) = 6$. In table 4.1, $T_{n=3} \rightarrow r_q = \sqrt{\frac{3}{4}}$, associated with $\zeta(2)$, marks chord $h_{init} = \frac{\sqrt{5}}{2} \rightarrow (\angle 50.77^\circ)$ in fig. 5.2. This matches with table 7.1 $n = 3 \rightarrow c_3 = 0.8660254038$ because $\frac{cl_3}{cl_6} = c_3$. By this the absolute value $T_{n=3} \rightarrow r_q = \left| \sqrt{\frac{3}{4}} \right| = 0.8660254038$ reflects the scale invariant $b = \sin\left(\frac{\pi}{3}\right)$ proportional to any hexagon. The obvious difference is that cl_n is the hypotenuse and $b = \sin\left(\frac{\pi}{3}\right)$ a right angle side. The interchange of sides b and c is one aspect, the fact that $b : c$ as $1 : \sin\left(\frac{\pi}{3}\right)$ means that although $b = \sin\left(\frac{\pi}{3}\right)^2 = \frac{3}{4}$ is a proportion that can occur, but not if b is approached as the absolute value $r_q = \sqrt{\frac{3}{4}} \rightarrow (\angle ABC = 50.77^\circ)$, e.g. the circumference of a circle with radius $|1|$ is $|2\pi|$, the circumference of a circle with radius $|2\pi|$ is proportionally 2π , but in absolute terms $(2\pi)^2$. As is with $r_q = \left| \sqrt{\frac{3}{4}} \right|$ if for a right angled triangle $c = \left| \sqrt{\frac{3}{4}} \right|$ then $r_q \neq \left| \sqrt{\frac{3}{4}} \right|$

7.2.2 Where does the unity chord live

The right angled sides associated with a unity chord are derived from the chord (hypotenuse) by $a = 2 \left(\frac{cl}{1 \frac{1}{4}} \right) - cl$ and $b = \frac{0.5}{a}$. From b derive the value

a for the associated A_{\square} projection

$$\begin{aligned} a &= 2 \left(\frac{\left| \sqrt{\frac{3}{4}} \right|}{1\frac{1}{4}} \right) - \left| \sqrt{\frac{3}{4}} \right| \\ &\approx 0.5196152423 \\ b &= \frac{0.5}{a} \approx 0.9622504486 \end{aligned} \tag{7.1}$$

Derive the associated area A for both planes

$$\begin{aligned} a &= \sqrt{2A} \\ A_{\square} &= \frac{T_n}{4 \times n^2} \rightarrow \frac{a^2}{2} = \frac{0.27}{2} = \frac{27}{200} = \frac{54}{400} \\ A_{\triangle} &= \frac{T_n}{n^2} = \frac{54}{100} = \frac{54}{10} = 5.4 \\ T_n &= 10 \times 5.4 = 54 \end{aligned} \tag{7.2}$$

Pinpoint n in the triangular cycle (inverse triangular formula)

$$\begin{aligned} n &= \frac{\sqrt{(8x) + 1} - 1}{2} \\ x &= T_n = 54 \\ x &= \frac{\sqrt{(8 \times 54) + 1} - 1}{2} \\ &\approx 9.904326023 \sim \pi^2 \end{aligned} \tag{7.3}$$

Contrast with the enclosing T_n for integer n=9 and n=10

$$\begin{aligned} T_{n=9} &= \left(\frac{9}{2} \right) \times (9 + 1) = 45 \\ T_{n=10} &= \left(\frac{10}{2} \right) \times (10 + 1) = 55 \\ \frac{T_{n=10}}{T_{n=9}} &= \frac{55}{45} = 1\frac{1}{10} \times T_h = 1.222222\dots \end{aligned} \tag{7.4}$$

The ratio is the same as encountered in figure 6.6 where for each cycle the affected area is divided in $\triangle AED = \frac{9}{60}$ and $\square EBCD = \frac{1}{60}$, a function of area dependent on the angle and “calibrated” to exact $\frac{A}{60}$. The interpretation is that in physical systems this margin translates to apparent spatial aspects, but abstract geometry can not, does not enforce spatial aspects, a method for independent emergent behavior that underlays the QGF must exist.

7.2.3 The primorial connection

The ratio is related to the primorial function by the following observation:

$$\angle \theta A = \frac{10}{60} \rightarrow \tan^{-1} \left(\frac{1}{3} \right) \approx 18.43494882^\circ \quad (7.5)$$

The primorial oscillation, table 3.2, column $\frac{lb}{ub} \rightarrow P_{n=\infty} = 0.32$ gives

$$\begin{aligned} \frac{60}{18.75} &= 10 \times 0.32 = 3.2 \\ h &\sim 2\pi \times \frac{\frac{1}{3}}{\tan^{-1} \left(\frac{2\pi}{360^\circ} \times 18.75^\circ \right)} \approx 6.62228\dots \end{aligned} \quad (7.6)$$

Application of the quadrature constant gives a lower and upper bound for the occurrence of Planck's constant in this range.

$$\begin{aligned} h &\sim 2.5^2 \times \frac{\frac{1}{3}}{\tan^{-1} \left(\frac{2\pi}{360^\circ} \times \frac{18.75^\circ}{\frac{6\pi}{\pi}} \right)} \approx 6.620000375\dots \\ h &\sim 2\pi \times \frac{\frac{1}{3}}{\tan^{-1} \left(\frac{2\pi}{360^\circ} \times \frac{18.75^\circ}{\frac{11.28820573}{2}} \right)} \approx 6.655156257\dots \end{aligned} \quad (7.7)$$

The rational fraction $18.75 = 3 \times 2.5^2 = \frac{6\pi}{\pi}$ indicates 6 chords of length π or $\frac{1}{0.32} = 3.125$, therefor we assume 18.75 correct.

$$\begin{aligned} T_{primor} &= 18.75^\circ \\ n_{primor} &= \frac{\sqrt{(8 \times T_{primor}) + 1} - 1}{2} \\ n_{primor} &= \frac{\sqrt{(8 \times 18.75) + 1} - 1}{2} \\ n_{primor} &= \frac{11.28820573}{2} \approx 5.644102865 \end{aligned} \quad (7.8)$$

Wedged between the nearest integer neighbors indicates that area is proportional to angle.

$$\begin{aligned} T_{n=5} &= \left(\frac{5}{2} \right) \times (5 + 1) = 15 \\ T_{primor} &= \left(\frac{n_{primor}}{2} \right) \times (n_{primor} + 1) = 18.75^\circ \\ T_{n=6} &= \left(\frac{6}{2} \right) \times (6 + 1) = 21 \end{aligned} \quad (7.9)$$

Some relations

$$\begin{aligned}
 T_n &\rightarrow [15 < 18.75 < 21] \\
 \frac{360^\circ}{T_n} &\rightarrow \left[24 > 19.2 \star > 17\frac{1}{7} \right] \\
 \frac{T_n}{2.5^2} &\rightarrow [2.4 < 3 < 3.36] \\
 Ratio &\rightarrow \left[\frac{4}{5}, 1, 1\frac{2}{5} \right] \\
 Inverse ratio &\rightarrow \left[\left(1\frac{1}{4} \right)^{-1}, 1, \sim \left(\sqrt{2} \right)^{-1} \right]
 \end{aligned} \tag{7.10}$$

Example interchange between $\mathbb{R} \leftrightarrow \mathbb{Q}$:

$$\begin{aligned}
 \left(\frac{\pi^2}{6} \right)^{-1} \times (\dagger^2) &= \left(\frac{3.125^2}{6} \right)^{-1} \\
 2 \left(\frac{\pi^2}{6} \right)^{-1} \times (\dagger^2) &= 2 \left(\frac{3.125^2}{6} \right)^{-1} = \frac{4 \times 1.92 \star}{2.5^2}
 \end{aligned} \tag{7.11}$$

7.2.4 The forties

Because the total cycle over the quadrant stretches $90^\circ \rightarrow \frac{3}{2} \times \frac{1}{60} = \frac{1}{40}$ must be the unit increment per cycle, $\frac{360^\circ}{40^\circ} = 9^\circ$. Each 60° period represented by $\zeta(2) = \frac{\pi^2}{6}$, projects on a 90° plane and represents the traversed angle 90° as function of area. The angle progresses in steps of $\frac{1}{10}90^\circ = 9^\circ$ or $\frac{1}{10}60^\circ = 6^\circ$ dependent on chosen projection ($\frac{1}{40}360 = \frac{1}{10}90^\circ = 9^\circ$) or ($\frac{1}{10}60^\circ = 6^\circ$). In short, the decimal system emerges from the sexagesimal expanding/decreasing area as it takes 10 incremental periods to complete 60 parts. Note that these 10 periods are grouped in 2 cycles of $5 \times 9^\circ = 45^\circ$.

7.2.5 Powers of ten to infinity

In table 5.1 the column $c_h \rightarrow n = 2 \rightarrow \sqrt{\frac{1}{4}}\sqrt{5} = \frac{\sqrt{5}}{2}$ indicates that $10\frac{\sqrt{5}}{2} = 5\sqrt{5} = 10\sqrt{1\frac{1}{4}}$ occurs in the span of 60° . This translates to a span of $(\frac{1}{40}360 = \frac{1}{10}90^\circ = 9^\circ)$ in which 2 cycles of $5 \times 9^\circ = 45^\circ$ each account for $5\sqrt{5} = 10\sqrt{1\frac{1}{4}}$, a tenfold increase of the chord $\sqrt{1\frac{1}{4}}$ over the span of the triangular projection, see table 4.1 and figure 5.2, and likewise the primorial root 2 approach , table 3.1. By some measure, the chords expand or decrease in size with a factor 10 and everything apparently blows up. But there is a

solution that at its core has dark energy and zeta zero's intimately entangled in a numerical expansion that will make perfect sense. But first why chords do not resize absolutely, only relatively. In the QGF configuration the length of the chords of each n -gon is $cl_n = 2n \times c_n$ and approaches a length of 2π , $\lim_{n \rightarrow \infty} cl_n = 2\pi$. This limit to the chord length is the key that allows us to define a physical model from which the QGF as first principle emerges and by this the foundation under the otherwise unreasonable effectiveness of mathematics in modeling the observed universe and its physical interactions.

7.3 The natural state as repository of potential

The n -chords in the QGF have their own “orbits” at the geometric radius $x = \frac{4n}{2.5^2} = n \times 0.16$ (relative to the pole at $\frac{25}{25}$). All QGF chords are periodic chords, but will only be revealed as such when expressed by a modulated repository of potential. In the physical implementation of the QGF the pole at $x = 2.5^2$ is absolute, it represents the outer limit of a complete convex set. In figure 7.3 the horizontal shaded bar encloses a vertical range, $y = [(2\pi \times \sin(\frac{\pi}{3})), 2\pi]$ and stretches over the range $x = [\pi, \infty]$. The lower end is $b = 2\pi \times \sin(\frac{\pi}{3})$ because the chord at $c = 2\pi$ is in fact the 90° orthogonal chord at infinity projected as a hexagonal chord under 60° . Herein we find the two configurations responsible for the 90° vs 60° as mentioned under section 7.2.5. The whole range between the pole and infinity gets confined to the maximum radius $x = 2\pi$ and the accumulated sum translates, because orthogonal, to $A = (2\pi)^2 = 4 \times \pi^2$. At coordinate $x=1$, the circle has a circumference of $c = 2\pi$. This is to be considered the chord at infinity as shown on the right of the picture at $x = \infty$. The chord at infinity is the evolution of the circle at $x=1$. The remaining chords at $n = [2, \infty)$ progressively project at a steeper angle until at the limit, $\lim_{n \rightarrow \infty} \angle_n = 90^\circ$ all chords stack up to an infinite line orthogonal to the x-axis, a circle of sorts, just like the circle at coordinate 1 is a line of sorts.

7.3.1 A box of chords

Figure 7.3 shows that all chords fit the box, the maximum length is $\lim_{n \rightarrow \infty} 2n \times \sin(\frac{2\pi}{2n}) = 2\pi$. The number of chords contained in the box is $\#chords \rightarrow T_n = \binom{n}{2} (n + 1)$, or a triangular infinity of them, $C_{box} = \{1\text{ gon}, 2\text{ gon}, 3\text{ gon}, 4\text{ gon}, \dots\} \rightarrow T_n = \sum_{n \rightarrow \infty} n = \{1 + 2 + 3 + 4 + \dots\}$ In figure 7.3 the shaded area between the 6-gon chord at $x=6$ and the $2\pi - \text{gon}$ at $x = 2\pi = \text{pole}$ is the range of

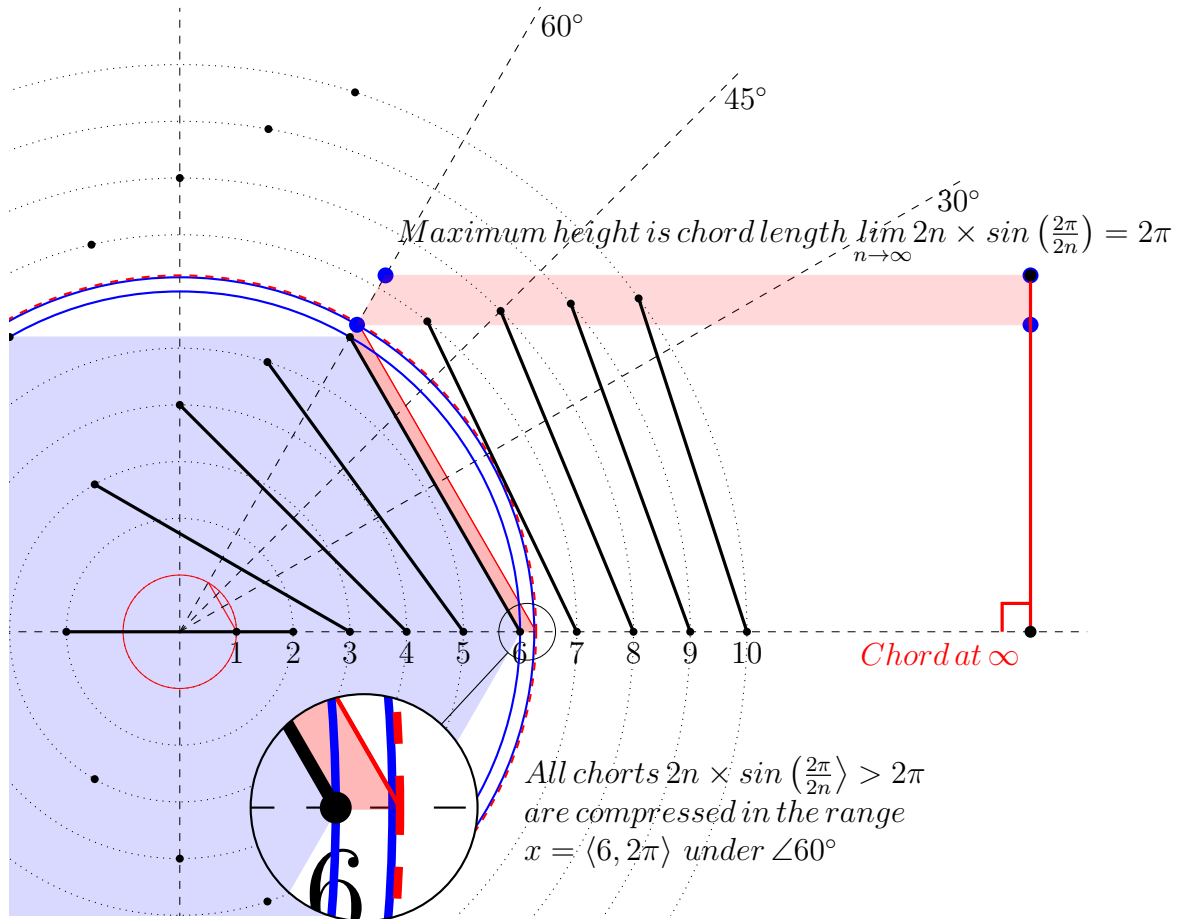


Figure 7.3: QGF natural state

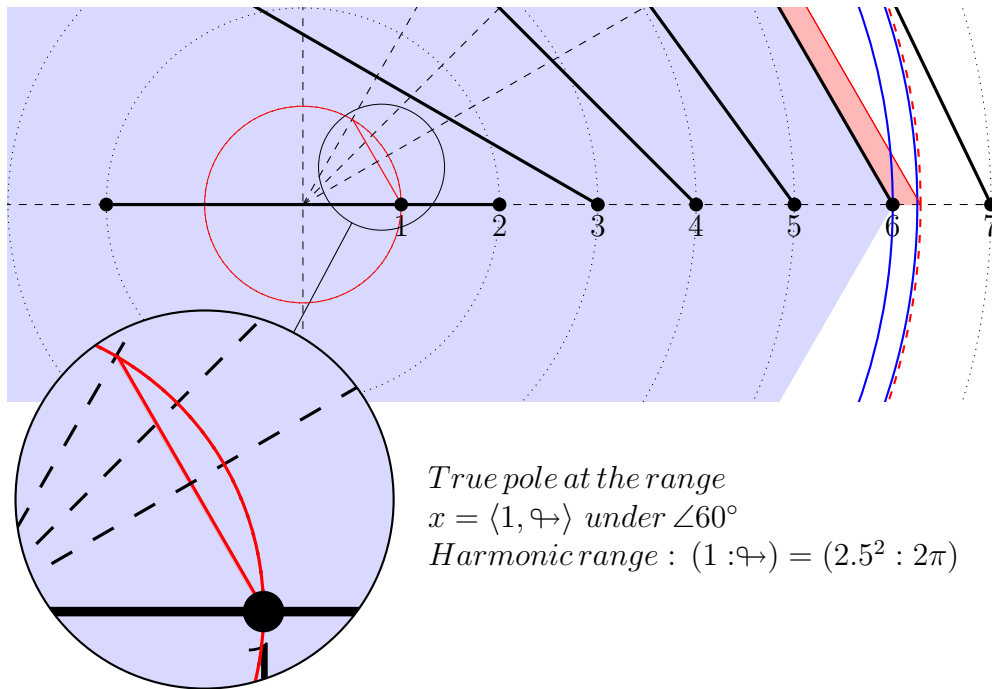


Figure 7.4: QGF natural state normalized pole

the C_{box} , labeled the harmonic range $\{1, \frac{1}{2}, \frac{1}{3}, \frac{1}{4}, \frac{1}{5}, \dots\}$ because that shaded area only holds $\frac{1}{n}$, the first chord of each n-gon. Each coordinate in the range $x = [6, 2\pi]$ is a radius for a hexagon with radius x and chord size x. In figure 7.3 x-coordinate is normalized to $C_{box}x \forall n \rightarrow x = \frac{2n \times \sin(\frac{2\pi}{2n})}{6} = [1, \frac{\pi}{3}]$ which is the range for column $\frac{cl_n}{cl_6}$, table 7.1 for $n = 6$ to $n = \infty$. The question is how to confine the infinite set of chords to C_{box} , and more pressing (no pun intended), how to fit for example a 10-gon in a 6-gon box. Compression is the answer to surplus chords , in table 7.2 the column n starts at n=6. In their geometric identity all chords for $n \geq 7$ can be inscribed n times at x=n. The chords for $n \leq 6$ that are part of the same set do not fit any other x-coordinate because the QGF framework is designed this way, absolute position, absolute size, each chord represents a unique coordinate. The column x_n in table 7.2 lists the calculated length of the chords at their designated geometric x coordinate, starting with $x_n = 6$ and thereafter the chords get progressively larger. The chord at $n = \infty$ is exactly 2π and allows for a hexagon with radius $r = 2\pi$ to fit inside the pole. This means that each x_n fits the C_{box} as hexagon at coordinate x_n . The column ρ_n lists the normalized x_n and column $\frac{1}{6}n$ lists how many such chords are available for coordinate x_n . Column “surplus” shows the amount of chords the local hexagon does not allow for if

Table 7.2: Chord length and relative density

n	$x_n = 2n \times \sin\left(\frac{2\pi}{2n}\right)$	$\rho_n = \frac{x_n}{x_6}$	$\frac{1}{6}n$	surplus
6	6	$1 = \frac{6}{6} = \frac{24}{24}$	$1 = \frac{6}{6}$	0
7	6.0743723476	1.012395391	$1\frac{1}{6} = \frac{7}{6}$	1
8	6.122934918	1.020489153	$1\frac{2}{6} = \frac{8}{6}$	2
9	6.15636258	1.02606043	$1\frac{3}{6} = \frac{9}{6}$	3
10	6.180339887	1.030056648	$1\frac{4}{6} = \frac{10}{6}$	4
11	6.198116251	1.033019375	$1\frac{5}{6} = \frac{11}{6}$	5
12	6.211657082	1.03527618	$2 = \frac{12}{6}$	6
13	6.2222072771	1.037034545	$2\frac{1}{6} = \frac{13}{6}$	7
14	6.230586151	1.038431025	$2\frac{2}{6} = \frac{14}{6}$	8
15	6.237350725	1.039558454	$2\frac{3}{6} = \frac{15}{6}$	9
16	6.242890305	1.040481717	$2\frac{4}{6} = \frac{16}{6}$	10
∞	2π	$\frac{\pi}{3}$	$\frac{1}{6}$	\mathbb{N}

not expressed as density/compression factor $\rho_n = \frac{x_n}{x_6}$. Each chord is part of a hexagon representing a snare compressed into to n-6 integer parts that define the harmonic to which the snare is tuned. In fact there are n radii that define a circumference behaving like a “particle in a box” configuration. Figure 7.5 shows a particle in a box and quantum harmonic oscillator configuration.

The n-chords $n \geq 6$ exist on their own unique radius between $x=6$ and $x=2\pi$. For each radius the resulting chord length is unique, $(\forall n > 6) (\exists! x \in \mathbb{R}) \left(\frac{2\pi}{x} \in \langle 6, 2\pi \rangle \right)$. The first possible fit is a hexagon, the radius defines the chord length and hence the compression factor. This sets up a stack of hexagons that in the surplus chords mimic the configuration of a quantum harmonic oscillator with energy level n_{surplus} . The layers are tuned to the integer surplus for each hexagon, see table 7.2, but that integer surplus defines n-chords that are unique real values $x_n = 2n \times \sin\left(\frac{2\pi}{2n}\right)$. E.g. The 7-chord projects geometrically beyond $x = 2.5^2$. The 7-chord has a length of $cl_7 = 14 \times \sin\left(\frac{2\pi}{14}\right) \approx 6.074372348$, that is, all 7 chords of them, but only 6 chords will fit the circumference at $x = 6.074372348$, the remaining chord (wave) can be envisioned as bouncing between the walls forming a standing wave, see figure 7.5, first level. The largest n-gon in the QGF that fits the circumference is the 6-gon, this is the lowest energy state equivalent in a physical setting, fits snug without surplus to bounce around. Given a repository of potential with a infinitely hard rigid border, the ultimate particle in a box example must be the universe itself.

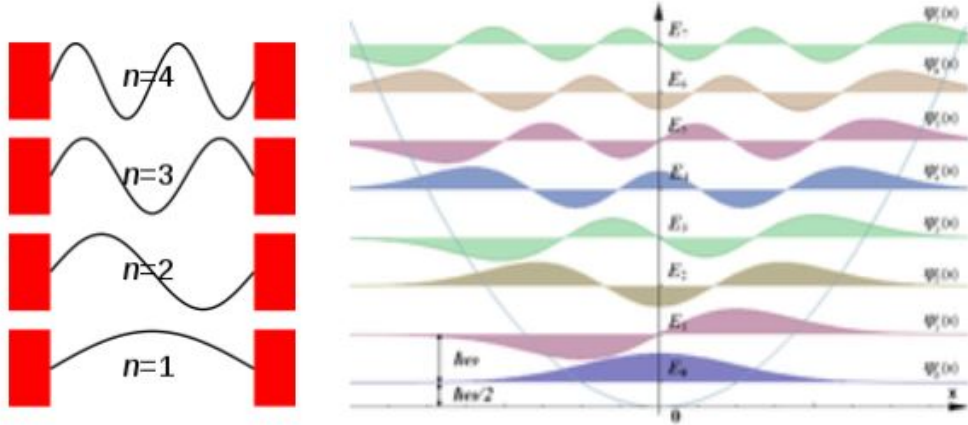


Figure 7.5: Particle in a box and Harmonic oscillator

7.4 Prime interference

The surplus as listed in table 7.2 is at first glance represented by the set of Natural numbers \mathbb{N} , but column x_n tells a different story. In fact it is not even a triangular number set because each diagonal has n copies of column x_n , as it should because the diagonals represent all the chords of the associated n -gon.

$$\begin{bmatrix} x_7 \\ x_6 & x_7 \\ x_5 & x_6 & x_7 \\ x_4 & x_5 & x_6 & x_7 \\ x_3 & x_4 & x_5 & x_6 & x_7 \\ x_2 & x_3 & x_4 & x_5 & x_6 & x_7 \\ x_1 & x_2 & x_3 & x_4 & x_5 & x_6 & x_7 \end{bmatrix} \quad (7.12)$$

Using the analogy of a De Broglie wave we can envision each diagonal to represent a string of specific density ‘surplus’. Like tuning a snare on an instrument the ‘surplus’ can be envisioned as a measure of tension on the string. Note that in abstract geometric sense there is no such thing as a C_{box} , all n -gons occupy their natural coordinate, ‘fit snugly’ and have no ‘surplus’ chords. The relative density is given by the quotient $\rho_n = \frac{x_n}{x_6}$ and of vital importance. Unlike $n \in \mathbb{N}$ the surplus consists of values that are not unit values but are more prime-like. It is as if putting the primes in one to one correspondence with the natural numbers, but not by assigning a number, instead grouping those primes in n copies, as in matrix [eq:chord-

diagonal-matrix-prime].

$$\begin{bmatrix} 17 \\ 13 & 17 \\ 11 & 13 & 17 \\ 7 & 11 & 13 & 17 \\ 5 & 7 & 11 & 13 & 17 \\ 3 & 5 & 7 & 11 & 13 & 17 \\ 2 & 3 & 5 & 7 & 11 & 13 & 17 \end{bmatrix} \quad (7.13)$$

This does not seem very useful, but equation [eq:chord-diagonal-matrix] is in fact analogues to this arrangement. The set of chords within a n-gon are equivalent but differ from all other chords in the QGF. The hexagonal structure splits those n-chords per diagonal over 6 chords and gives the relative density ρ_n for each diagonal, forming a string with a specific density. This specific density in physical sense is of vital importance, the resonance frequencies of such ‘strings’ can be equated to the set of prime numbers among the Natural numbers , each chord acts like a snare uniquely tuned for the n-gon. The comparison with prime numbers is a valid one, be it that every hexagon consists of 6 chords of that specific density. Naively one could make the comparison that electrons, all possessing the same set of properties could be modeled by a n-gon of the size n-electrons in the universe. The QGF is broader than representing one singular set, a less naive representation is forthcoming. All being well, but can the assumption of a repository of potential structured like the QGF be verified in natural systems.

7.4.1 Observations

This specific density is probably linked to observed features like present in hexagonal basalt, the fracture pattern of gradually dried mud planes or for instance the hexagonal features at the north pole of Saturn. A volatile environment comes slowly to rest and at certain point the system organizes into an equilibrium. Mud flats dry out faster than a few $1000m^3m^3$ of basalt cools down, the hexagonal structure is more obvious in columnar basalt than in the crack pattern of a mud plane. The specific pattern at Saturn’s north pole exists in a rather volatile atmosphere as the pattern is thought to be caused by jet streams and can be modeled to appear in simulations of atmospheric conditions. The more granular the subset, the less obvious the hexagonal equilibrium. Recognizing any odd pattern is part of being human, so we need a process to connect the dots. Geometrically we can appreciate numerical indicators that might be labeled as “density” , but a label does not cause behavior.

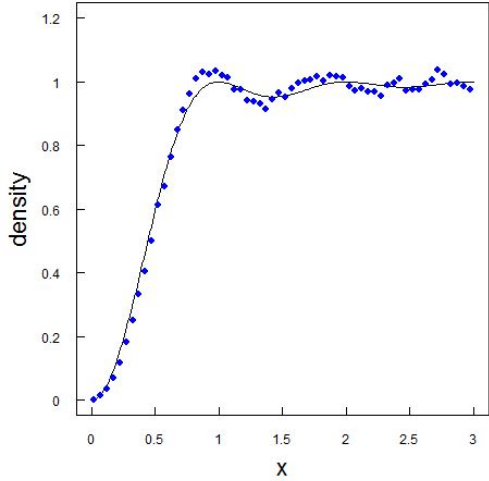


Figure 7.6: Pair correlation numerical calculation by Odlyzko

7.5 Geometric, density dependent primes

No such thing as abstract density, but in a physical system any variation in density can cause “strings” to match density with adjacent “strings” (hexagons) in the C_{box} lattice. A propagating wave on one n-gon can reroute, either temporarily or periodically during density fluctuations. This dynamic enables strings that in the base state differ in density to transfer potential, to and fro notably quantified in character. Of course for something to fluctuate it needs to exist. Particle accelerators collide blobs of energy, those do exist, scientist wack those blobs and study the way the energy dissipates. But what do those “blobs” consist off is the question we hope to answer. The link between the abstraction of chords and physics can be made via the pair correlation function.

7.5.1 Pair correlation

In 1972 at the Institute of Advanced Study Freeman Dyson and Hugh Montgomery compared notes. Hugh Montgomery found that $1 - \left(\frac{\sin(\pi x)}{\pi x}\right)^2$ is the theoretical prediction for two-point correlations in the distribution of the zeros of the Riemann zeta function. According to Freeman Dyson $1 - \left(\frac{\sin(\pi x)}{\pi x}\right)^2$ states exactly the pair-correlation for the eigenvalues of a random Hermitian matrix and for the energy levels in a heavy nucleus like U-238.

Figure 7.7 shows two series. The upper series simply plots the relative

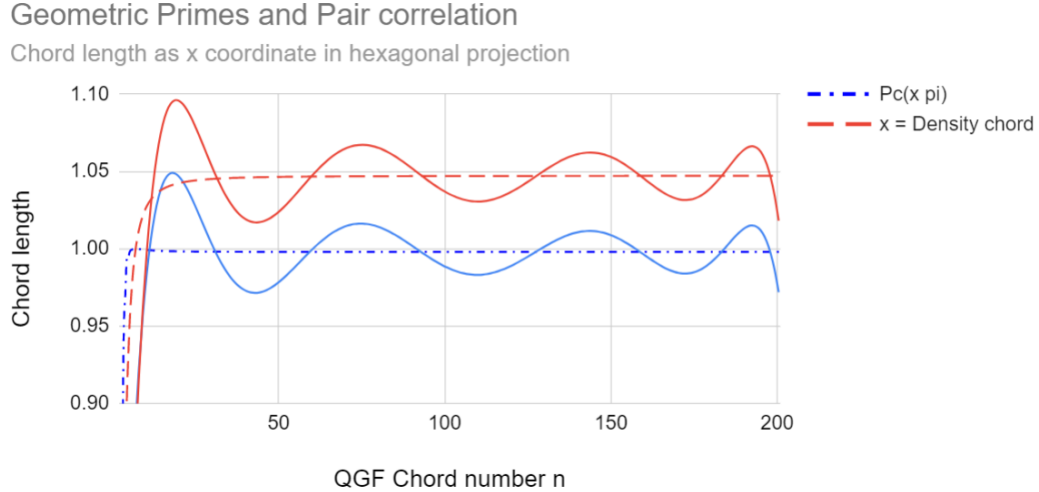


Figure 7.7: Geometric Primes and Pair correlation

density ρ_n from the normalized chord length $\forall n > 0 \rightarrow x = \frac{2n \times \sin(\frac{2\pi}{2n})}{6}$. This is an absolute value which in the physical implementation of the QGF is the x-coordinate of the hexagon shaping ‘the box’ that the n-chords project into. The bottom series inputs the $x = \frac{2n \times \sin(\frac{2\pi}{2n})}{6}$ into the Montgomery/Dyson pair-correlation formula $1 - \left(\frac{\sin(\pi x)}{\pi x} \right)^2$. Clearly $1 - \left(\frac{\sin(\pi x)}{\pi x} \right)^2$, seems to model the magnitude of the chords in the range C_{box} . The limit for $\rho_n = \frac{\pi}{3} = 60^\circ$ represents the equilibrium, passing ρ_n to the pair correlation function yields $\rho_n = \frac{\pi}{3} \rightarrow x = 1 - \left(\frac{\sin(\rho_n)}{\rho_n} \right)^2 \approx 0.316020104$. If we assume x equivalent to area $A \approx 0.316020104\dots$ then we can derive the associated context of the projection plane A_\square :

$$\begin{aligned}
 a &= \sqrt{A} = 0.5622117132\dots \\
 r_q &= \frac{0.5}{a} = 0.8893446869 \\
 r_x &= \frac{r_q}{\sqrt{0.96 \times (\dagger \rightarrow)^{-1}}} = 0.9100901707 \\
 SA &= 4\pi (r_x)^2 = 10.40827388 \\
 \Delta\pi^2 &= \frac{SA}{\pi^2} \approx 1.054578629 \\
 h &= 2\pi \times \Delta\pi^2 \approx 6.62611295
 \end{aligned} \tag{7.14}$$

Planck’s constant as discrepancy in surface area seems significant, we found

for the fractal argument for zeta (section ??) $T_h = 0.9^{-1}$ as the equilibrium for volume and surface area, a value $c_h = \sqrt{1\frac{1}{4}}$ for the hexagonal chords and here a rather precise value without using a fudge factor.

7.6 Looking back from infinity

In figure 7.8 the second quadrant on the left shows some sample angles and the square of the sine function J to M. The right side shows two of those, $M = \square EBGH$ and $K = \square ABCD$. The square of the sine function for M and K shows the equilibrium in the shared diagonal $\overline{BHD} \rightarrow B_x = 1\frac{1}{2} = 0^\circ, H_x = \sqrt{\frac{3}{4}} = 30^\circ, D_x = \frac{1}{2} = 60^\circ$. This is equivalent to $60^\circ \times \frac{3}{2} = 90^\circ \rightarrow \overline{BHD} \rightarrow B_x = 1 = 0^\circ, H_x = \frac{1}{2} = 45^\circ, D_x = 0 = 90^\circ$

7.6.1 Pair correlation as function of volume

The Montgomery/Dyson pair-correlation formula $1 - \left(\frac{\sin(\pi x)}{\pi x}\right)^2$ and the geometric primes are in intimate relation (see figure 7.7). How intimate becomes clear if we observe the following:

$$\begin{aligned} \rho_\infty &= \frac{\pi}{3} \\ p_{cor} &= 1 - \left(\frac{\sin(\rho_\infty)}{\rho_\infty}\right)^2 = 1 - \left(\sqrt{\frac{3}{4}} \times P_*\right)^2 \\ p_{cor} &= 1 - \frac{1\frac{1}{8}}{\zeta(2)} \rightarrow 1 - \frac{V}{\zeta(2)} \\ 1\frac{1}{8} &\rightarrow \left(1\frac{1}{8}\right) \times T_h = \left(1\frac{1}{4}\right) \end{aligned} \tag{7.15}$$

We are right back at volume over zeta, equation [eq:volume over zeta], but now on the other side of a primorial cycle indicated by P_* . Here we truly look back from infinity, $1\frac{1}{8} = \frac{9}{8}$ is in fact $V_1 + V_0 = \frac{8}{9} \times \frac{9}{1} = V_{current}$, or simply the scale invariant state of volume. This must be true because $(1\frac{1}{4}) = (1\frac{1}{8}) \times T_h \equiv (c_{n=1} = c_h)$, see figure 5.6. This indicates the QGF correctly models a universal first principle for both abstract number sets and physical implementation thereof.

$$x = \frac{1}{6} (2n \times \sin(\frac{2\pi}{2n})) \text{ and } P_{cor} = 1 - \left(\frac{\sin(\pi x)}{\pi x} \right)^2$$

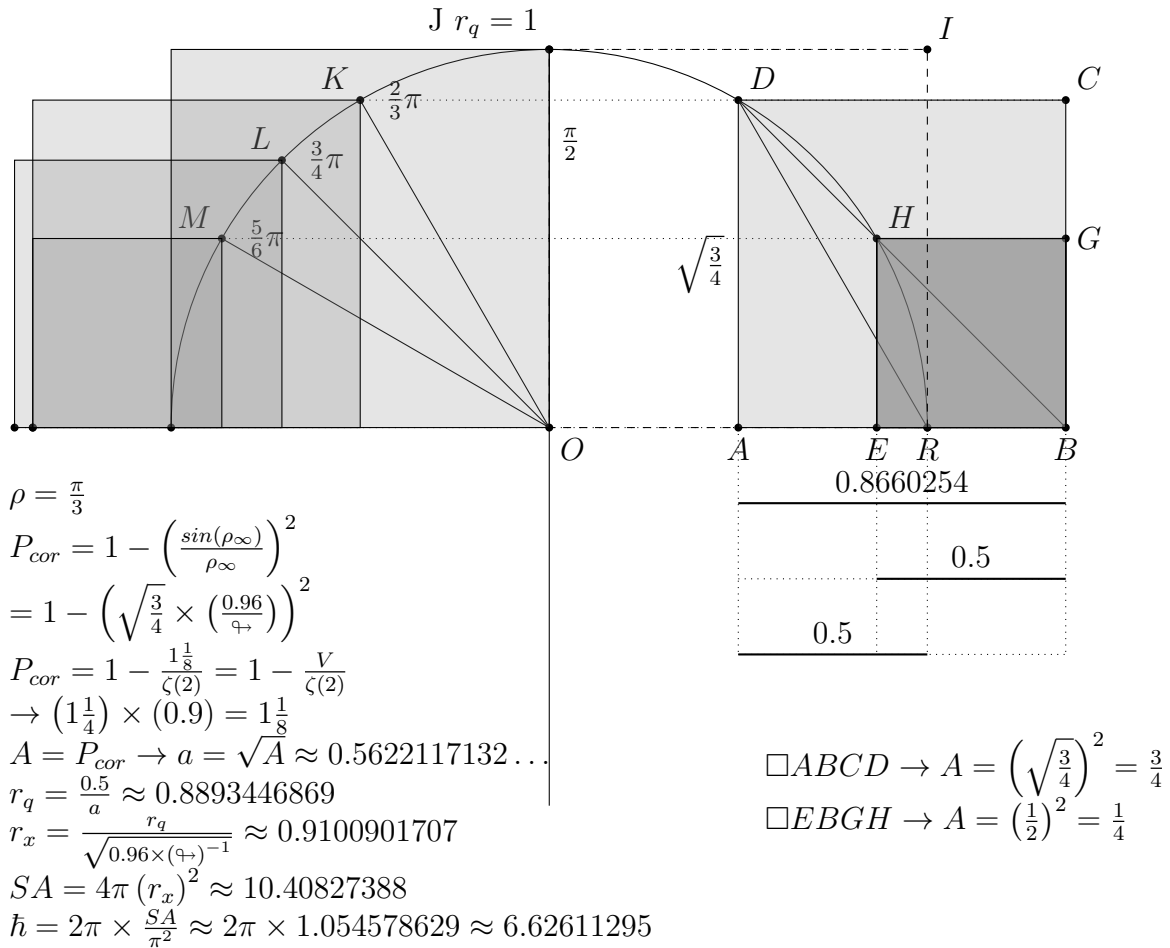


Figure 7.8: Pair correlation proportional chord

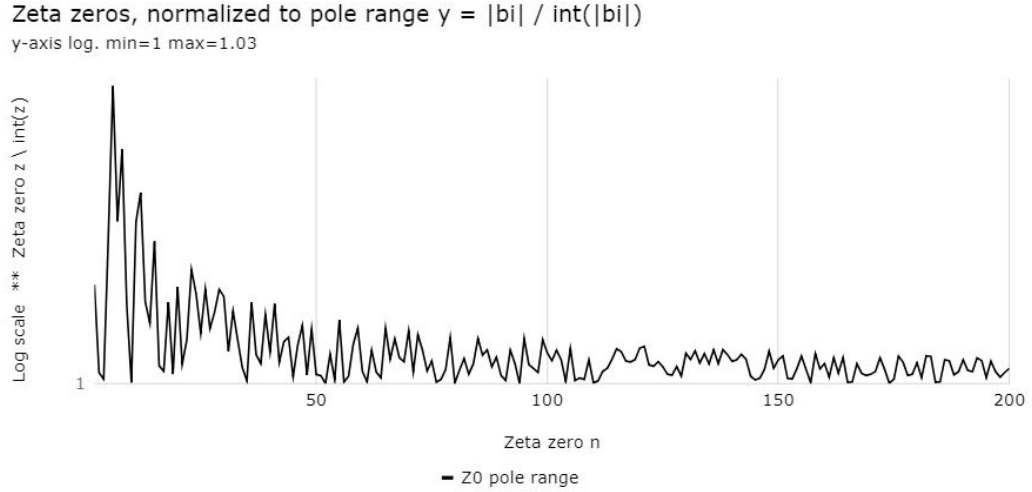


Figure 7.9: Zeta zeros normalized to pole range

7.7 Zeta zero to proportional QGF chord

To bring the zeta zeros into the range C_{box} one can simply apply $y = \frac{|bi|}{\lfloor |bi| \rfloor} = 1 + \epsilon$. Figure 7.9 shows the oscillatory character of the normalized values. This characteristic oscillation is recognizable in the logarithmic integral function $\sum_{\rho} Li(x^{\rho})$ summing over the non trivial zeros. We need not go there, we will make sense of the zeta zeros in terms of the QGF.

If the non trivial zeros from the complex analysis can be localized in the QGF schema, then the modulus $|a| = \sqrt{a^2 + bi^2}$ is the prime candidate (maybe pun intended). Table 7.3 lists the first 25 zeta zeros, up to 8 decimals will suffice for constructing the model, but it will become clear that the decimal expansion can not be ignored as the sample set increases. There are two sets of columns, “Complex” shows the real, imaginary and the derived modulus in their familiar form, set “ C_{unity} Hexagonal unity chords” is where the complex modulus is normalized. The normalization assumes the zeta zeros to represent D_4 values en reduces them to D_1 by taking the fourth root of the modulus, $d = \sqrt[4]{|a|}$ and then normalize this to $d \rightarrow C_{box}$ by $x = \frac{\sqrt[4]{|a|}}{\lfloor \sqrt[4]{|a|} \rfloor}$. The list makes no use of any sorting, the zeta zeros are listed in order of appearance and as such match the structure of the QGF. The zeta zeros $\forall n \rightarrow z_n = \{z_1, z_2, z_3, \dots, z_\infty\}$ do not represent individual $n \in \mathbb{N}$ from the set of natural numbers but are sets of n-zeros for each $n \in \mathbb{N}$ as represented in matrix [eq:chord-diagonal-matrix] and [eq:chord-diagonal-matrix-prime]. In table 7.2 the column level starts with $L_{n=1} = 0$ for 1 zeta

Table 7.3: Non trivial zero to Unity chord

n	a	Complex		d	C_{unity}	C_{box}
		bi	c (modulus)			
$Real$	$Zero$ (imaginary)	$ a = \sqrt{a^2 + bi^2}$	$\sqrt[4]{ a }$		$x = \frac{\sqrt[4]{ a }}{\sqrt[4]{ a }}$	
1	0.5	14.13472514	14.14356585	1.939276475	0	1.939276475
2	0.5	21.02203964	21.02798494	2.141407968	1	1.070703984
3	0.5	25.01085758	25.01585491	2.23642242	1	1.11821121
4	0.5	30.42487613	30.42898433	2.348669263	1	1.174334631
5	0.5	32.93506159	32.93885672	2.395670749	1	1.197835375
6	0.5	37.58617816	37.5895037	2.476091264	1	1.238045632
7	0.5	40.91871901	40.92177373	2.529231677	1	1.264615838
8	0.5	43.32707328	43.32995822	2.565647973	1	1.282823987
9	0.5	48.00515088	48.0077547	2.632254329	1	1.316127165
10	0.5	49.77383248	49.77634377	2.656169272	1	1.328084636
11	0.5	52.97032148	52.97268124	2.697820118	1	1.348910059
12	0.5	56.4462477	56.44846215	2.741025202	1	1.370512601
13	0.5	59.347044	59.34915022	2.775579213	1	1.387789606
14	0.5	60.83177852	60.83383334	2.792777236	1	1.396388618
15	0.5	65.11254405	65.11446377	2.840660727	1	1.420330364
16	0.5	67.07981053	67.08167396	2.861877056	1	1.430938528
17	0.5	69.54640171	69.54819905	2.887828992	1	1.443914496
18	0.5	72.06715767	72.06889215	2.913647184	1	1.456823592
19	0.5	75.7046907	75.70634183	2.949735435	1	1.474867717
20	0.5	77.14484007	77.14646038	2.963664248	1	1.481832124
21	0.5	79.33737502	79.33895055	2.984500204	1	1.492250102
22	0.5	82.91038085	82.91188849	3.017548102	2	1.005849367
23	0.5	84.73549298	84.73696815	3.03401854	2	1.011339513
24	0.5	87.42527461	87.42670439	3.057813734	2	1.019271245
25	0.5	88.80911121	88.81051871	3.069842552	2	1.023280851

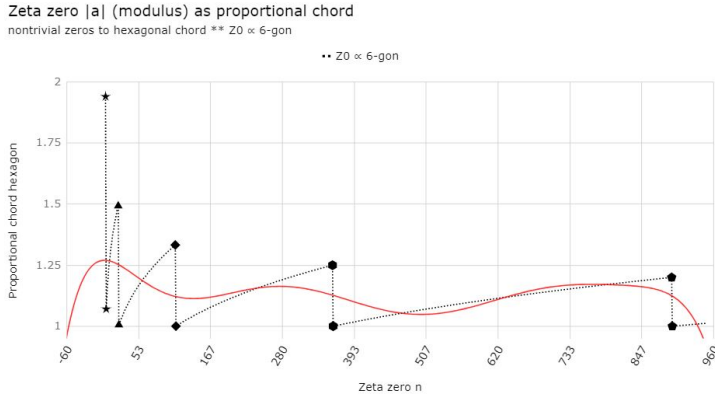


Figure 7.10: Zeta zero modulus as proportional chord

Table 7.4: Non trivial zeros - Levels

Level	ζ zero index			$z_{max} \in T_n$	$z_n \propto$ chord	
	z_{min}	z_{max}	Δz	$n \in \mathbb{N}$	z_{min}	z_{max}
0	0	1	1	1	0	1.939276475
1	1	21	20	6	1.070703984	1.492250102
2	22	111	90	14.41	1.005849367	1.332429741
3	112	359	258	26.3	1.000372059	1.24963489
4	360	894	535	41.79	1.000407544	1.199853089
5	895	—	—	—	1.000154518	—
∞				\mathbb{N}	1	1

zero, then $L_{n=2} = 1$ continues on to $L_{n=21} = 1$ and $L_{n=22} = 2$, the level simply counts of ranges of increasing $x = \frac{\sqrt[4]{|a|}}{\sqrt[4]{\sqrt[4]{|a|}}}$ in order of appearance in the list of zeta zero. In this configuration we find again a upper bound and lower bound, and a very distinct pattern in the zeta zeros, see figure 7.10. Zeta zero modulus as proportional chord

From left to right the first step indicated with \star mark the first and the second zeta zero. Next indicated by \blacktriangle , the zeros Z_{21} and Z_{22} , then by \diamond the zeros Z_{111} and Z_{112} . Table 7.4 lists the first 4 complete levels.

7.7.1 Stable QGF configuration

From those zeros only indices $Z_1 \rightarrow n = 1$ and $Z_{21} \rightarrow n = 21$ are elements of the set of triangular numbers, all other Z_n land somewhere between triangular numbers. The number $T_6 = 21$ as culmination of the first cycle has

great significance for the QGF. $T_6 = 21$ is the number of chords (including for $n=1$) that project inside the pole, $1 + 2 + 3 + 4 + 5 + 6 = 21$. From zero Z_{21} to zero Z_{111} is exactly 90 zeta zeros. 111 is not a triangular number, the triangular numbers nearest to 111 are $T_{14} = 105 \Delta - 6$ and $T_{15} = 120 \Delta 9$. This positions Z_{111} at a $\frac{6}{9}$ ratio. This is recognizable in the $\zeta(2)$ configuration of the triangular plane and shows the mechanism of the continuously decreasing surface area encoded in the zeta zeros. The area inside the QGF pole is represented by the 21 zeta zeros in level 1 and therefore all chords that project inside the pole for every scale invariant natural state of the QGF are represented.

7.7.2 Interlaced zeta and repulsion

Each of the levels has a fixed number of zeros and a fixed range in which the zeros project, this is illustrated in figure 7.11. It is in the projection of level 1, $Z_2 L_1 x = 1.070703948 \rightarrow Z_{21} L_1 x = 1.492250102$ that the characteristic level repulsion, pattern of spacing between zeta zeros begins to show. Interlaced zeta zeros The progression of the levels as seen in figure 7.10 shows that the lower range becomes progressively denser. Level 2 $Z_{22} L_2 x = 1.005849367 \rightarrow Z_{111} L_2 x = 1.332429741$ only starts intruding into Level 1 at $Z_{33} L_2 x = 1.072498831$ as it projects past $Z_2 L_1 x = 1.070703948$.

7.7.3 Naturally in pieces

All the natural numbers are interlaced in parts. For every $n \in \mathbb{N}$ there are n zeta zeros representing that number that diffusely interlace on the real axis. The number of zeta zeros is an area $A = \lim_{n \rightarrow \infty} T_n \rightarrow \frac{1}{2} N^2$ and each zero is an area the size of $\frac{1}{n}$, e.g. to represent the number $n=7$, 7 uniquely sized Z_0 project on the real axis, not as a continuous string of zeros, but spread out as dots on a rubber sheet, like galaxies spreading with the expansion of space. As shown in figure ?? this is not a loosely formulated analogy, it is a quite accurate description of the process involved. The figure shows the geometric spreading of zeta zeros where the first zero on the left of level 1 is from number $n = 2 \rightarrow Z_2 = 1.070703984$. The eight squares on level 2, making up the range for number $n = 8 \rightarrow Z_{29} = 1.051002249$ to $Z_{36} = 1.089959968$ enclose also one of two zeros for number $n = 2 \rightarrow Z_2$ but not $n = 2 \rightarrow Z_3$.

In fact there are more numbers interlaced in the range for $n = 8$ ■. From the first 950 zeta zeros (up to 9 decimal places suffices in this region), 134 zeros spread over the first 4 levels are included in the range $n = 8 \rightarrow Z_{29}$ to Z_{36} .

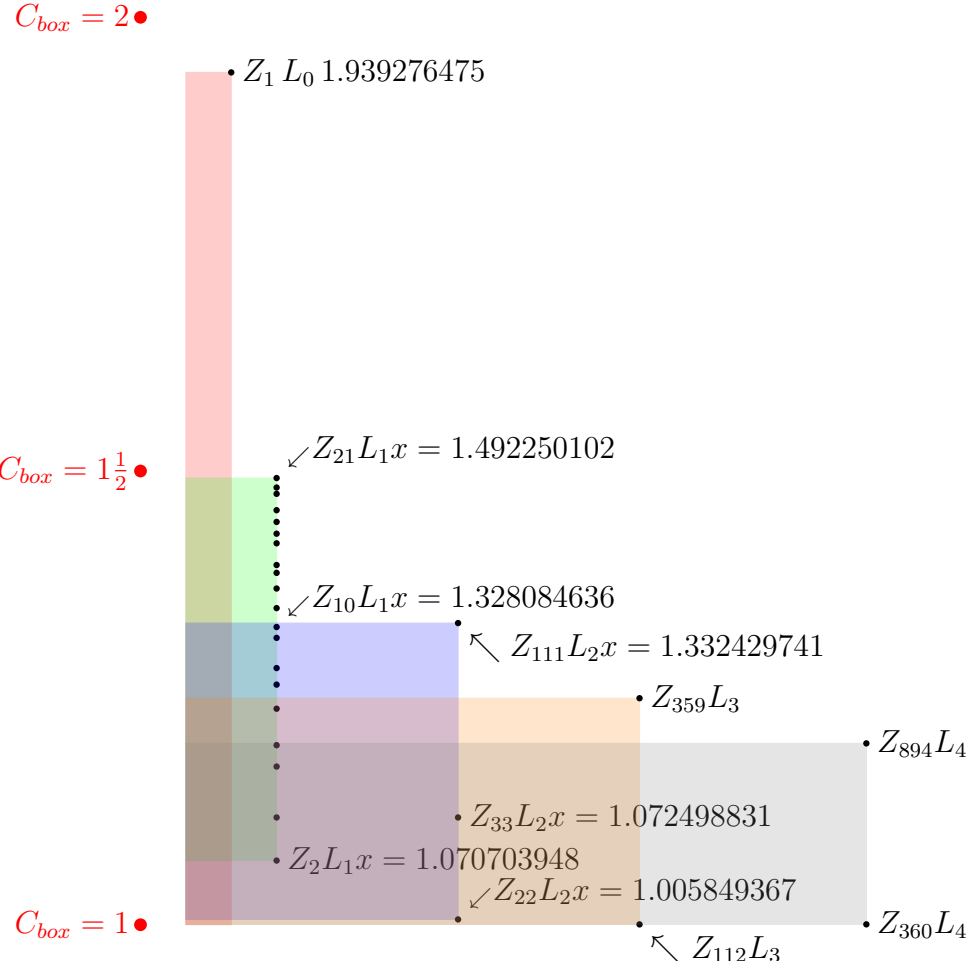


Figure 7.11: Interlaced zeta zeros

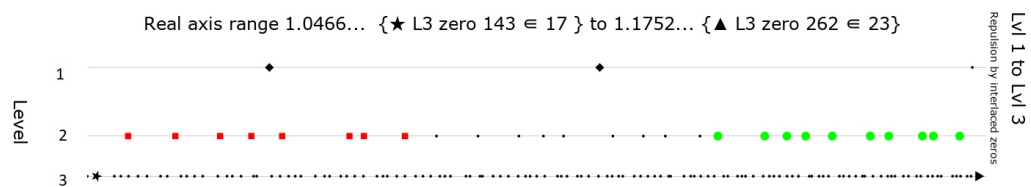


Figure 7.12: Interlaced zeta zero detail

- 1 zero from level 1, our $n = 2 \rightarrow Z_2$
- 8 zeros from the second level (obviously)
- 32 zeros from level 3
- 93 zeros from level 4

All between $n = 8 \rightarrow Z_{29}$ to Z_{36} , see the diagonal indicated by \star in matrix [eq:n-in-pieces].

$$\left[\begin{array}{ccccccccc} z_{46} & & & & & & & & \\ z_{37} & z_{47} & & & & & & & \\ \star z_{29} & z_{38} & z_{48} & & & & & & \\ z_{22} & \star z_{30} & z_{39} & z_{49} & & & & & \\ z_{16} & z_{23} & \star z_{31} & z_{40} & z_{50} & & & & \\ z_{11} & z_{17} & z_{24} & \star z_{32} & z_{41} & z_{51} & & & \\ z_7 & z_{12} & z_{18} & z_{25} & \star z_{33} & z_{42} & z_{52} & & \\ z_4 & z_8 & z_{13} & z_{19} & z_{26} & \star z_{34} & z_{43} & z_{53} & \\ z_2 & z_5 & z_9 & z_{14} & z_{20} & z_{27} & \star z_{35} & z_{44} & z_{54} \\ z_1 & z_3 & z_6 & z_{10} & z_{15} & z_{21} & z_{28} & \star z_{36} & z_{45} & z_{55} \end{array} \right] \quad (7.16)$$

This does not mean that the distribution is solved by the depiction of levels in matrix [eq:n-in-pieces] because as seen $n_2\text{gon} \rightarrow Z_2$ wedges between $n_8\text{gon} \rightarrow Z_{32} < Z_2 < Z_{33}$ and the second zero of $n_2\text{gon} \rightarrow Z_3$ does not. The diagonals must depict a unique sequence of area that can be equated to a natural number, but as seen that area gets stretched out, fragmented beyond recognition. But seemingly not ad infinitum so, it is like a shifting panel of affected area (figure 7.11). What happens is that when a larger range is selected, observed granularity increases proportionally. In fact we know of such a property occurring in the physical realm and we alluded to it before, it is the expansion of space itself. It seems that with the expansion of space the energy content does not get diluted, local conditions remain stable while space expands into oblivion. What is proposed here is not to interpret the measured effect as “expansion of space”, but as artifact of observing space from a regressing surface area. One that continuously decreases its radial distance to the singularity at the center, but expressed as a phase shift that enforces local parameters to maintain stability. e.g. similar to the constant temperature at the melting point of water ice, or boiling point of water. Selecting a greater subset by application of some arbitrary coordinate system increases local granularity relative to that coordinate system. This intuition seems confirmed by figures 7.10 and 7.11 as it is clear that the levels condense ever increasing sets of zeta zeros in proportionally compacter stretches

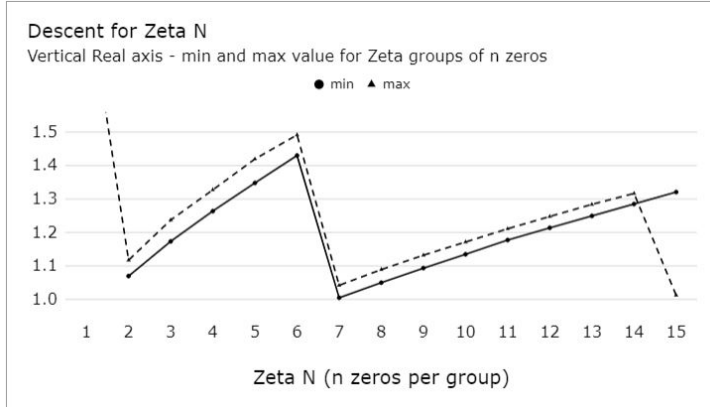


Figure 7.13: Decent for Zeta N

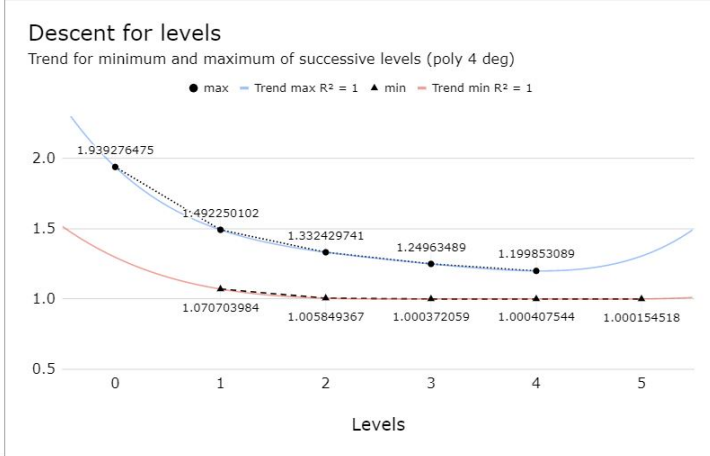


Figure 7.14: Decent for levels

of the real line (y-axis), see figures 7.13 and 7.14. From a perspective of scale in variance each level must in some sense be the fractal sibling of the previous level. This implies that the stable configuration, section [Stable-QGF-configuration], holds the complete set of prime numbers, $\{2, 3, 5\}$ and all other primes are in some sense ghost of future levels.

Not “ghosts” in the sense of figments of the imagination, we can all count and apply the sieve of Eratosthenes, but like a mirage projects a distant image in the dessert. There is something projected that definitely does exist, only not there were its images appears to be. Figure 7.14) implies that all cycles lay within the previous cycles, where figure 7.11 provides kind of a mirage where each level seems to project some distinct part of the continuum. It is a bit counter intuitive but the things being stuffed are not numbers, what

is stuffed are markers of spaces between numbers, as if becomes apparent that those spaces are conglomerates of a finer grained subset. What seems to be the case is that prime numbers are in some sense coordinates on the M-brane mono-surface from where the horizon encloses rational fractions of the available space. It seems that prime numbers are defined by being rational multiples of zeta zeros, and not just rational multiples, but groups of multiples in specific order that exactly match some set of units shaping some exact curvature of (prime) unit surface area. The conclusion must be that although $n \in \mathbb{N}$ are seen as the sum of equal partitions, $1 + 1 + 1 + 1 \dots$ each 1 of them is one of a kind and has a specific size (area / curvature). E.g. $(2 - 1) \neq (3 - 2) \neq (4 - 3) \neq (5 - 4) \dots$ Those spaces together are responsible for the expanding surface area, filling the diagonal of the triangular plane $c = \sqrt{2 \times \lim_{n \rightarrow \infty} T_n} \sqrt{2}$ level by level, each level unique in number and spread of zeta zeros.

7.7.4 Prime like distribution for all n

This of course means that the zeta zeros by themselves say nothing special about the distribution of primes. Each level spreads the represented natural numbers out over that level in n parts. E.g $L_1 = \{2 + 3 + 4 + 5 + 6\} = 20$ zeros. The cumulative effect is the apparent accretion of surface area as found in the projection plane model. The zeta zeros by their triangular distribution represent an area $A = \lim_{n \rightarrow \infty} T_n \rightarrow \frac{1}{2} \mathbb{N}^2$, the area fills up over the diagonal as $\{Z_0\}, \{Z_1, Z_2\}, \{Z_3, Z_4, Z_5\}, \{Z_6, Z_7, Z_8, Z_9\}, \dots$ see matrix [eq:n-in-pieces]. Returning to the triangular plane and its diagonal $c = \sqrt{2 \times \lim_{n \rightarrow \infty} T_n} \sqrt{2}$, at the end only \mathbb{N} remains but yes, the zeta zeros all line up on that diagonal, because in the triangular projection all of them lay on the diagonal of the triangular plane. In the limit the whole \mathbb{N} of them, any natural number, prime or not. QED for the Riemann hypothesis, at least for as far as the QGF goes. It is a bit frustrating to look at this picture and realize that the nth (prime) number is distributed over that area in n parts, infinitely diffuse in spread, how many time one wonders “where the (expletive) does that number live”. The geometric primes as n-gon are as prime as it gets. But how to make the connection between prime numbers having a specific location in \mathbb{N} , the distinct x coordinate for the geometric primes and the, ever shifting, distribution of the zeta zeros. One answer is that the zeta zeros are even more prime than the geometric primes, literally so because $\forall n \in \mathbb{N} \exists n \times Z_n \rightarrow \#Z_n = [T_n - (n - 1), T_n]$ e.g. $n = 3 \rightarrow T_3 = 6 \rightarrow \{Z_4, Z_5, Z_6\}$, 3 zeros each representing a unique chord as we are about to see.

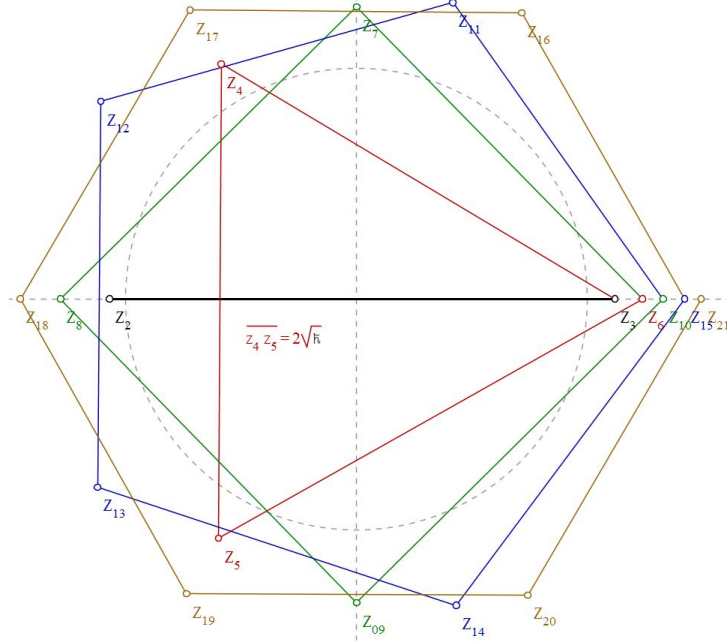


Figure 7.15: Zeta zeros walk about

7.7.5 Zetas walk about on the diagonal.

The QGF chords resemble geometric primes in abstract sense, none divides the other, each can be seen as a uniquely tuned string. The zeta zeros however do something different in the sense that they clearly define a n-gon that is not regular, but has ever increasing chord length defined by consecutive zeta zeros. Unlike the geometric chords that describe those of a hexagon, the chords represented by the zeta zeros have a slightly higher value for each converted zero. The zeros are grouped according to the triangular schema, but each zeta zero produces a unique chord length. Because of this unique chord length the zeta zeros cannot form a regular n-gon. We know however by the triangular order that they are n-gon like. One interpretation is that the deflection of the angles is as expected for an n-gon $\angle\theta = \frac{2\pi}{n}$, and thus the discrepancy in size must be due to “departing the circumscribed arc at $\angle\theta$ ” under condition of a actively shrinking radius and “landing on the circumscribed arc at $\angle\theta$ ”. This is what is modeled in figure 7.15.

The zeta zeros follow some intermediate path that seem to describe chords of a spiral that for each set add up to 360 degrees, see matrix [eq:zeta-angle-

progression].

$$\begin{bmatrix} 60_{16} \\ 72_{11} & 60_{17} \\ 90_7 & 72_{12} & 60_{18} \\ 120_4 & 90_8 & 72_{13} & 60_{19} \\ 180_2 & 120_5 & 90_9 & 72_{14} & 60_{20} \\ 360_1 & 180_3 & 120_6 & 90_{10} & 72_{15} & 60_{21} \end{bmatrix} \quad (7.17)$$

The construction of figure 7.15 is straight forward. Project the x-value, rotate anti clockwise over the associated accumulative angle and connect to the end of the previous chord. The interval between z_n progressing on the x-axis follow the harmonic series if the interval is defined to full 360° or 2π periods, $1 + 1 + 1 + 1 + 1 + \dots$. The z_n along the x-axis follow the triangular numbers $Z_n \rightarrow n = T_{index} = \frac{\text{index}}{2}(\text{index} + 1) = \left\{ 1 + \frac{1}{2} + \frac{1}{3} + \frac{1}{4} + \frac{1}{5} + \dots \right\}$

Zeta zeros walk about The angle for each z_n is deterministic because the zeta zero lives on a known n-gon. The last chord always lands on $x = z_n$, $y=0$ where the x-coordinate is simply the proportional chord C_{unity} (see table 7.3). The coordinates of the vertices for $n = 3 \rightarrow T_n = 6$ are

$$\begin{aligned} \phi(n = 3 \rightarrow T_n = 6) &\rightarrow \left[\frac{1}{n}2\pi, \frac{n}{n}2\pi \right] = \left\{ \frac{1}{3}2\pi, \frac{2}{3}2\pi, \frac{3}{3}2\pi \right\} \\ Z_n(n = 3 \rightarrow T_n = 6) &\rightarrow Z_{[T_n - (n-1), T_n]} = \{Z_4, Z_5, Z_6\} \\ Z_4(x, y) &= \left(Z_4 \times \cos\left(\frac{1}{3}2\pi\right), Z_4 \times \sin\left(\frac{1}{3}2\pi\right) \right) \\ &= (-0.5871673155, 1.017003632) \\ Z_5(x, y) &= \left(Z_5 \times \cos\left(\frac{2}{3}2\pi\right), Z_5 \times \sin\left(\frac{2}{3}2\pi\right) \right) \\ &= (-0.5989176875, 1.037355864) \\ Z_6(x, y) &= \left(Z_6 \times \cos\left(\frac{3}{3}2\pi\right), Z_6 \times \sin\left(\frac{3}{3}2\pi\right) \right) \\ &= (1.238045632, 0) \end{aligned} \quad (7.18)$$

The chord $\overline{z_4 z_5} = 2\sqrt{\hbar} \approx 2.0543531002$, is the first and largest orthogonal chord in the sequence. Planck's constant seems to define the point of equilibrium as pivoting point where the chord at infinity starts to morph into a orthogonal x-axis.

Table 7.5: Level 1 coordinate listing

n	C_{unity}	$ngon$	$chrd$	$\cos\left(\frac{idx}{ngon}2\pi\right)$	$cl \times x$	$\sin\left(\frac{idx}{ngon}2\pi\right)$	$cl \times y$
	$cl = \frac{\sqrt[4]{ a }}{\sqrt[4]{ a }}$	idx	idx	x	x'	y	y'
2	1.070703984	2	1	-1	-1.070703984	0	0
3	1.11821121	2	2	1	1.11821121	0	0
4	1.174334631	3	1	-0.5	-0.5871673155	$\sqrt{\frac{3}{4}}$	1.017003632
5	1.197835375	3	2	-0.5	-0.5989176875	$-\sqrt{\frac{3}{4}}$	-1.037355864
6	1.238045632	3	3	1	1.238045632	0	0
7	1.264615838	4	1	0	0	1	1.264615838
8	1.282823987	4	2	-1	-1.282823987	0	0
9	1.316127165	4	3	0	0	-1	-1.316127165
10	1.328084636	4	4	1	1.328084636	0	0
11	1.348910059	5	1	0.3090169944	0.4168361321	0.9510565163	1.282889702
12	1.370512601	5	2	-0.8090169944	-1.108767985	0.58778522523	0.855670579
13	1.387789606	5	3	-0.8090169944	-1.122745376	-0.58778522523	-0.8157222261
14	1.396388618	5	4	0.3090169944	0.4315078137	-0.9510565163	-1.328044494
15	1.420330364	5	5	1	1.420330364	0	0
16	1.430938528	6	1	0.5	0.715469264	$\sqrt{\frac{3}{4}}$	1.239229117
17	1.443914496	6	2	-0.5	-0.721957248	$\sqrt{\frac{3}{4}}$	1.250466634
18	1.456823592	6	3	-1	-1.456823592	0	0
19	1.474867717	6	4	-0.5	-0.7374338585	$-\sqrt{\frac{3}{4}}$	-1.27727291
20	1.481832124	6	5	0.5	0.740916062	$-\sqrt{\frac{3}{4}}$	-1.283304264
21	1.492250102	6	6	1	1.492250102	0	0

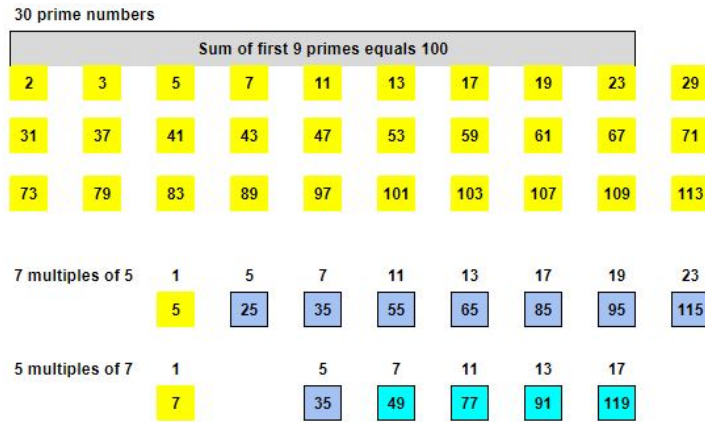


Figure 7.16: Prime number triangular core set

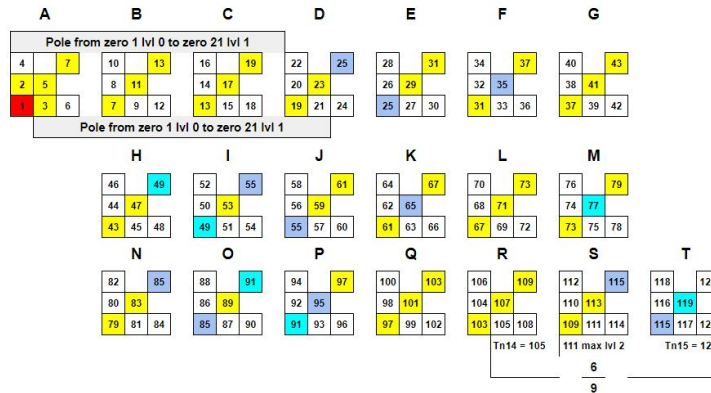


Figure 7.17: Stacking the core

7.8 Prime stretching in the projection plane

There are in total 30 primes involved in the mechanics of the projection plane model, see figure 7.16.

The prime number ‘5’ takes a pivotal role and presents itself in eighth identities, one in its original role as the prime number 5, and then consecutive as the multiples $5 \times 5 = 25$, $5 \times 7 = 35$, $5 \times 11 = 55$, $5 \times 13 = 65$, $5 \times 17 = 85$, $5 \times 19 = 95$, $5 \times 23 = 115$. Also we see 5 extra identities for prime 7, of which $7 \times 5 = 35$ is just the same as $5 \times 7 = 35$, further $7 \times 11 = 77$, $7 \times 13 = 91$, $7 \times 17 = 119$ complete the range of composites for this section. Prime numbers triangular core set The prime distribution for the triangular plane starts with the stacking of the familiar triangular plane $\frac{6}{9}$ occupied cells along the orthogonal diagonal, see figure 7.17. stacking the core

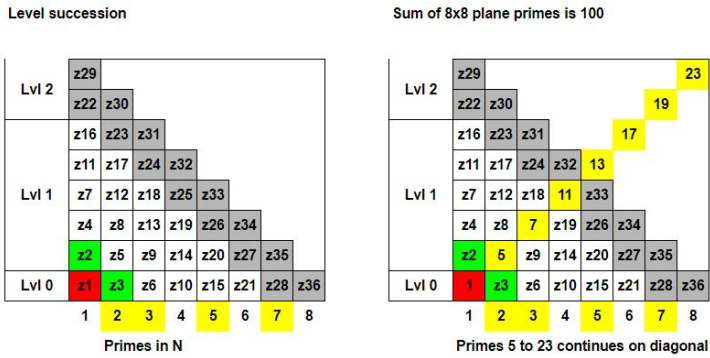


Figure 7.18: Orthogonal succession

For the configuration inside the pole 4 such $\frac{6}{3 \times 3} = \frac{6}{9}$ blocks affected area, labeled A to D are stacked along the diagonal. The total affected area $A_{AD} = \frac{4 \times \frac{6}{9}}{64} = \frac{1}{24}$. Each $\frac{6}{3 \times 3} = \frac{6}{9}$ block shows a upper right value that is there as chain link to the left lower cell of the following block, indicating the chain along the diagonal. Thus a diagonal of 7 primes plus the initial lower left 1 is formed summing up to $1 + 5 + 7 + 11 + 13 + 17 + 19 + 23 = 96$. The total of primes in this $8 \times 8 = 64$ configuration sum op to 100 (excluding the lower left 1), including primes 2 and 3 not on the orthogonal diagonal. This gives a $\frac{96}{100}$ ratio that we register as the primorial delta $P\Delta = \frac{24}{25}$. The pattern follows figure 4.9 in its stacking of affected area,

- {[1], [2, 3], [4, 5, 6]}
- {[7], [8, 9], [10, 11, 12]}
- {[13], [14, 15], [16, 17, 18]}
- {[19], [20, 21], [22, 23, 24]}

and causes the primes {5, 7, 11, 13, 17, 19, 23} to line up along the diagonal. In the next image, 7.18, on the left the ordering of the zeta zeros is superimposed on the triangular plane. On the right we find numerically a bad fit for the stack of primes to the zeta zero indices, however, the affected area did not change, merely a swapping of square units occurred. Orthogonal succession

The zeta zeros are projected in their ‘natural’ n-gon position. The columns are numbered according to the n-gon diagonals and therefor map the zeta groups to individual natural numbers. The prime numbers in the index row below (shaded yellow) do not line up to the superimposed stack of primes. The index row is there to indicate the zeta groupings and have no direct

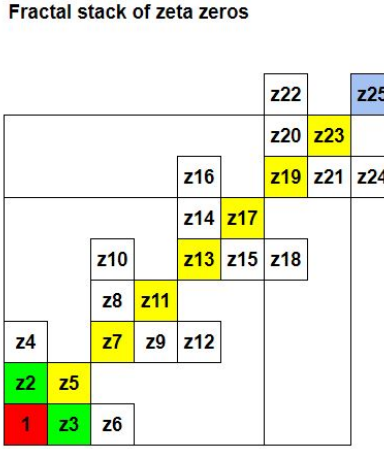


Figure 7.19: Orthogonal fractal stack zeta

relation to the stack of primes. We find the relation in the fractal argument for zeta, see section ???. The fractal stack , see figure 7.19 does project the zeros conform figure 7.17 and as such matches the indices of specific zeta zero to either a prime number or composite without obvious relation to the associated n -gon. e.g. $z_{13} \in \{z_{11}, z_{12}, z_{13}, z_{14}, z_{15}\} \rightarrow 5 - gon$. Notice that top right z_{22} , z_{24} and z_{25} project outside the 8×8 grid. Further notice that the accommodation for completing the diagonal requires expansion of the 6×6 grid by a factor $\frac{64}{36} = P\Delta \times 1.6$. Equation [eq:surface-2-area-ratio] in relation to the hexagonal equilibrium indicates how the golden ratio appears in the root of curvature, and the curvature along lines of sight postulated in section 6.0.2. Orthogonal fractal stack zeta

The consequence of the stacking is a numerical additive sequence visiting primes and composites on the diagonal $1+4+2+4+2+4+2, \dots, \{1, 5, 7, 11, 13, 17, 19, 23, (25) \dots\}$, see equation [eq:stack-additive-sequence], indicated are the composites (n) and how they break down.

$$\begin{aligned}
 1\Delta 5 &= 4 \rightarrow 2 = 5\Delta 7 \\
 7\Delta 11 &= 4 \rightarrow 2 = 11\Delta 13 \\
 13\Delta 17 &= 4 \rightarrow 2 = 17\Delta 19 \\
 19\Delta 23 &= 4 \rightarrow 2 = 23\Delta (25) \rightarrow (5^2 = 25) \\
 (25)\Delta 29 &= 4 \rightarrow 2 = 29\Delta 31 \\
 31\Delta (35) &= 4 \rightarrow 2 = (35)\Delta 37 \rightarrow (7 \times 5 = 35)
 \end{aligned} \tag{7.19}$$

The initial $\frac{6}{9} block = A \begin{Bmatrix} 4 \\ 2 & 5 \\ 1 & 3 & 6 \end{Bmatrix}$ structure is replicated with each iteration,

giving the pattern of (combinations of) numbers each cell can hold.

$$\begin{aligned}
 & \left\{ \begin{matrix} 4 \\ 2 & 5 \\ 1 & 3 & 6 \end{matrix} \right\} \rightarrow \left\{ \begin{matrix} 2 \\ 1 & \star \\ \star & 1 & 2 \end{matrix} \right\} \rightarrow \left\{ \begin{matrix} 2 & 0 \\ \star & 0 \\ 0 & \star & 2 \end{matrix} \right\} \rightarrow \left\{ \begin{matrix} \star \\ 1 & 0 \\ 0 & 1 & \star \end{matrix} \right\} \\
 & \left\{ \begin{matrix} +3 \\ +1 & +4 \\ 1 & +2 & +5 \end{matrix} \right\} \rightarrow \left\{ \begin{matrix} even \\ even & odd \\ odd & odd & even \end{matrix} \right\} \rightarrow \left\{ \begin{matrix} (2 \times e) \\ (2 \times e) & (o \times o) \\ o & (3 \times o) & (2 \times o) \end{matrix} \right\} \\
 & \left\{ \begin{matrix} D_2 \\ D_1 & D_0 \\ D_0 & D_1 & D_2 \end{matrix} \right\} \rightarrow \left\{ \begin{matrix} p_n (< 5) \cap D_0 = \emptyset & \rightarrow \{1 + |4, 2, 4, 2, \dots\} \\ p_n (2 \wedge 3) \cap D_1 = \emptyset & \rightarrow \{2 + |1, 5, 1, 5, \dots\} \\ p_n (2 \vee 3) \cap D_2 = \emptyset & \rightarrow \{4 + |2, 4, 2, 4, \dots\} \end{matrix} \right. \tag{7.20}
 \end{aligned}$$

All $n \in \mathbb{N}$ are represented in the stack therefore the clear areas in figure 7.19 is either compressed into the diagonal stack, or irrelevant.

7.8.1 The size of the plane

The diagonal sets the size of the triangular plane at $A_{\Delta} = 8 \times 8 = 64$, this gives us a measure for the size of the diagonal $d_p = \sqrt{64}\sqrt{2} = \sqrt{128}$, there is however another measure that we can follow. The sum of the values on the diagonal is $d_p = 96$ or 12×8 , the proportional area of a square with a diagonal $d_p = 96 \rightarrow A_{prop} = (96\sqrt{2}^{-1})^2 = 4608$. The ratio between both areas is $A_r = \frac{A_{prop}}{A_{\Delta}} = \frac{4608}{64} = 72$ or $\frac{4608}{360} = 12.8 = \frac{80}{2.5^2}$ and $\frac{64}{360} = \frac{P\Delta}{2.5^2} = 0.16 \times P\Delta$ and thus of relevance for this model. Figure 7.20 projects the sum of the first 9 primes on a circumference of 100 units. The x-axis is subdivided in units of $\frac{1}{2.5^2} = \frac{16}{100}$ conform the QGF standard for $n \in \mathbb{N} \propto n^{\frac{4}{25}}$. Orthogonal diagonal as circumference

The sectors are delimited by the 9 primes, labeled $(+2, +3, +5, +7, +11, +13, +17, +19, +23)$. The circumference is subdivided in units of arc $U_{arc} = \frac{1}{50}360^\circ = 7.2^\circ$, derived from the spread of prime 2. By applying U_{arc} the diagonal of 100 units is stretched over a Archimedes spiral¹ of 720° . In total 115 points are projected because $5 \times 23 = 115$ concludes the 38 unit orthogonal diagonal. This $115 \times 7.2^\circ = 828^\circ$ is intriguing because $\frac{828}{2.3} = 360^\circ$ and exponential number $e \approx \frac{2\pi}{2.3} \leftrightarrow^{-1} \approx (1 + \frac{1}{1600})^{1600}$ indicates the ratios are significant. The $e \propto 360^\circ$ invites to explore further: $\sqrt[8]{828} \approx 2.316081256$ then try $\frac{2\pi}{\sqrt[8]{828}} \approx 2.712851843 \rightarrow \Delta e \approx \sqrt[8]{\frac{2\pi}{\sqrt[8]{828}}}$ and find $\frac{e^8}{828} \approx \frac{U_{arc}}{2} \approx 3.600190806$.

¹wikipedia: Archimedes spiral

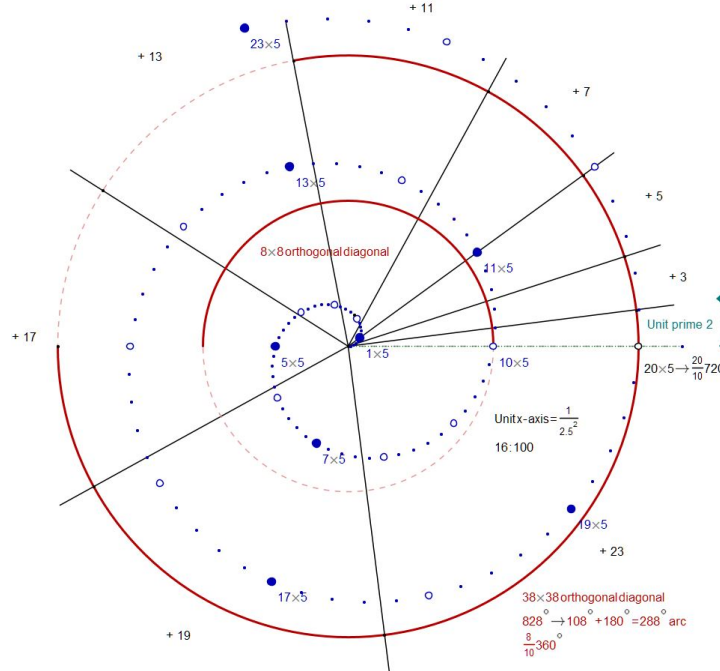


Figure 7.20: Orthogonal diagonal as circumference

Not to venture too far into a numerologists exercise, $\alpha^{-1} \approx \frac{2\pi}{828} \times 9^{-8}$. Back to figure 7.20, the inner arc labeled “ 8×8 orthogonal diagonal” indicates the part of the spiral that defines the pole section. It covers $x=0$ to $x=-4$, ($25 \times -0.16 = -4$) radial units of $\frac{1}{2.5^2}$. This 180° of arc holds the 9 primes under 25, (2, 3, 5, 7, 11, 13, 17, 19, 23), see figure 7.17, pole section A1 to D25. The outer arc labeled “ 38×38 orthogonal diagonal” continues on to 108° for a total of $180^\circ + 108^\circ = 288^\circ$, covering the remainder of the stack E25 to T115. The pole terminating at 180° is significant because $\frac{288^\circ}{180^\circ} = 1.6^\circ \rightarrow 10 \times \frac{1}{2.5^2} = \frac{1}{10}$. By the factor U_{arc} the radius gets stretched a factor 7.2, each 5 point displacement along the radius represents $5nU_{arc} = n\frac{360^\circ}{10}$, the model integrates the base 10 and 60 number system. 7.9 Spectrum 7.9.1 Prime edges, vertices and 10 The minimum increment $U_{arc} = \frac{1}{50}360^\circ = 7.2^\circ$, and $5U_{arc} = \frac{1}{10}360^\circ = 36^\circ$ indicates there are 10 radii available for any distinct arithmetic sequence $n(x \times U_{arc})$ to project on. This aspect causes a skeletal structure of five radii (36° stretched to 72°) where multiples of 5 land on. The radial distance between each projection is forced by $U_{arc} \times 5 = \frac{360^\circ}{10}$, it takes 50 steps on the x-axis to project a full 360° further, this makes the radial distance a consistent $50 \times U_{arc} = 8$ and the spiral Archimedean. Figure 7.20 plots the complete stack A to T, see figure 7.17, as continuous succession of

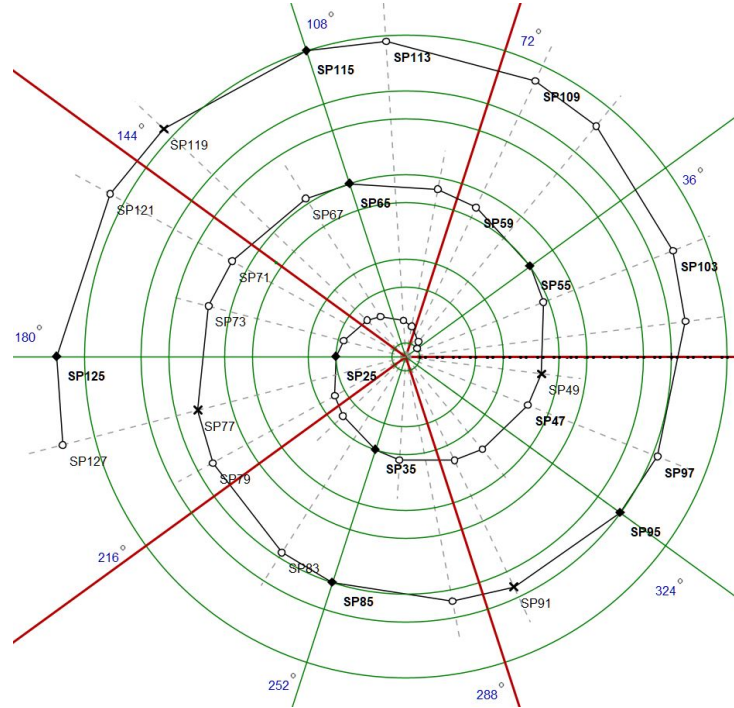


Figure 7.21: Projecting the stack

$\angle n = (n \times U_{arc}) \bmod 360$. In bold face, indicated by the black diamond, the composites 25, 35, 55, 65, 85, 95 and 115 project on 5 radii at 72° interval. All values on the x-axis with an interval of 50 units project on the same radial, e.g. $180^\circ = \{0, 25, 75, 125, 175, \dots\}$, $64.8^\circ = \{0, 9, 59, 109, 159, \dots\}$ and $54.72^\circ = \{0, 7.6, 57.6, 107.6, 157.6, \dots\}$. Projecting the stack

Figure 7.22 shows the effect of plotting this sequence $n(x \times U_{arc})$ on a 2-dimensional plane. When $p=5$ we find that all intersections represent integer angles and that each fifth value is either $(180^\circ \rightarrow 360^\circ)$ or $(0^\circ \rightarrow 720^\circ)$. With $n=10$ the same applies but consequently each fifth iteration projects at $(0^\circ \rightarrow 720^\circ)$. Stack rhythm in the plane

Application of any other value preserves an integer angle for the fifth iteration because it will contain some factor of prime 5. The pattern for sums of five do not simply repeat. As seen in figure 7.22 the values 5, 10, 25 and 50 generate distinct patterns. These patterns are the analogue of strange attractors in the QGF, the intermediate values vary considerably. Figure 7.22 depicts the two dimensional plot for the primes 7 and 11. Prime rhythm in the plane

The result as seen in figure 7.20 is that in the limit all prime numbers combined address the whole continuum $\frac{n \times 7.2^\circ}{7.2^\circ} = n \text{on } \frac{7.2^\circ}{720^\circ} = \frac{1}{100}$ part of the

P5											N10										
	x_5	x_{10}	x_{15}	x_{20}	x_{25}	x_{30}	x_{35}	x_{40}	x_{45}	x_{50}	x_{10}	x_{20}	x_{30}	x_{40}	x_{50}	x_{60}	x_{70}	x_{80}	x_{90}	x_{100}	
7.2	36	72	108	144	180	216	252	288	324	0	7.2	144	216	288	0	72	144	216	288	0	
14.4	72	144	216	288	0	72	144	216	288	0	14.4	288	72	216	0	144	288	72	216	0	
21.6	108	216	324	72	180	288	36	144	252	0	21.6	72	288	144	0	216	72	288	144	0	
28.8	144	288	72	216	0	144	288	72	216	0	28.8	216	144	72	0	288	216	144	72	0	
36	180	0	180	0	180	0	180	0	180	0	36	0	0	0	0	0	0	0	0	0	
43.2	216	72	288	144	0	216	72	288	144	0	43.2	144	216	288	0	72	144	216	288	0	
50.4	252	144	36	288	180	72	324	216	108	0	50.4	144	288	72	216	0	144	288	72	216	0
57.6	288	216	144	72	0	288	216	144	72	0	57.6	216	72	288	144	0	216	72	288	144	0
64.8	324	288	252	216	180	144	108	72	36	0	64.8	288	216	144	72	0	288	216	144	72	0
72	0	0	0	0	0	0	0	0	0	0	72	0	0	0	0	0	0	0	0	0	

P25											P50										
	x_{25}	x_{50}	x_{75}	x_{100}	x_{125}	x_{150}	x_{175}	x_{200}	x_{225}	x_{250}	x_{50}	x_{100}	x_{150}	x_{200}	x_{250}	x_{300}	x_{400}	x_{450}	x_{500}		
7.2	180	0	180	0	180	0	180	0	180	0	7.2	0	0	0	0	0	0	0	0	0	
14.4	0	0	0	0	0	0	0	0	0	0	14.4	0	0	0	0	0	0	0	0	0	
21.6	180	0	180	0	180	0	180	0	180	0	21.6	0	0	0	0	0	0	0	0	0	
28.8	0	0	0	0	0	0	0	0	0	0	28.8	0	0	0	0	0	0	0	0	0	
36	180	0	180	0	180	0	180	0	180	0	36	0	0	0	0	0	0	0	0	0	
43.2	0	0	0	0	0	0	0	0	0	0	43.2	0	0	0	0	0	0	0	0	0	
50.4	180	0	180	0	180	0	180	0	180	0	50.4	0	0	0	0	0	0	0	0	0	
57.6	0	0	0	0	0	0	0	0	0	0	57.6	0	0	0	0	0	0	0	0	0	
64.8	180	0	180	0	180	0	180	0	180	0	64.8	0	0	0	0	0	0	0	0	0	
72	0	0	0	0	0	0	0	0	0	0	72	0	0	0	0	0	0	0	0	0	

Figure 7.22: Stack rhythm in the plane

P7											P11										
	x_7	x_{14}	x_{21}	x_{28}	x_{35}	x_{42}	x_{49}	x_{56}	x_{63}	x_{70}	x_{50}	x_{100}	x_{150}	x_{200}	x_{250}	x_{300}	x_{400}	x_{450}	x_{500}		
7.2	50.4	100.8	151.2	201.6	252	302.4	352.8	43.2	93.6	144	7.2	79.2	158.4	237.6	316.8	36	115.2	194.4	273.6	352.8	72
14.4	100.8	201.6	302.4	43.2	144	244.8	345.6	86.4	187.2	288	14.4	158.4	316.8	115.2	273.6	72	230.4	28.8	187.2	345.6	144
21.6	151.2	302.4	93.6	244.8	36	187.2	336.4	129.6	280.8	72	21.6	237.6	115.2	352.8	230.4	100	345.6	223.2	100.8	338.4	216
28.8	201.6	43.2	244.8	86.4	288	129.6	331.2	172.8	14.4	216	28.8	316.8	273.6	230.4	187.2	144	100.8	57.6	14.4	331.2	288
36	252	144	36	288	180	72	324	216	108	0	36	72	108	144	180	216	252	288	324	0	
43.2	302.4	244.8	187.2	129.6	72	14.4	316.8	259.2	201.6	144	43.2	115.2	230.4	345.6	100.8	216	331.2	86.4	201.6	316.8	72
50.4	352.8	345.6	338.4	331.2	324	316.8	305.6	302.4	295.2	288	50.4	194.4	28.8	223.2	57.6	252	86.4	280.8	115.2	305.6	144
57.6	43.2	86.4	129.6	172.8	216	259.2	302.4	345.6	28.8	72	57.6	273.6	187.2	100.8	14.4	288	201.6	115.2	28.8	302.4	216
64.8	93.6	187.2	280.8	14.4	108	201.6	295.2	28.8	122.4	216	64.8	352.8	345.6	338.4	331.2	324	316.8	305.6	302.4	295.2	288
72	144	288	72	216	0	144	288	72	216	0	72	144	216	288	0	72	144	216	288	0	

Figure 7.23: Prime rhythm in the plane

circumference or simply put the surface collapses to $\frac{8 \times 8}{100} = 0.64 \propto \frac{50 \times 50}{100} = 25$, the pole, or more illustrative perhaps, that simple beginnings at figure 7.17 at the start of the orthogonal diagonal, n=1.

Chapter 8

Spectrum of volume

That we arrived at the Archimedes spiral to model the volume of number might be labeled a “historic mathematical coincidence”, being Archimedes discovering the principle cause of buoyancy. But this aside, the patterns of figure 7.22 are drawn on a Cartesian plane representing volume. Table 8.1 lays out a two dimensional array that extends to 50 rows and columns of U_{arc} . The $U_{arc} = 7.2^\circ$ ensures that 50 iterations suffice to complete a full cycle, $\angle U_{arc} \rightarrow [7.2^\circ, 360^\circ]$. The variable $q \in \mathbb{Q}$ determines the value for which $50^2 = 2500$ data points represent intersecting radii. The radius subdivides into units $\frac{1}{2.5^2} = \frac{8}{50}$. The proportion $50^2 \propto 8^2$ models the reduction in volume as function of surface area. Table 8.1 represents just one out of an infinite number of gradients that represent a 8-fold increase in volume. The proportion $2500 \propto 64$ can also be stated as the circumference of a circle with radius $|2\pi|$, the limit of mapping the zeta function to a circumference, see table 2.2, $c = \frac{|2\pi| \times 2\pi}{q^2} = 39\frac{1}{16} = \frac{2500}{64}$.

8.1 Interval, chaos and strange attractor

Projected as a 50×50 surface, enhanced with a gradient, the spectrum of the $50^2 = 2500$ possible intersections per unique value tells a story that culminates with a primordial connection.

Figure 8.1 shows the spectrum for each of the 7 primes on the orthogonal diagonal, the starting value 1, and the first composite in the sequence, 25. Where ever the color is absent the angle is 0, progressively the gradient lightens until $\angle n \bmod 360 = 0$. The set for $q=1$ is the baseline. The diagonal from lower right to upper left is the inverse of the orthogonal diagonal, the figure is symmetric over 180° . The division in 4 quadrants is presents in all spectra, the least discernible in $q=25$. There is an evolution visible in Cartesian

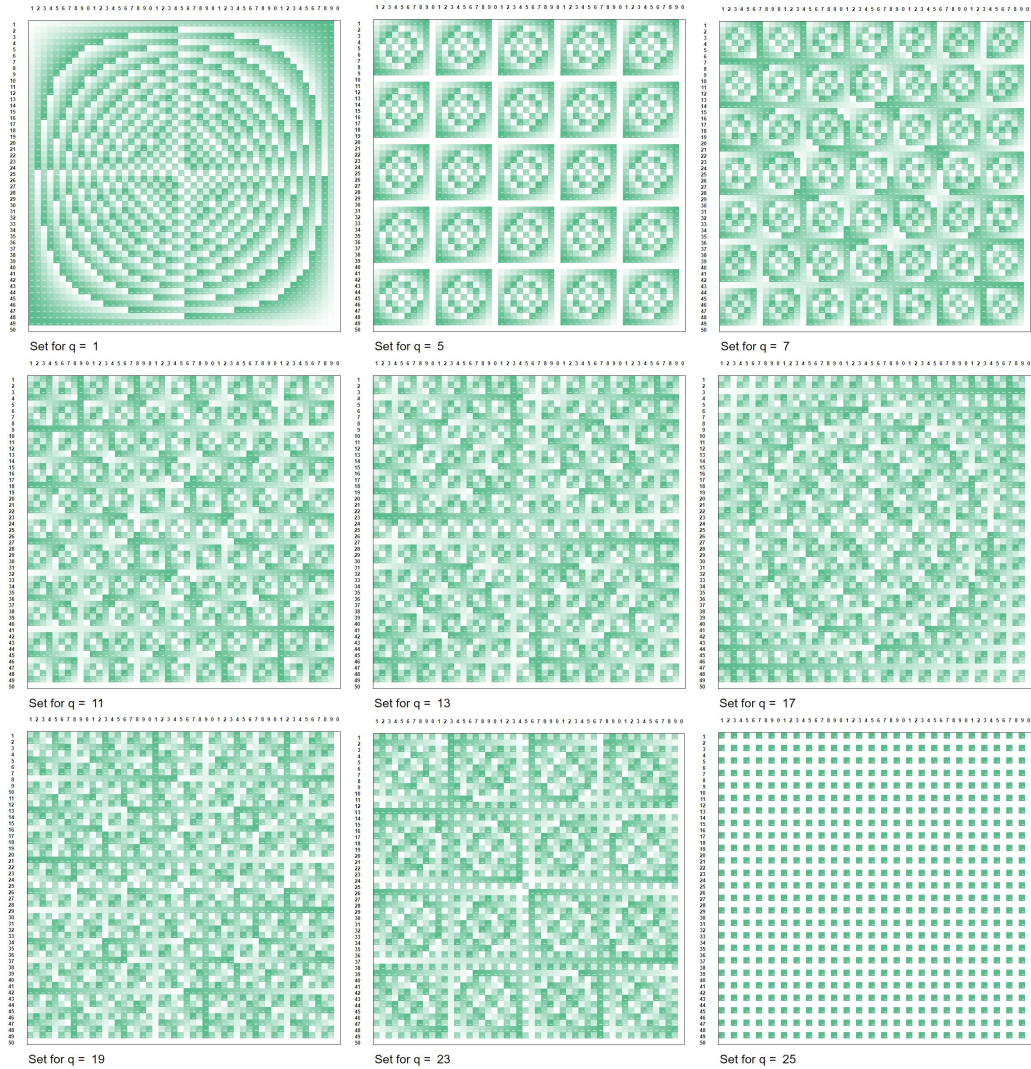


Figure 8.1: Spectrum core orthogonal diagonal

Table 8.1: Spectrum orthogonal diagonal full cycle

$U_{arc} = \angle 7.2^\circ$		Spectrum 50 periods for q							
q	$q(n\angle 7.2^\circ)$	n	1	2	3	4	5	..., 50	
1	7.2°	1	7.2°	14.4°	21.6°	28.8°	36°	...	
1	14.4°	2	14.4°	28.8°	43.2°	57.6°	72°	...	
1	21.6°	3	21.6°	43.2°	64.8°	86.4°	108°	...	
1	28.8°	4	28.8°	57.6°	86.4°	115.2°	144°	...	
1	36°	5	36°	72°	108°	144°	180°	...	
1	43.2°	6	43.2°	86.4°	129.6°	172.8°	216°	...	
1	50.4°	7	50.4°	100.8°	151.2°	201.6°	252°	...	
1	57.6°	8	57.6°	115.2°	172.8°	230.4°	288°	...	
1	64.8°	9	64.8°	129.6°	194.4°	259.2°	324°	...	
1	72°	10	72°	144°	216°	288°	0°	...	
..., 50, 50	

patterns and patterns of spherical geometry. It seems that at the transition between $q=23$ and $q=25$ Descartes wins the fight. This is the core set, A to D, eight transitions $\{1, 5\}, \{5, 7\}, \{7, 11\}, \{11, 13\}, \{13, 17\}, \{17, 19\}, \{19, 23\}, \{23, 25\}$, at transition $\frac{6}{9} \rightarrow \{13, 17\}$ we find the clearest intermediate pattern between Cartesian and spherical features. Spectrum core orthogonal diagonal

8.2 Spectrum chain links

In the total stack, see figure [fig:stacking-the-core], we find 7 values

$$\{25, 49, 55, 85, 91, 115, (121)\}$$

, that link between the $\frac{6}{9}$ blocks. Those chain links are displayed in figure 8.2. The spectrum for $q=25$ is familiar, $25 + (n \times 50) \rightarrow \angle 180^\circ$. The next spectrum for $q=49$ looks similar to $q=1$ but is in fact rotated over 45° , the diagonals are flipped and the whole configuration remains symmetrical over 180° . It is as if we shifted perspective from above to underneath the plane. The sets for $q = [I55, N85, S115]$ are member of the sets $[5, 15, 35] + (n \times 50)$. They project on $55 \times 7.2^\circ = \angle 36^\circ, 85 \times 7.2^\circ = \angle 252^\circ, 115 \times 7.2^\circ = \angle 108^\circ$. The set for $q=91$ is from $7 \times 13 = 91$ or $41 + (n \times 50) \rightarrow \angle 295.2^\circ$, set 41 is in fact the midfield value for $\frac{6}{9}G$ in figure 7.17. In this we see that a loop occurs connecting two values $\{G41, P91\}$ both along the spiral, and orthogonal to the spiral, through the bulk. The

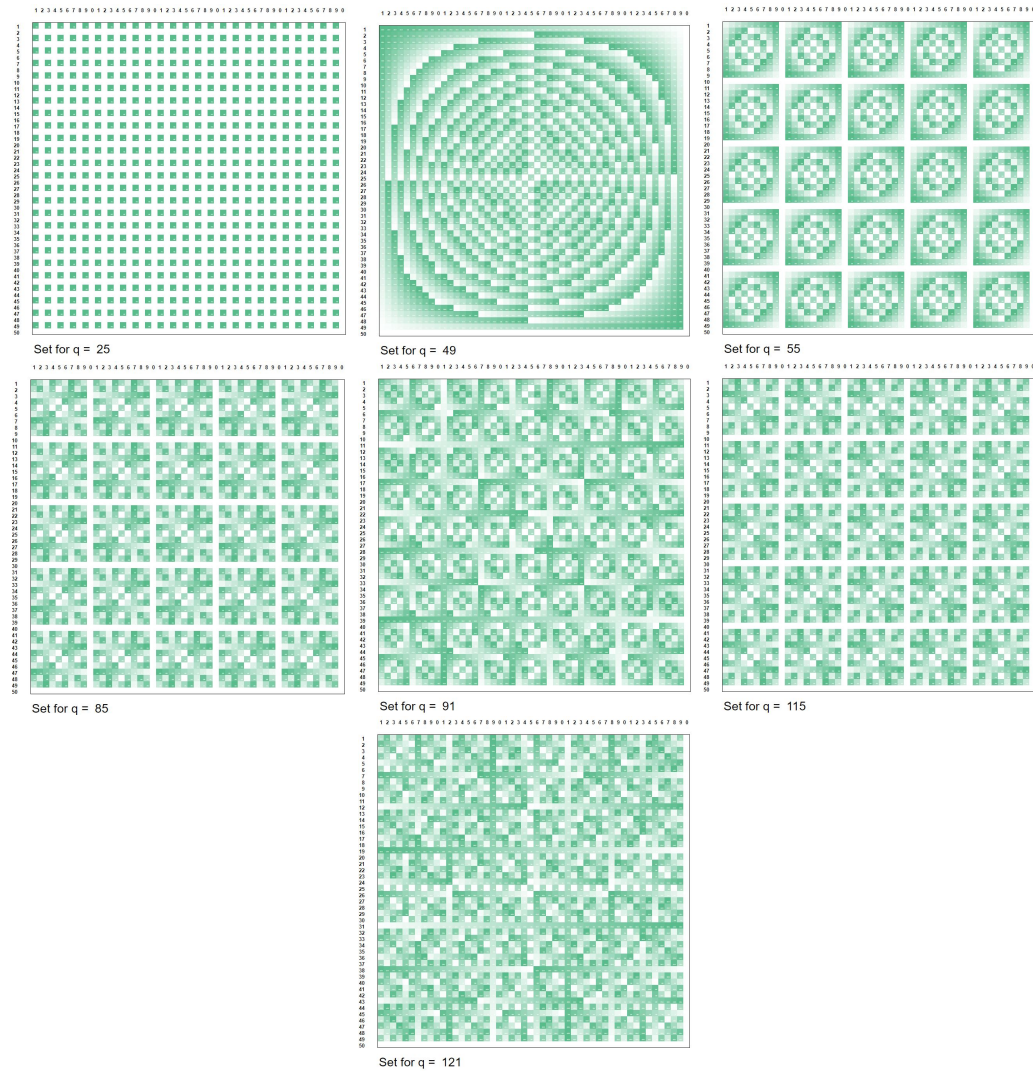


Figure 8.2: Spectrum composite stack links

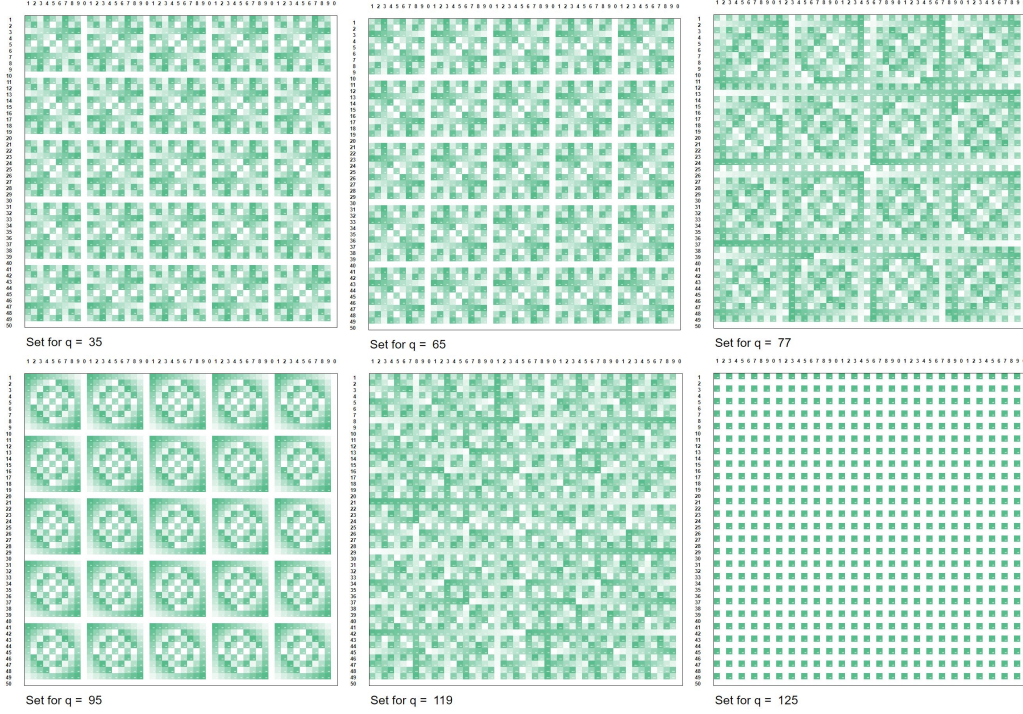


Figure 8.3: Spectrum composite stack midfield

same goes for $\{A5, I55\}$, $\{B11, J61\}$, $\{C17, K67\}$, $\{D23, L73\}$, etc. Each represents an interval of 50 (8), which is significant as a function of volume, causing specific (surface) coordinates to line up, see figure 5.6 where chords merge forming a polar triangle, proportionally reducing $SA = 1$ to $SA = \frac{1}{8}$ as function of volume. Spectrum composite stack links

8.3 Spectrum midpoint composite

The sets for $q = [F35, K65, P95]$ are member of the sets $35 + (n \times 50) \rightarrow \angle 252^\circ$, $15 + (n \times 50) \rightarrow \angle 108^\circ$ and $45 + (n \times 50) \rightarrow \angle 324^\circ$, and project accordingly.

The midfields as shown, do not merely connect along the spiral, but share radii with the 9th $\frac{6}{9}block$ further up the stack. The midfield clearly ends a sequence of eighth $\frac{6}{9}block$, but does so scale independent, as chain link in a continuous flow. In principle the spiral represents a continuum, but comes prefixed with a rational set of coordinates enforced by units. Those units emerge from integer wavelength resonating in the repository of potential. Mathematics follows nature in the sense that applying mathematics involves

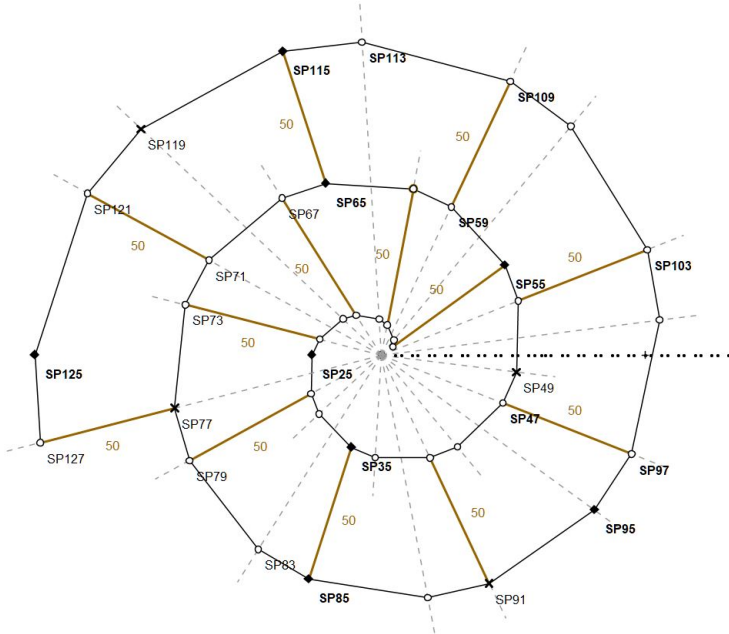


Figure 8.4: Midfield radial connections

counting and manipulating units. Nature does not know math, it necessarily organizes by simple resonance patterns.

Figure 8.4 shows radial connections between midfields and start of other $\frac{6}{9}$ blocks. All of those radial segments are of length 50 (8) as they connect arcs of the Archimedes spiral. Just like the QGF 2-gon chord, the radius of $50U_{arc} = 8$ appears as a linear segment from a previous cycle. In an infinity of steps it completes a 720° cycle passing along the way all conceivable angles with the x-axis, until the radius stretched to $x=16$ at which point the doubling of radius indicates a completed cycle. In the QGF representation, figure 7.2, the chord at infinity stands orthogonal to the x-axis after two triangular, or primorial cycles of 45° . Here 90° is proportional to $\frac{90^\circ}{288^\circ} = \frac{\pi}{104^\circ}$. There are intermediate values that seem to be missing. These missing values represent nodes intersecting with diagonal D_1 or D_2 and do not appear on the spiral, which of course represents diagonal D_0 , see matrix [eq:block-stamp]. Note for instance $SP95 \in [H47, P95, X145]$ and $SP113 \in [C13, K63, S113]$. Resp. $3 \times 3 \times 5 = 45$ and $3 \times 3 \times 7 = 63$, both on diagonal D_1 . Some other

examples,

$$\begin{aligned} D_2 96 &= \{2 \times 2 \times 2 \times 2 \times 2\} \times \{3\} \\ D_1 99 &= \{3 \times 3 \times 3\} \times 11 \\ D_1 105 &= \{3\} \times \{5\} \times \{7\} \\ D_2 108 &= \{2 \times 2 \times 2\} \times 23 \end{aligned} \tag{8.1}$$

The connection with 40 units, see section 7.2.4, re-emerges by $\frac{288}{U_{arc}} = 40$. The model can be projected on $\frac{12.5}{40} = \frac{1.25}{4} \propto \frac{\pi}{10^{\frac{1}{2}}}$ which makes sense by a repetitive scale invariant projection of pole $AD = 180^\circ$. A sub sequential repetition will result arithmetically in $\frac{\pi}{100}$, but in a physical implementation taken from a view of scale invariance, the observer will just measure two cycles $2 \times 180^\circ = 360^\circ$. In section 5.5.1 the statement made was: “The question to ask is however, did you not notice your radius decreasing?”. This question implies that somehow the physical universe is in a state of continuous collapse, and thus a further statement keeps the energy flowing: “At which set of points does the energy of a blast project at any given point in time?”

8.4 At the edge of chaos, the primorial spectrum

Fractal recurrence in shape like the Mandelbrot set shows, does not cause motion, nor does it cause “time” or can it be equated to “energy”. It is however observable, measurable and can be modeled to produce beautiful images, preferably zoom-able on our computer screens. The beauty disappears from the vantage of one particular point on some arbitrary line, nothing changes from the points perspective because none of its neighbors changes.

8.4.1 25, primorial equilibrium

We are not in such a dire clueless state, but we are like such points nonetheless. If all changes in relation with all other things, then at first glance no change occurs. Taking a closer look at figure 7.19, the set of diagonals D_0, D_1, D_2 provide some answers that connect the QGF intimately with the primorial function. In figure 8.5 each prime on the fractal core stack is amended with the quotient $\frac{P_n \#}{2 \times 3} = n$, and $n \bmod 25 = \frac{n}{5}$. The orthogonal diagonals subdivide the primorial product in two distinct factors, $D_1 = 2 \times 3 = 6$ and $D_0 = 5 \times P_{n>5} \# \dots = n \rightarrow D_0 \bmod 5 = 0$.

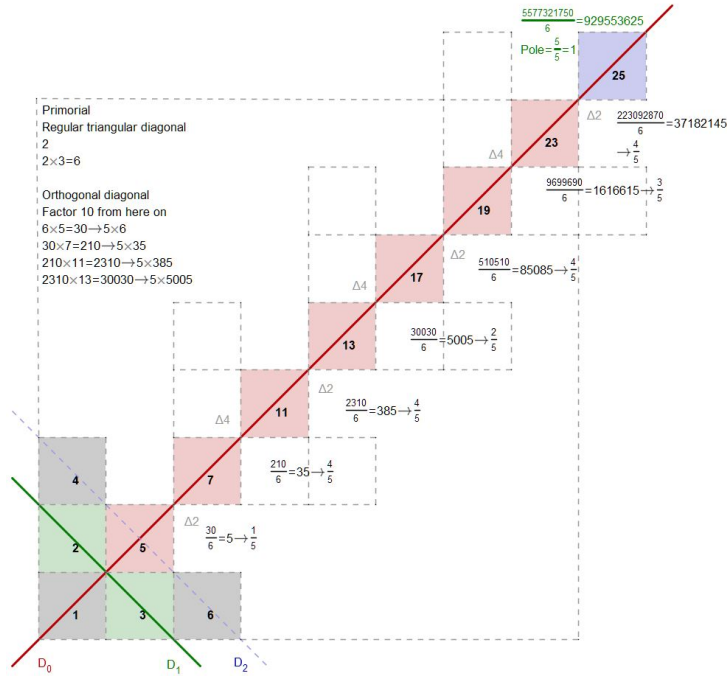


Figure 8.5: The primorial stack

The pole at 2.5^2 and the subdivision in units of $\frac{1}{25}$ is the foundation under the QGF, in the stack prime 5 and composite 25 indicate a connection. In the fractal core stack we find in D_0 indications of a winding path along a continuous curve that at each prime interval finds a cusp of $\frac{n}{5}$. The “path along a continuous curve” must be true, because the prime after 23 is 29 and yields $\frac{223092870 \times 29}{6} = \frac{6469693230}{6} = 1078282205 \rightarrow \left\lfloor \frac{1078282205}{25} \right\rfloor = \frac{1}{5}$. Instead the curve passes the composite $5 \times 5 = 25$ along the way, and $\frac{223092870 \times 25}{6} = \frac{5577321750}{6} = 929553625 \rightarrow \left\lfloor \frac{929553625}{25} \right\rfloor = 0$, indicating a full cycle just occurred. This occurrence of some integer composite in this sequence can only be meaningful if the intermediate integer 24 has some profound reason not to appear on D_0 as the first next integer in line. Aside from the fact that division by 25 then would not yield an integer result, “24” would know neither decide not to be there because of that fact, as would 2, 3, 4, 6, 8, 9, 10, etc, no numerical consciousness present is the best guess. End of fun section. It does have one reason that is not immediately obvious but can be derived from the location of prime 23. Composite 24 appears to belong to D_1 , above 23, but in fact it claims position at $\frac{24}{6} = 4$, the 6th position of block number 4, $\frac{6}{9}blockD$ on diagonal D_2 , see figure 7.17. This condition of pattern was postulated in eq. [eq:block-stamp] and the primorial stack nails down the

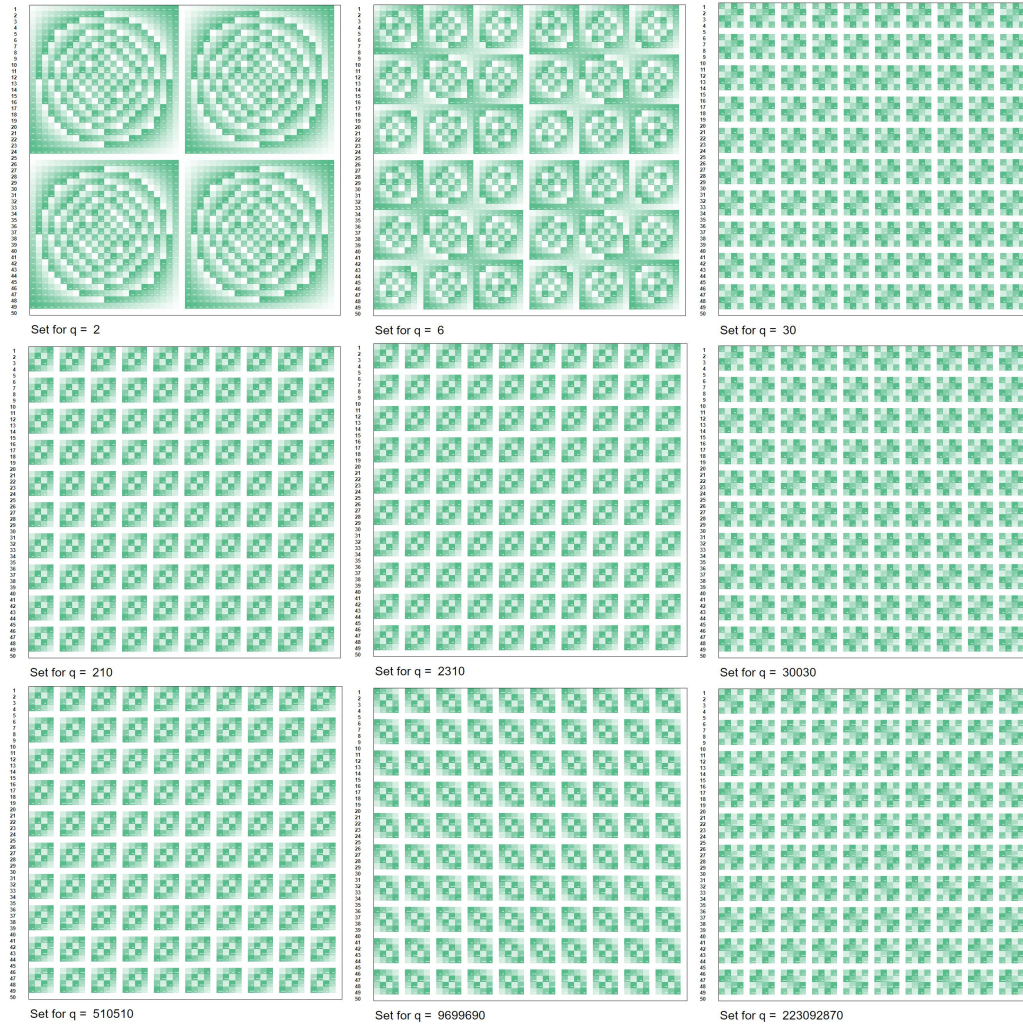


Figure 8.6: Primorial spectrum

case for the fractal argument and might provide a pathway towards a closed formula for the number and location of primes $\prod(n)$.

8.4.2 The spectrum for the primorials

The primorial function is a product of primes, see table 3.1 column $P_n\# = \{2, 6, 30, 210, 2310, \dots\}$, and those intermediate products have a spectrum, see figure 8.6. The sets for $q = [2, 6]$ are those residing on diagonal D_1 , all the following lay on diagonal D_0 and those show a nice consistency in discrete cycles. Primorial spectrum However, from $(2 \times 3) \times 5 = 30$ on, all following $P_n\#$ products are a factor of 10, and because the prime factors are odd, only

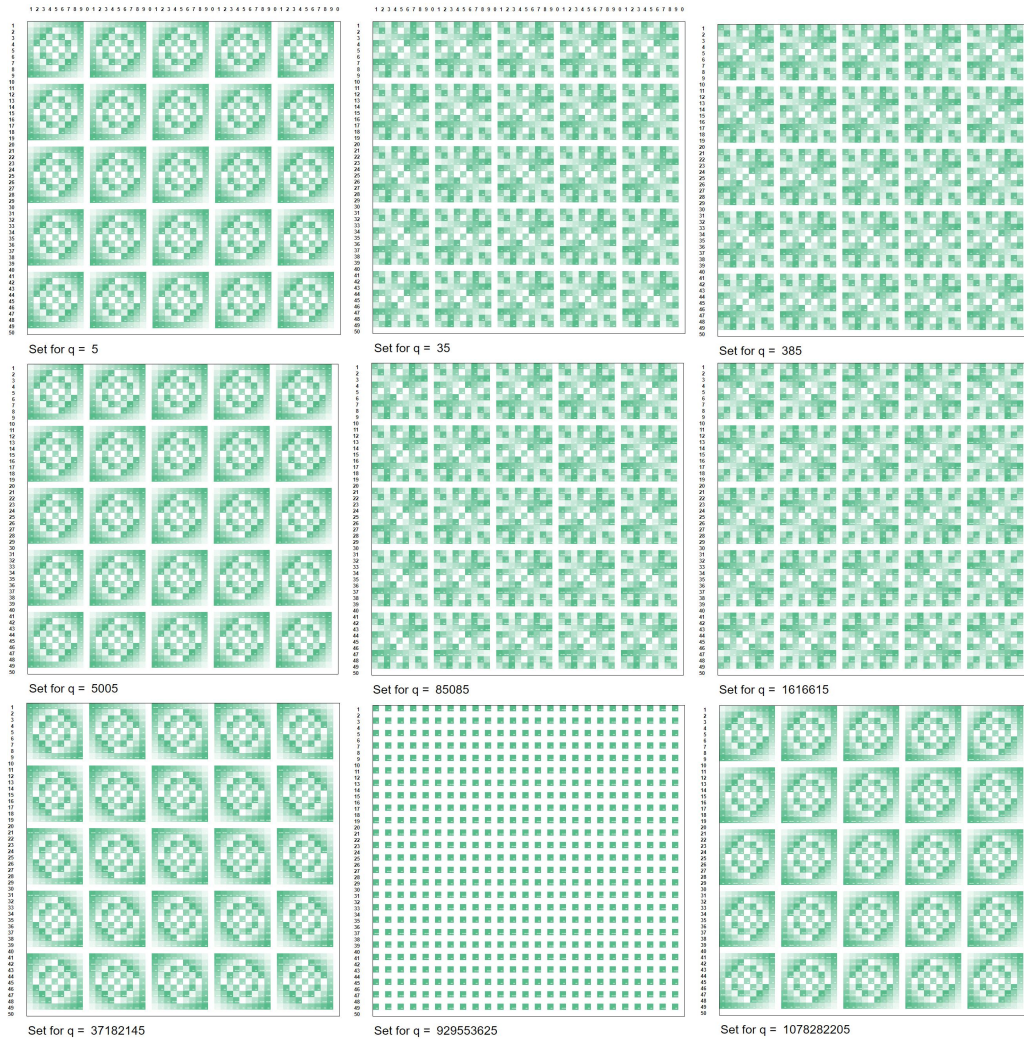
the 4 spectra will be generated that end in $q = [10, 30, 70, 90]$. This does not take into account though, that these spectra, with exception of the first two, are the products of two orthogonal diagonals.

8.4.3 Factors on the orthogonal diagonal

To obtain the spectra of the factors on the orthogonal diagonal we use a simple quotient. Each factor on that diagonal is $\frac{P_n \#}{D_1} = \frac{1}{6} P_n \#$ which is a familiar pattern indicating proportionality with $\zeta(2)$ by $P_n \# \propto \pi^2$ as a function of area, and follows the pattern of expansion in figure 6.5. By $\frac{P_n \#}{D_1}$ we find the spectra as shown in figure 8.7. Depicted are the spectra of the first eight (8) $\frac{P_n \#}{D_1} = \frac{1}{6} P_n \#$ and for making the order clear, including the spectrum of $\frac{P_{9 \rightarrow 23} \# \times 25}{D_1}$, found at position E1 in figure 7.17, the pole.

8.4.4 Equilibrium at the bow shock

In “QGF in its natural configuration” there was mention of a “repository of potential” needed for explaining the dynamic behavior we were about to invoke in describing dynamical behavior of the physical implementation of the QGF. At this point we only have a first principle that might account for the emergence of a quantum harmonic oscillator in a complete convex set when the abstraction of the QGF is superimposed on that set. How does one account for a repository of potential that, by observation and experimentation, has real tactile properties, spatial and temporal qualities. It is not sufficient to ‘declare’ such a space into existence and explain its properties in terms of (analogies to) the QGF. Wikipedia: Energy In physics, energy is the quantitative property that must be transferred to an object in order to perform work on, or to heat, the object. Energy is a conserved quantity; the law of conservation of energy states that energy can be converted in form, but not created or destroyed. The SI unit of energy is the joule, which is the energy transferred to an object by the work of moving it a distance of 1 meter against a force of 1 newton. Spatial qualities are in fact non existent. The QGF models a dimensionless point that can neither expand nor collapse. But we observe both collapse and expansion at all conceivable scales, so how to account for spatial displacement if, as proposed, there are no such things as spatial qualities in the dimensionless point. There is no mystery here, looking out into the universe is receiving signals from times long gone. The M-brane mono surface stretches out in time, is in a excited state and is in a entropic process similar to a damped oscillator eventually coming to absolute rest. Yes, “absolute” in clear defiance of the zero point energy

Figure 8.7: Primorial P_n over 6 spectrum

attributed to Heisenberg's uncertainty principle. The notion of what energy exactly is has a clear explanation under this framework. It is the nature of circumstances that led to the observation that energy evidently is conserved and must be some eternal quantity that can not be destroyed. The repository of potential that we occupy is structured such that observation must lead to that conclusion. Then what is it? The Planck constant represents the staccato transfer of potential from unity chord to unity chord at some point of equilibrium as if part of a zone of constant pressure in a shock wave. A continuous gradient of collapsing surface area. It is at the front of a shock wave that we envision the conditions that at first sight energy, and by extension information, is preserved. The universe that we experience to be a spatial realm, expanding in time, is in fact an illusion of ever decreasing 'surface area'. This surface area that we are part of close to atomic scale, has a cross section that stretches out from the Planck scale to the center of the great voids at universal scale. This thin layer of activity is the M-brane mono surface coming to rest by shifting potential from layer to layer, the absolute surface area of the bow shock reduces with the radius, and us observers are integral part of that surface. It is space that apparently expands in relation to that for the observer static surface area, but in fact is just an illusion caused by re-configuring potential. Spatial qualities are an illusion of shifting potential traversing the zero dimensional point. This equilibrium at the bow shock is our universe, a phase transition akin to a boiling kettle of water, a constant 100°C until there is nothing to evaporate left. At which point the bow shock ran its course, Heisenberg's uncertainty principle is no more and the potential called "time" reduced to nothing. Wikipedia: to interpret UN (the vibrational energy of N oscillators) not as a continuous, infinitely divisible quantity, but as a discrete quantity composed of an integral number of finite equal parts. Let us call each such part the energy element – Planck, On the Law of Distribution of Energy in the Normal Spectrum

8.5 The size of the mathematical universe

Our mathematical universe, given the 8 units on D_0 , has the definite size of $A = 8 \times 8 = 64$. Not every angle, line or pattern, no matter how appealing, has to have structural meaning in the context of this thesis. Humans are pattern seeking animals by evolutionary necessity and find patterns even where non exist. D_0, D_1 and D_2 represent areas by triangular projection. In the limit of the triangular projection we are left with a field of dimensionless points, a surface which only structure exists by the linear relation of the natural numbers, a line for short. In this context we are justified to interpret

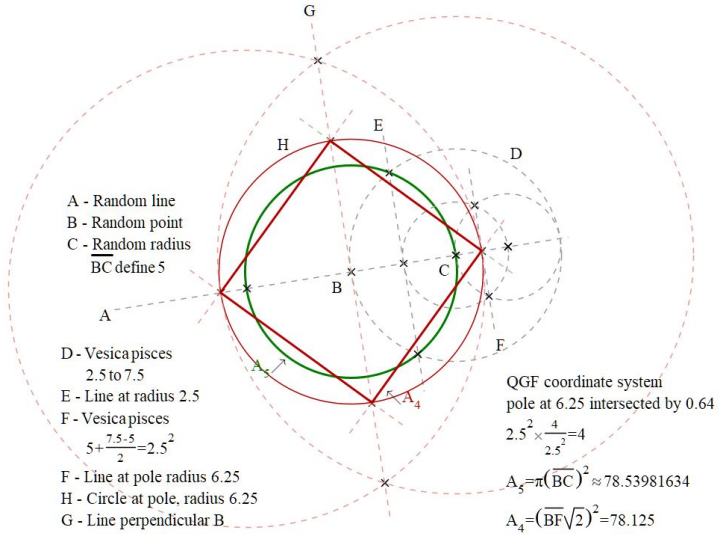


Figure 8.8: QGF Solution

the sum of primes as a linear feature, one that exists on two diagonals. As shown in figure 8.4, there exist a configuration at which those two diagonals line up, and in essence represent the diagonal \overline{BHD} in figure 7.8 at the point of equilibrium. In figure 6.3, line $\overline{AG} = \sqrt{2}$, the longest line in our universe is a diagonal of a square. All this we find sufficient corroboration to postulate the size of our (mathematical) universe. But then again, “64” is not that poetic standing there alongside “42”, no cult status just yet. So let us see what 64 has to offer, maybe a slice of history is possible. Taken the sum of primes as line $\overline{AG} = \sqrt{2}$, the we find $A_{universe} = \left(\frac{100}{\sqrt{2}}\right)^2 = 5000$, and this provides us with a universal unit of area $A_1 = \frac{1}{64}5000 = 78.125$, this all is a bit nondescript until we unlock some beautiful relation and take some time to ponder on the following.

$$\begin{aligned}\circ A_5 &= \pi 5^2 = 78.53981634 \\ \diamond A_4 &= \left(2.5^2 \sqrt{2}\right)^2 = 78.125 \\ \frac{\circ A_5}{\diamond A_4} &= \varphi^2\end{aligned}\tag{8.2}$$

List of Tables

2.1	Zeta function values	5
2.2	Zeta as a scale invariant proportion	16
3.1	Primorial root 2 approach	18
3.2	Primorial lb/ub oscillation	19
4.1	Discrete triangular - Continues projection plane	31
4.2	Projection plane range for all s	32
4.3	The base of Planck's constant	40
4.4	Zeta, the SA/Volume equilibrium	42
5.1	Hexagonal equilibrium	52
6.1	4/5 proportion Spherical vs Cartesian projection (exc. \leftrightarrow) . .	65
7.1	QGF standard chord and deviation	70
7.2	Chord length and relative density	77
7.3	Non trivial zero to Unity chord	85
7.4	Non trivial zeros - Levels	86
7.5	Level 1 coordinate listing	94
8.1	Spectrum orthogonal diagonal full cycle	105

List of Figures

1.1	The sum formula	2
1.2	The product formula	3
2.1	SA as a Volume	10
3.1	Quadrature constant - leap	20
3.2	Quadrature continuum	21
3.3	Quadrature reference frame	22
3.4	Primorial hexagon	23
4.1	The sum formula and first six triangular numbers	25
4.2	The projection plane	26
4.3	The triangular plane	27
4.4	Triangular to projection plane	29
4.5	Exceeding the bounds of the Triangular plane	30
4.6	Projection plane extended zeta	34
4.7	Projection plane bulk	37
4.8	The triangular plane bulk	38
4.9	Projection plane regression	41
4.10	Fractal stack	43
5.1	Hexagonal chord versus \hbar	45
5.2	Planck base - Unity chord	46
5.3	Triangular numbers - (a, R_q) chord density	48
5.4	Plot Triangular $T_{n=1}$ and $T_{n=2}$	49
5.5	Planck base - Transition $T_{n=3}$ to $T_{n=4}$	50
5.6	Root 2 equilibrium	53
5.7	Spherical triangle	54
5.8	M-brane hemisphere mono surface	55
6.1	Some $\frac{1}{6}$ affected area configurations	57
6.2	M-brane mono surface $\sqrt{2}$ contraction	58

6.3	M-brane mono surface radii group III	59
6.4	M-brane mono surface area contraction	61
6.5	M-brane mono surface zeta equilibrium	62
6.6	M-brane mono surface - detail 9 over 60	64
7.1	Convex set	67
7.2	Quadrature Geometric Framework	69
7.3	QGF natural state	75
7.4	QGF natural state normalized pole	76
7.5	Particle in a box and Harmonic oscillator	78
7.6	Pair correlation numerical calculation by Odlyzko	80
7.7	Geometric Primes and Pair correlation	81
7.8	Pair correlation proportional chord	83
7.9	Zeta zeros normalized to pole range	84
7.10	Zeta zero modulus as proportional chord	86
7.11	Interlaced zeta zeros	88
7.12	Interlaced zeta zero detail	88
7.13	Decent for Zeta N	90
7.14	Decent for levels	90
7.15	Zeta zeros walk about	92
7.16	Prime number triangular core set	95
7.17	Stacking the core	95
7.18	Orthogonal succession	96
7.19	Orthogonal fractal stack zeta	97
7.20	Orthogonal diagonal as circumference	99
7.21	Projecting the stack	100
7.22	Stack rhythm in the plane	101
7.23	Prime rhythm in the plane	101
8.1	Spectrum core orthogonal diagonal	104
8.2	Spectrum composite stack links	106
8.3	Spectrum composite stack midfield	107
8.4	Midfield radial connections	108
8.5	The primordial stack	110
8.6	Primordial spectrum	111
8.7	Primordial Pn over 6 spectrum	113
8.8	QGF Solution	115